Downloaded from orbit.dtu.dk on: May 05, 2023

DTU Library

Sensitivity analysis of nacelle lidar free stream wind speed measurements to wind-induction reconstruction model and lidar range configuration

Svensson, Elin; Borraccino, Antoine; Meyer Forsting, Alexander Raul; Troldborg, Niels; Wagner, Rozenn

Publication date:
2017

Document Version
Publisher's PDF, also known as Version of record

Link back to DTU Orbit

Citation (APA):
Svensson, E., Borraccino, A., Meyer Forsting, A. R., Troldborg, N., & Wagner, R. (2017). *Sensitivity analysis of nacelle lidar free stream wind speed measurements to wind-induction reconstruction model and lidar range configuration*. DTU Wind Energy. DTU Wind Energy E Vol. 152

General rights
Copyright and moral rights for the publications made accessible in the public portal are retained by the authors and/or other copyright owners and it is a condition of accessing publications that users recognise and abide by the legal requirements associated with these rights.

- Users may download and print one copy of any publication from the public portal for the purpose of private study or research.
- You may not further distribute the material or use it for any profit-making activity or commercial gain
- You may freely distribute the URL identifying the publication in the public portal

If you believe that this document breaches copyright please contact us providing details, and we will remove access to the work immediately and investigate your claim.

UniTTe

Innovation Fund Denmark
RESEARCH, TECHNOLOGY & GROWTH

DTU

Sensitivity analysis of nacelle lidar free stream wind speed measurements to wind-induction reconstruction model and lidar range configuration

DTU Wind Energy E-Report-0152

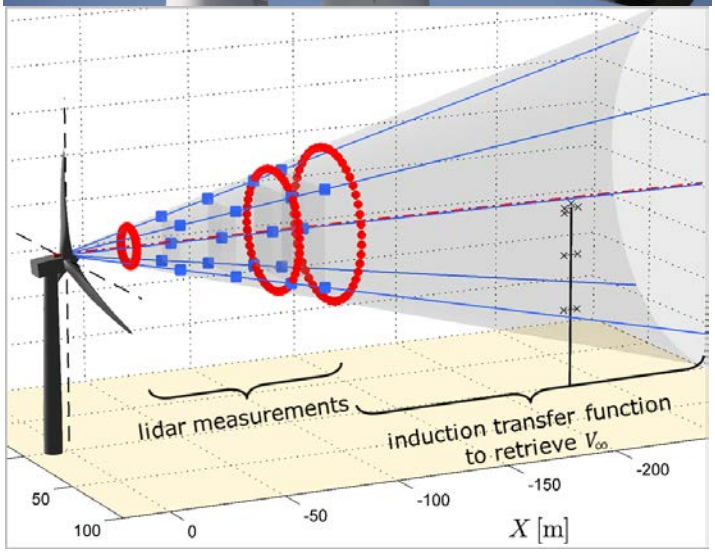

E. Svensson, A. Borraccino, A.R. Meyer Forsting,
N. Troldborg, R. Wagner

DTU Wind Energy E-0152

December 2017

DTU Wind Energy
Department of Wind Energy

Authors: E. Svensson, A. Borraccino, A.R. Meyer Forsting, N. Troldborg, R. Wagner

Title: Sensitivity analysis of nacelle lidar free stream wind speed measurements to wind-induction reconstruction model and lidar range configuration

Department: DTU Wind Energy

Abstract:
The sensitivity of nacelle lidar wind speed measurements to wind-induction models and lidar range configurations is studied using experimental data from the Nørrekær Enge (NKE) measurement campaign and simulated lidar data from Reynold-Averaged Navier Stokes (RANS) aerodynamic computational fluid dynamics (CFD) simulations. In both approaches, the data correspond to measurements (or simulations) from a five-beam Demonstrator (5B-Demo) unit developed by *Avent Lidar Technology* and a ZephIR Dual-Mode (ZDM) unit developed by *Zephir Lidar*. The 5B-Demo was configured to measure at ten distances while the ZDM was configured to measure at five distances.

From the configured distances, a large number of range configurations were created and systematically tested to determine the sensitivity of the reconstructed wind speeds to the number of ranges, minimum range and maximum range in the range configurations. The wind speeds were reconstructed using both a one-dimensional and two-dimensional induction model to test the sensitivity towards the wind-induction model. In all cases, the sensitivity of the reconstructed wind speed was determined from the wind speed error and root mean square error (RMSE) of the fitting residuals.

The results demonstrate that it is not possible to use RANS CFD simulated lidar data to determine optimal range configurations for real-time nacelle lidars due to their perfect (unrealistic) representation of the simulated flow field. The recommended range configurations are therefore based on the NKE sensitivity analysis results. Based on these results, it is recommended to configure nacelle lidars to measure at approximately 3-5 ranges. The minimum distance should be configured to roughly 0.5 rotor diameters (D_{rot}) while it is recommended that the maximum range lay within 1-1.5D_{rot}. In addition, the results show that the reconstructed wind speeds are insensitive to the wind-induction reconstruction model.

DTU Wind Energy E-0152

December 2017

ISBN: 978-87-93549-20-3

Contract no.: InnovationsFondens 1305-00024B

Project: UniTTe
http://www.unitte.dk/

Funding:
Innovation Fund Denmark

Pages: 84
Tables: 6
Figures: 25 (+ 44 in annexes)
References: 16

Technical University of Denmark
DTU Wind Energy
Risø Campus
Frederiksborgvej 399
DK-4000 Roskilde
Denmark

www.vindenergi.dtu.dk

Table of contents

Figures and tables

Preface

This technical report studies the influence of lidar range configuration on the accuracy of estimating the free stream wind speed using a simple wind-induction model from nacelle-mounted lidars.

The report was written within work package 4 of the Unified Turbine Testing project (UniTTe, http://www.unitte.dk/) funded by *Innovation Fund Denmark*. UniTTe aims at developing power performance testing procedures using profiling nacelle-mounted lidars applicable in all types of terrain. Work package 4 focuses specifically on developing methods for power curve verification using nacelle-mounted lidar systems.

The sensitivity analysis aims at providing recommendations for the configuration of nacelle lidar ranges when using the so-called "combined wind-induction" model to estimate the free stream wind speed (V_∞) from nacelle lidar measurements close to the turbine rotor.

The technical report is deliverable D4.9.

Elin Svensson (Research Assistant)
Antoine Borraccino (Postdoctoral Researcher)

Acknowledgements

We, Elin Svensson and Antoine Borraccino, would like to say "Tusind tak", "Merci beaucoup", many thanks to Rozenn Wagner for four years of terrific project leading and team work within UniTTe and for providing us with the opportunity to perform this study. Thanks to Alexander R.M. Forsting and Niels Troldborg for the close collaboration that allowed us to push the boundaries of lidar measurements and the scientific understanding of a turbine's induction zone. Finally, we acknowledge the support to UniTTe by *Innovation Fund Denmark*.

Joint author statement

Elin Svensson was in charge of the research work under the direct supervision of Antoine Borraccino. The report was co-written by these two authors.

Rozenn Wagner extensively contributed to the definition of the tasks and to the analysis of the results and lead the UniTTe project. Niels Troldborg and Alexander R.M. Forsting performed the numerical simulations necessary for the second part of the study. They participated in the analysis of the results and the technical discussions relating to the numerical parts of the study.

1 Introduction

1.1 Nacelle lidars and power curve verification

Nacelle-mounted lidars have in recent years become a mature measurement technology. This is particularly true for the application of power performance testing ([1], [2]) where they are used in forward-looking mode. As nacelle-mounted lidars follow the turbine's yawing motion, they measure the wind directly upstream of the rotor. This means that nacelle lidars provide more representative wind measurements than conventional meteorology towers. In fact, nacelle-mounted lidars might even provide more representative measurements than ground-based profilers. In addition, nacelle lidars are cost-efficient, especially offshore.

Nacelle lidars – as other monostatic Doppler anemometers – do not measure wind field characteristics (WFC) directly. Instead, they measure the component of the wind vector that is projected onto the line-of-sight (LOS) of the laser beam, the so-called LOS velocity ($\mathrm{V_{LOS}}$). The LOS velocity is thus an intermediate measurand in the lidar measurement chain. In order to retrieve useful information on the wind vector, LOS velocity measurements along multiple beams have to be combined using assumptions on the wind field (defining a wind model). This process is commonly known as "Wind Field Reconstruction" (WFR).

In power curve verification (PCV), the primary aim is to correlate the turbine electrical power output to the energy present in the wind. The wind's kinetic energy is quantified through the proxy of wind speed and air density. The wind driving the turbine is characterised in the PCV standard (IEC 61400-12-1:2017, [3]) to be the so-called free stream wind speed at hub height ($\mathrm{H_{hub}}$) (see definition in [4]) or a suitable average of the wind profile over the rotor swept area. Practically, the IEC 61400-12-1 standard describes the normative procedures used to test the power performance of a wind turbine. This standard requires measurements of the wind speed, which typically are obtained using a meteorological mast or a ground-based profiler located between two and four rotor diameters ($\mathrm{D_{rot}}$) from the turbine. At such distance, the wind speed is assumed to be within 1% of the free stream wind speed $\mathrm{V_{\infty}}$.

In [5], it was demonstrated using experimental data from a full-scale campaign that the free stream wind speed – "*the wind at the turbine position as if the turbine were not there*" by definition unmeasurable – can be estimated using nacelle lidar measurements taken at multiple distances close to the rotor. Here, the wind is strongly influenced by the turbine operation effects and experiences significant wind speed deficits (induction). The lidar LOS velocity measurements are used as inputs to a WFR algorithm, which fits the measurements to a simple model of the wind speed evolution in the induction zone of a wind turbine. This innovative method allowed to estimate $\mathrm{V_{\infty}}$ solely from nacelle lidar measurements and showed promising results, with wind speed deviations less than 0.7% in comparison to measurements from a top-mounted cup anemometer on an IEC-compliant met. mast.

1.2 Research questions

Although the nacelle short-range measurement method estimating $\mathrm{V_{\infty}}$ was successfully demonstrated using the Nørrekær Enge (NKE) measurement campaign – a 7-month full-scale measurement campaign for the primary purpose of PCV ([5], [6]) – an essential question remained unanswered; what is the sensitivity of the nacelle lidar-reconstructed (fitted) wind field characteristics to:

1) The range configuration:
    a. How many ranges are required?
    b. What values should the ranges take? What should be the minimum range, maximum range and separation between the configured ranges?
2) The combined wind-induction model:
    a. Is the simple one-dimensional induction model sufficient or should it be two-dimensional and account for the radial dependency of the induction profile?

In order to answer these research questions, an extensive sensitivity analysis was conducted, taking two different approaches. The first approach makes use of the experimental data of the NKE campaign. In NKE, two commercially developed nacelle-mounted profiling lidars were installed on the nacelle of a Siemens wind turbine of 2.3MW rated power and 93m rotor diameter: one five-beam Demonstrator (5B-Demo) unit developed by *Avent Lidar Technology* and one ZephIR Dual-Mode (ZDM) unit developed by *Zephir Lidar*.

The second part of the study is entirely based on numerical simulations using computational fluid dynamics (CFD). Reynold-Averaged Navier Stokes (RANS) aerodynamic simulations – running in steady-state – were performed for the aerodynamic model of the Siemens 2.3-93 wind turbine of NKE ([7], [8]). A variety of wind conditions were simulated, with different free stream wind speeds (at hub height), yaw misalignments, and wind shear profiles. The nacelle lidar measurements were simulated to match the beam trajectories and range configuration of the 5B-Demo and ZDM lidar systems during the NKE campaign.

For both approaches, we applied the model-fitting wind field reconstruction technique ([5], [9]) using lidar measurements at several ranges and the so-called “combined wind-induction model” (either one- or two-dimensional). A large number of range configurations were systematically tested (see Chapter 4). For both approaches, the analysis focuses on the wind speed error between the lidar-reconstructed and reference wind speed values. The reference wind speed is measured by the top-mounted cup anemometer in the NKE approach, while for the CFD it is taken from the boundary conditions of the simulations. Additionally, the sensitivity analysis is also focused on the LOS velocity residual statistics.

1.3 Outline

This technical report is structured as follows:

- Chapter 1 introduces the study, its purposes and aims.
- Chapter 2 describes the NKE data and the CFD simulated data used in the sensitivity analysis.
- Chapter 3 provides the necessary technical information related to the wind field reconstruction technique and wind-induction models.
- Chapter 4 describes the methods employed in the sensitivity analysis.
- Chapter 5 provides the results of the sensitivity analysis based on the NKE experimental data. The results are split into several sub-sections in order to identify the impact of the induction models, lidar range configurations and lidar trajectory and technology.
- Chapter 6 provides the result of the sensitivity analysis based on the CFD simulations. Its structure is identical to that of Chapter 5.
- Chapter 7 discusses several aspects directly related to the study, such as the adequacy of the simple induction model. It also contains recommendations for the lidar configurations in the WFR.
- The conclusions of the sensitivity analysis are summarized in Chapter 8.

2 Data

This chapter describes the data used in the study. The sensitivity analysis is based on two sets of data; experimental data from the NKE measurement campaign and simulated data from CFD simulations. The most important details on both data sets are described beneath.

2.1 Nørrekær Enge data

The first part of the sensitivity analysis (Chapter 5) is based on measurements from the NKE campaign. In the NKE campaign, seven months of data was collected between June 2015 and January 2016 from two nacelle-mounted lidars; a five-beam Demonstrator (5B-Demo) unit developed by *Avent Lidar Technology* and a ZephIR Dual-Mode (ZDM) unit developed by *Zephir Lidar*. The lidars can be viewed in Figure 1.

2.1.1 The lidars

The 5B-Demo (Figure 1 - left) is a pulsed system. It can therefore measure LOS velocities (V_{los}) at several distances along each LOS simultaneously by range gating. The 5B-Demo takes measurements along five LOS (see Figure 1 - left). The LOS are measured successively at 1Hz. Thus, a complete cycle takes 5s.

The ZDM (Figure 1 - right) is a continuous wave system featuring a variable focus to interrogate multiple distances successively. Each distance is conically scanned (see Figure 2, right). The ZDM samples V_{los} at a high frequency of approximately 50Hz. A specifically designed azimuthal averaging process yields a pseudo "48-beam lidar". More details on the two lidar systems can be found in their respective calibration reports, [10] for ZDM and [11] for 5B-Demo.

2.1.2 Lidar trajectories and configured distances

The lidar trajectories and range configurations used in the NKE campaign are visualized in Figure 2. All five LOS were used for the 5B-Demo while only six out of the 48 LOS (azimuthal sectors) were used for the ZDM. These were chosen such that four of the LOS would match the "corners" of the 5B-Demo square pattern, while the remaining two matched the hub height. Table 1 shows the configured measurement ranges (in the lidar coordinate system).

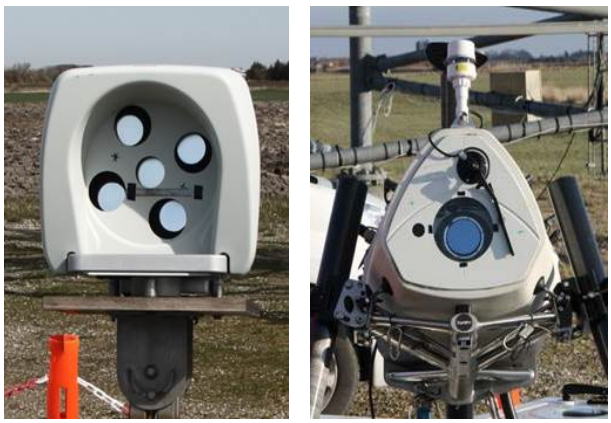

Figure 1. The two nacelle lidar systems used in this study and the Nørrekær Enge campaign: five-beam Demonstrator (left) and ZephIR Dual Mode (right).

Table 1. Configured measurement distances for the 5B-Demo and ZDM during the NKE campaign.

Lidar	**Configured measurement distances [m]**											
5B-Demo	-	-	49	72	95	109	121	142	165	188	235	281
ZDM	10	30	-	-	95	-	120	-	-	-	235	-
Lidar	**Non-dimensional distance in hub CS [D_{rot}]**											
5B-Demo	-	-	0.5	0.75	0.99	1.14	1.27	1.5	1.75	1.99	2.5	2.99
ZDM	0.08	0.30	-	-	0.99	-	1.26	-	-	-	2.5	-

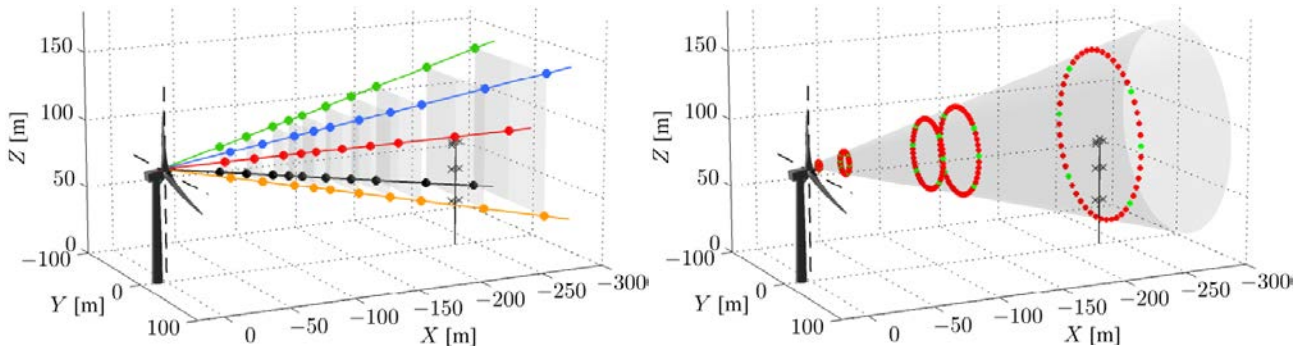

Figure 2. Lidar measurement trajectories in NKE: 5B-Demo (left), ZDM (right).

2.1.3 Filtering

In this study, the NKE data set corresponds to the filtering detailed in [5]. The data set consists of 2815 time periods of 10-minute data, and was obtained after filtering on:

- **Wind direction** – The wind direction measured by the wind vane mounted on the met. mast (at 78m a.g.l) is in the wake-free IEC sector $[110°; 219°]$.
- **Yaw misalignment** – The yaw misalignment measured by the spinner anemometer mounted on the turbine is in the range of $[-10°; +10°]$.
- **Turbine**
  – The turbine is operating normally and continuously.
  – The turbine is connected to the grid (status signals OK).
- **5B-Demo lidar**
  – The availability of V_{los} is higher than 30%.
  – The carrier-to-noise ratio (CNR) is above -20dB.
  – The tilt and roll measured by the lidar are real numbers.
  – All five beams pass the filtering at 49, 72, 95, 109 and 188m.

- **ZDM lidar** – The availability of V_{los} must be higher than 30%.
  – The considered 10-minute period contains at least 50 V_{los} measurements.
  – The tilt and roll measured by the lidar are real numbers.
  – No fog is detected.
  – All six LOS (azimuthal sectors) pass the filtering at 30, 95, 120 and 235m.

- **Joint data set** – The considered 10-minute period pass all of the above mentioned filters.

The 2815 time periods are valid for all ZDM range configurations as the filtering is based on the same ranges as used in this study. Furthermore, the data set was created specifically for the [49m, 72m, 95m, 109m and 188m] 5B-Demo range configuration. This means that some of the 10-minute periods can be invalid for the 121m, 142m, 165m, 235m and/or 281m range. The number of valid 10-minute periods (N_{10min}) therefore depends on the examined range configuration. A more detailed explanation of the valid periods is given in Chapter 4.

2.1.4 Wind conditions

Histograms of the reference wind speeds and yaw misalignments included in the data set are shown in Figure 3 and Figure 4, respectively. The reference wind speeds are given by the horizontal wind speeds measured by the top-mounted cup anemometer. Similarly, the reference relative directions are given by the yaw misalignments measured by the sonic anemometer mounted on the turbine's spinner.

The histograms show that most 10-minute periods feature wind speeds between 5ms^{-1} and 12ms^{-1} and a mean yaw misalignment of -3°. No measurements were made (or passed the filtering) below 3ms^{-1} and only a few above 15ms^{-1}. Situations with yaw misalignments below -6° or above 2° are also rare.

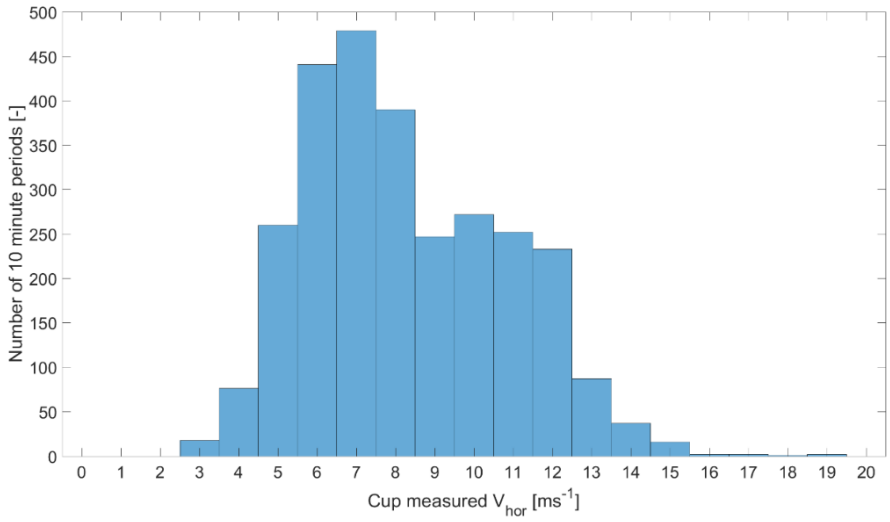

Figure 3. Histogram of 10-minute average wind speeds measured by the mast top-mounted cup anemometer.

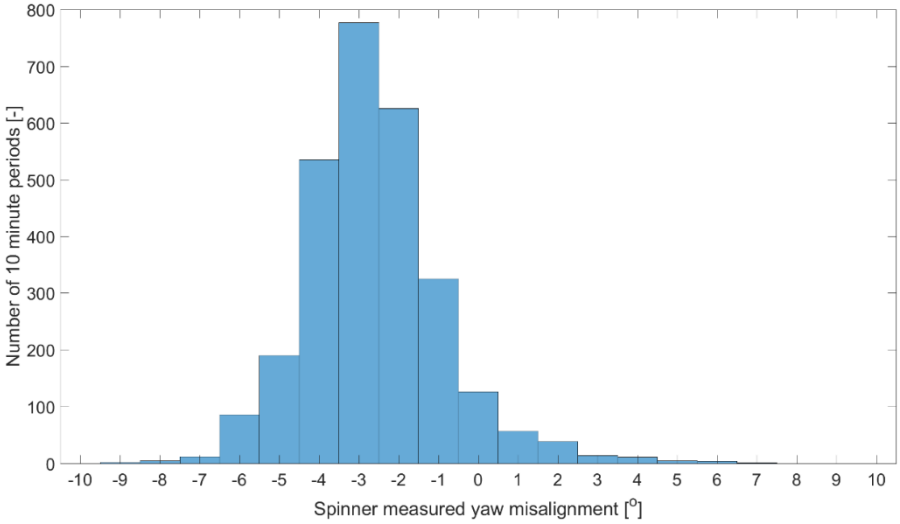

Figure 4. Histogram of 10-minute average yaw misalignments measured by the spinner anemometer.

2.2 CFD simulations

The second part of the sensitivity analysis (Chapter 6) is based on CFD simulations. The CFD simulations used in this study correspond to aerodynamic simulations. These were performed using the incompressible Reynold-Averaged Navier Stokes (RANS) solver EllipSys3D, which was running in steady-state. The simulations were performed using the aerodynamic model of the Siemens 2.3-93 wind turbine of NKE. For a more detailed introduction to the CFD modelling, see [7].

A variety of wind conditions were simulated:

- Free stream wind speeds (at hub height) ranging from 4 ms^{-1} to 18ms^{-1} (12 values).
- Yaw misalignment values of 0°, 2°, 5° and 10°.
- Four types of wind shear profiles (uniform, linear, power-law, log-law).

In total, 240 cases were simulated using CFD.

In this report, results are only presented for cases where the power-law shear profile was used. The power-law shear profile was simulated using a shear exponent (α_{exp}) of 0.3 at the boundary condition. Consequently, the "CFD data set" contains 48 simulations (N_{CFD}) of lidar measurements. This can be seen as 48 different time periods representing 12 different wind speeds and 4 different yaw misalignments.

The nacelle lidar measurements were simulated to match the beam trajectories and range configuration of the 5B-Demo and ZDM lidar systems used in the NKE campaign (see Table 1).

3 Wind field reconstruction technique

The purpose of this chapter is to describe the wind field reconstruction (WFR) technique used in the study. However, before the WFR technique can be described, we have to define the models that the WFR is based on. The wind model used in the study is presented in Section 3.2. This model is combined with both a one-dimensional (1D) and two-dimensional (2D) induction model to yield the so-called "combined wind-induction models". The 1D wind-induction model is described in Section 3.3 while the 2D wind-induction model is described in Section 3.4. Both models are used to estimate the free stream wind speed from the lidar-measured (or lidar-simulated) LOS velocities. The WFR technique used to estimate the free stream wind speed is presented in Section 3.5. Furthermore, it should be noted that both the models and WFR technique are described in the hub coordinate system (CS). The hub coordinate system is described in Section 3.1.

3.1 Hub coordinate system

The hub CS $(\mathcal{H}, \overrightarrow{x_{\mathcal{H}}}, \overrightarrow{y_{\mathcal{H}}}, \overrightarrow{z_{\mathcal{H}}})$ is a right-handed Cartesian orthonormal system with its origin at the center of the rotor plane (longitudinal direction). The x-axis of the hub CS is closely aligned with the rotor axis, which in reality is inclined by some degrees. The x-axis points downwind (i.e. measurements located upstream of the rotor plane correspond to negative $x_{\mathcal{H}}$ coordinates). $(\overrightarrow{x_{\mathcal{H}}}, \overrightarrow{y_{\mathcal{H}}})$ defines a horizontal plane. More details on the coordinate system can be found in [5].

3.2 Wind model

A wind model is defined by making assumptions on the flow field ([5], [9]). Such assumptions can (for example) include stationarity (static model), horizontal homogeneity, a wind shear profile and/or homogenous relative wind direction (no veer).

The wind model used in this study makes three assumptions on the spatial variability of the wind field. First of all, it assumes that the wind vector $\vec{V} = [u,\ v,\ w]$ is horizontal. This means that the vertical wind component w is forced to zero and that the wind vector becomes two-dimensional ($\vec{V} = [u,\ v,\ 0]$). Here, u and v are the longitudinal and transverse wind speeds, respectively. Secondly, it assumes that the wind speed $V = \sqrt{u^2 + v^2}$ is the same at any given height and distance upstream the rotor. Finally, it assumes that the shear profile is of power-law type. This means that the wind speed varies with height according to:

$$V(z_{\mathcal{H}}) = V_{hub}\left(\frac{z_{\mathcal{H}} + H_{hub}}{H_{hub}}\right)^{\alpha},$$

where V_{hub} is the wind speed at hub height $(z_{\mathcal{H}} = 0)$ and α is the shear exponent.

In addition, the wind model assumes stationarity. The reconstruction of wind characteristics is therefore performed on time-averaged data.

3.3 One-dimensional wind-induction model

The wind model described in Section 3.2 only accounts for the vertical variation of the wind. The turbine, by harnessing energy from the wind, also induces longitudinal wind speed gradients (negative). This means that the wind decelerates when approaching the rotor. This deceleration is here described by the 1D-induction model.

The 1D-induction model results from the vortex-sheet theory (vortex cylinder) applied to the actuator disk model of a wind turbine rotor (see [12]). The analytical expression for the 1D-induction model is given by:

$$u\left(\xi = \frac{x_{\mathcal{H}}}{R_{rot}}\right) = u_{\infty}\left(1 - a_{ind}\left[1 + \frac{\xi}{\sqrt{1+\xi^2}}\right]\right).$$

Here, a_{ind} is the so-called axial induction factor (directly related to the thrust forces exerted by the turbine on the wind flow), u_{∞} is the wind speed at a distance infinitely far away from the rotor (the free stream wind speed), R_{rot} is the rotor radius and $\xi = \frac{x_{\mathcal{H}}}{R_{rot}}$ is the non-dimensional longitudinal distance from the rotor plane. The effect of the turbine induction on the wind field is visualized in Figure 5 (one-dimensional model).

The induction model is combined with the wind model by assuming that only the longitudinal wind speed contributes to the generation of thrust. Consequently the transverse wind speed v remains constant when approaching the rotor. The final expression for the model flow field wind speed thus becomes:

$$V(x_{\mathcal{H}}, z_{\mathcal{H}}) = V_{\infty}\left(\frac{z_{\mathcal{H}} + H_{hub}}{H_{hub}}\right)^{\alpha} = \left(\frac{z_{\mathcal{H}} + H_{hub}}{H_{hub}}\right)^{\alpha} \sqrt{u_{\infty}^2\left(1 - a_{ind}\left[1 + \frac{\xi}{\sqrt{1+\xi^2}}\right]\right)^2 + v_{\infty}^2},$$

where $V_{\infty} = \sqrt{u_{\infty}^2 + v_{\infty}^2}$ is the free stream wind speed at hub height, θ_r is the relative wind direction (or yaw misalignment), $u_{\infty} = V_{\infty}\cos\theta_r$ is the axial speed of the free stream vector and $v_{\infty} = V_{\infty}\sin\theta_r$ is the transverse speed of the free stream wind vector.

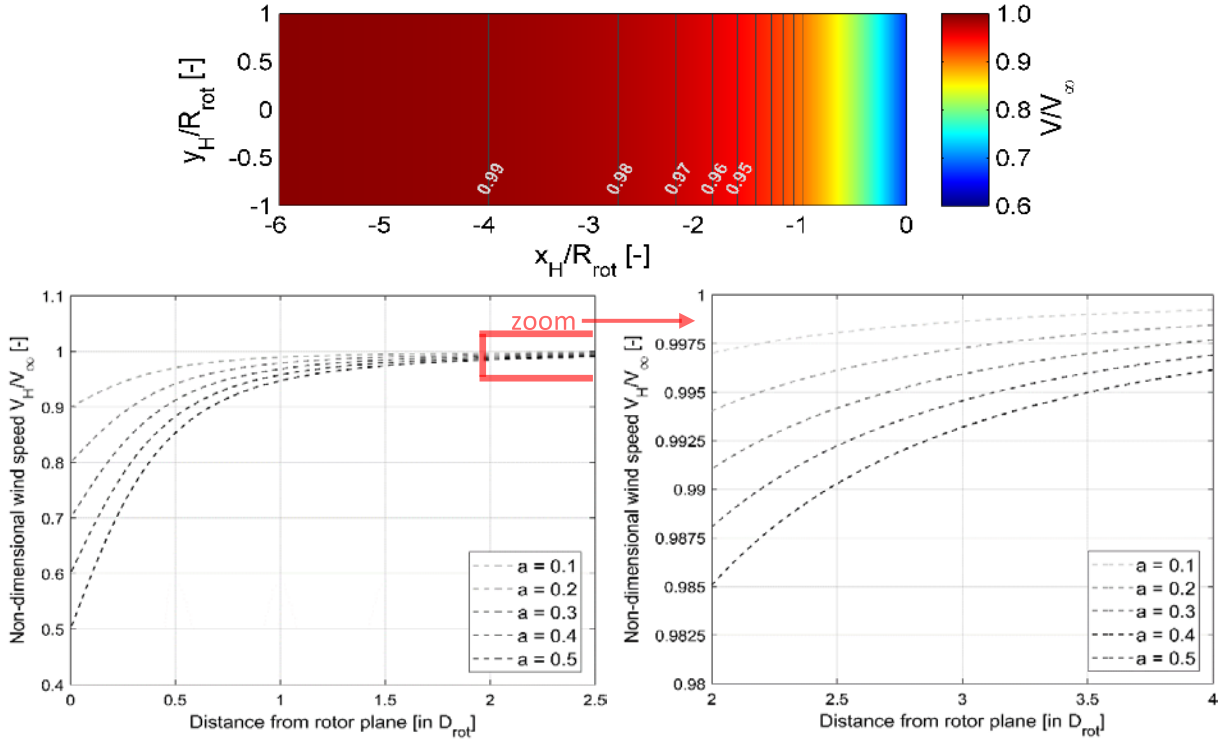

Figure 5. Wind speed evolution in the induction zone according to the one-dimensional induction model in the horizontal plane at hub height: with an induction factor a_{ind} = 0.334 (top); along the rotor centerline for various a_{ind} values (bottom).

3.4 Two-dimensional wind-induction model

In the actuator disk theory, the 1D-induction model is valid under the assumption of a constant uniformly loaded rotor. In reality, the thrust forces exerted by the turbine rotor on the wind are not evenly distributed due to the aerodynamic profiles of the blades.

The 2D-induction model presented in this section accounts for this radial dependency. The 2D model is semi-empirical since it was obtained by adapting the analytical 1D model (still valid along the rotor centerline) and fitting the radial variation of the induction to CFD simulations of five different modern rotors (study conducted by N. Troldborg and A.R. Meyer-Forsting, see [8] for more details).

The analytical expression of the 2D-induction model is given by:

$$u\left(\xi = \frac{x_{\mathcal{H}}}{R_{rot}}\right) = u_{\infty}\left(1 - a_{ind}\left[1 + \frac{\xi}{\sqrt{1+\xi^2}}\right] f(\varepsilon)\right).$$

The radial dependency is expressed through $f(\varepsilon)$, which is given by:

$$f(\varepsilon) = (\mathrm{sech}(\beta\varepsilon))^{a} = \left(\frac{2}{\exp(-\beta\varepsilon) + \exp(\beta\varepsilon)}\right)^{a}.$$

The parameters in the expression of $f(\varepsilon)$ are defined as:

- $\varepsilon = \frac{\rho}{\sqrt{\lambda(\eta+\xi^2)}}$ is a non-dimensional intermediate parameter that is both a function of the radial (ρ) and axial (ξ) non-dimensional coordinates.
- $\rho = \frac{r}{R_{rot}}$ is the non-dimensional radial coordinate in the hub system.
- $r = \sqrt{y_{\mathcal{H}}^2 + z_{\mathcal{H}}^2}$.
- a is a constant with the value 8/9.
- β is a constant with the value $\sqrt{2}$.
- λ is a constant with the value 0.587.
- η is a constant with the value 1.32.

The final expression for the model flow field wind speed thus becomes:

$$V(x_{\mathcal{H}}, z_{\mathcal{H}}) = V_{\infty}\left(\frac{z_{\mathcal{H}} + H_{hub}}{H_{hub}}\right)^{\alpha} = \left(\frac{z_{\mathcal{H}} + H_{hub}}{H_{hub}}\right)^{\alpha} \sqrt{u_{\infty}^2\left(1 - a_{ind}\left[1 + \frac{\xi}{\sqrt{1+\xi^2}}\right] f(\varepsilon)\right)^2 + v_{\infty}^2}.$$

Along the rotor axis ($\varepsilon = 0$), the expression matches the 1D model. The effect of the 2D induction on the wind field is visualized in Figure 6 and Figure 7.

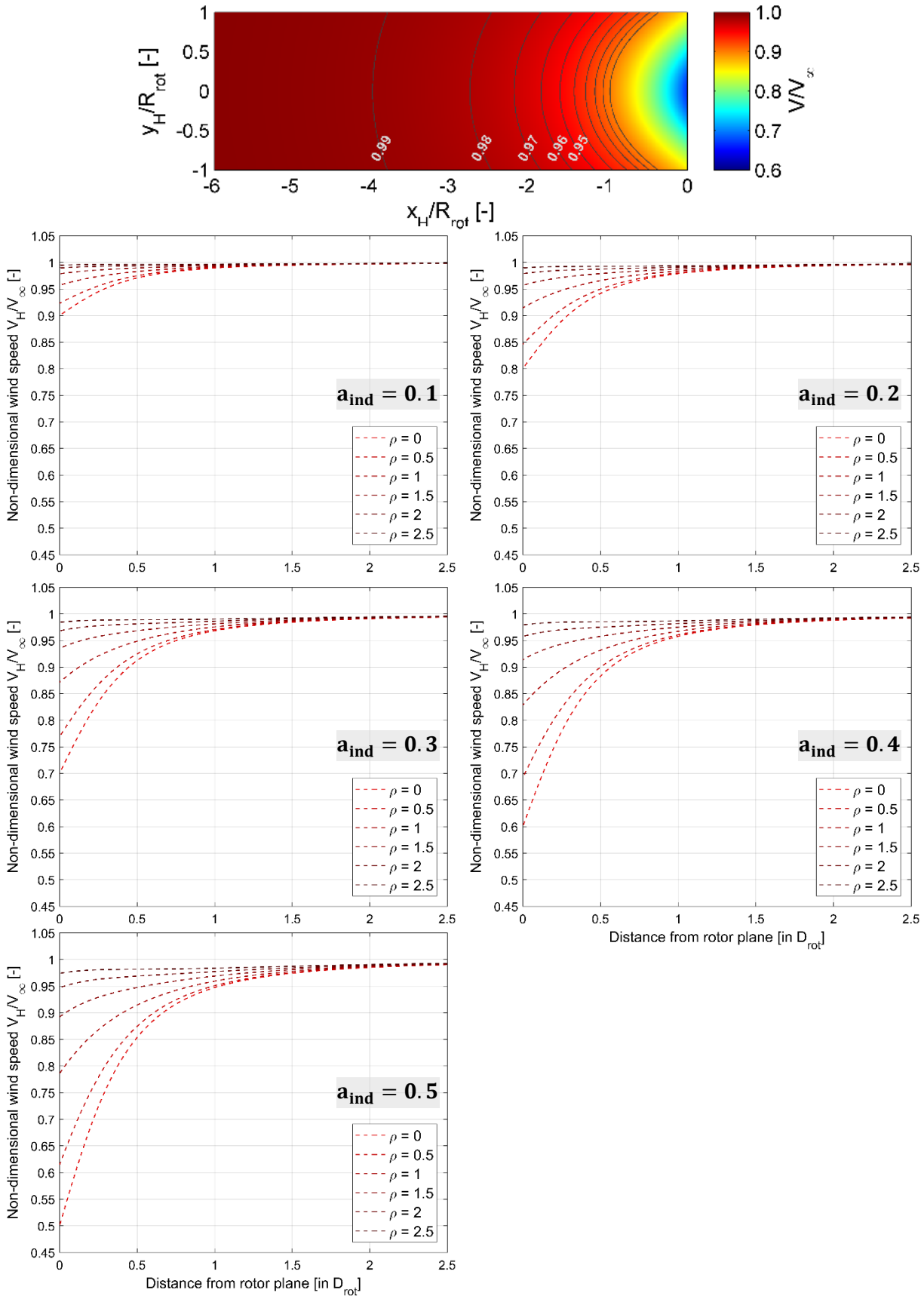

Figure 6. Axial evolution of wind speed in the induction zone according to the 2D-induction model: in the horizontal plane at hub height and an induction factor a_{ind} = 0.334 (top); at five radial positions, from 0 to 2.5 R_{rot} and for five different a_{ind} values (others).

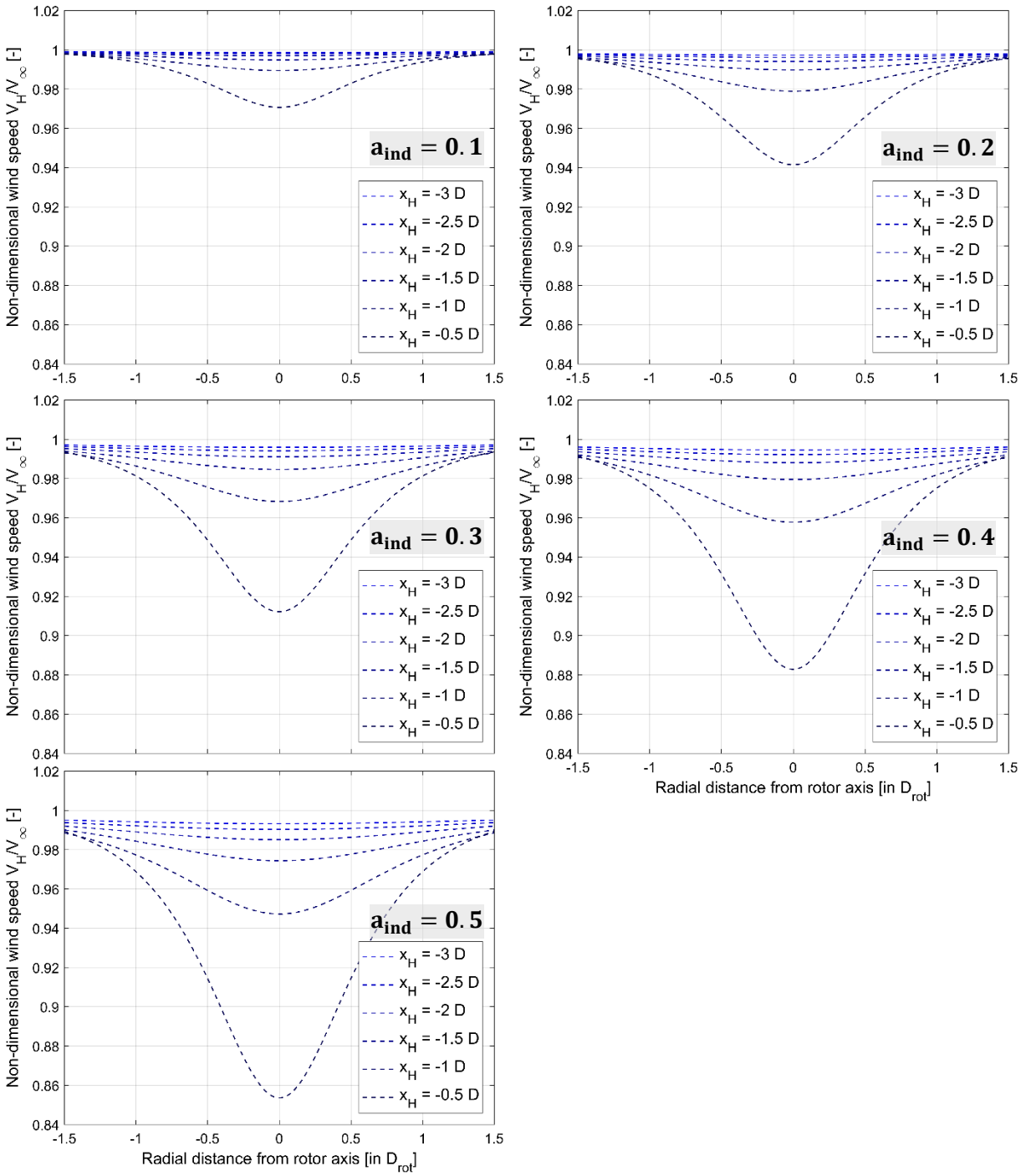

Figure 7. Radial evolution of wind speed in the induction zone according to the two-dimensional induction model: at five axial positions, from 0.5 to 3.0D_{rot} upstream and for five different a_{ind} values.

3.5 Model-fitting wind field reconstruction technique

In the model-fitting WFR technique, the lidar measurements (or CFD simulated lidar measurements) are used as inputs in an algorithm, which fits the lidar measurements to the chosen (1D or 2D) wind-induction model. In order to fit the lidar measurements to the flow model, the location of the lidar measurements must be known. The location of the lidar measurements are computed using knowledge of the laser beam trajectory (in the lidar coordinate system) and by accounting for the motion of the lidar (i.e. the tilting and rolling of the turbine itself). The tilting and rolling of the turbine is consequent to the forces exerted by the wind on the turbine structure (blades, nacelle, tower, etc).

In the model-fitting reconstruction technique, the optimization objective is to minimize the error between the lidar-measured $\mathbf{V_{los}}$ (vector of size equal to the number of measurement locations) and model-estimated $\widehat{\mathbf{V}}_{\mathrm{los}}$. This can be achieved by formulating a least squares problem, where the objective function f_{obj} is given by:

$$f_{\mathrm{obj}} = \mathrm{argmin}\left(\left\|\mathbf{V}_{\mathrm{los}} - \widehat{\mathbf{V}}_{\mathrm{los}}\right\|_2\right) = \mathrm{argmin}\left(\sqrt{\sum_{i=1}^{\mathrm{N_{los}}}(\mathrm{V_{los,i}} - \widehat{\mathrm{V}}_{\mathrm{los,i}})^2}\right),$$

where, $i = 1,2,\ldots,\mathrm{N_{los}}$ and $\mathrm{N_{los}} = \mathrm{N_{ranges}} * \mathrm{N_{beams}}$.

The model-based $\widehat{\mathbf{V}}_{\mathrm{los}}$ are simulated by projecting the modelled wind vector onto the LOS. As a result of the optimization, the solver outputs the wind field characteristics (e.g. wind speed, direction, shear parameter, induction factor, etc) that fit the lidar measurements best.

A by-product of the model-fitting reconstruction technique is the residual value for each measurement location, defined by:

$$\Delta \mathrm{V_{los,res,i}} = \mathrm{V_{los,i}} - \widehat{\mathrm{V}}_{\mathrm{los,i}}.$$

For each 10-minute period (or each simulation), a variety of residual statistics can be computed, such as mean bias, sum of squared errors (SSE), mean squared error (MSE), root mean squared error (RMSE) and normalized mean squared error (NMSE). In this sensitivity study, we only considered the RMSE of the LOS velocity in order to characterize the model adequacy (see definitions in [2]). The RMSE is given by:

$$\mathrm{RMSE} = \sqrt{\mathrm{MSE}} = \sqrt{\frac{1}{\mathrm{N_{los}}}\sum_{i=1}^{\mathrm{N_{los}}}\left(\mathrm{V_{los,i}} - \widehat{\mathrm{V}}_{\mathrm{los,i}}\right)^2}.$$

4 Description of sensitivity analysis

This chapter describes the methods employed in the sensitivity analysis. The objective of the sensitivity analysis is to determine the sensitivity of nacelle lidar-reconstructed (fitted) wind field characteristics to range configuration and wind-induction model. We therefore create a large number of range configurations in order to test the sensitivity to the minimum range, maximum range and number of ranges. The combinations of ranges are described in Section 4.1, while the grouping of the ranges is described in Section 4.2. The methods used to determine the sensitivity are described in Section 4.3.

4.1 Combination of ranges in the sensitivity analysis

The configured measurement distances for the 5B-Demo and ZDM are shown in Table 1. In total, it is possible to make range configurations using ten different ranges for the 5B-Demo and four different ranges for the ZDM – the 10m range is excluded as the combined wind-induction models are invalid for such short distance as the presence of the nacelle impacts the flow significantly. We decided to use all possible combinations using 2, 3 and 4 distances for the ZDM, and 3, 5 and 7 distances for the 5B-Demo.

The ZDM configurations used in the study are visualized in Figure 8. Each configuration is assigned a *point ID*, and the distances used for the specific point IDs are marked with circles. The figure differentiates between configurations using 2 (blue), 3 (green) and 4 (red) distances. In total, 11 different combinations are tested. In Figure 9, all possible configurations using 3 (blue), 5 (green) and 7 (red) distances are shown for the 5B-Demo lidar. In total, 492 different combinations are tested.

As explained in Section 2.1, the NKE data set was created specifically for the [49m, 72m, 95m, 109m and 188m] 5B-Demo range configuration. This means that some periods can be invalid for other range configurations. The number of valid 10-minute periods (N_{10min}) for each point ID is visualized in Figure 10. Here, it can be seen that the number of valid 10-minute periods varies from 2353 to 2815 depending on the range configuration.

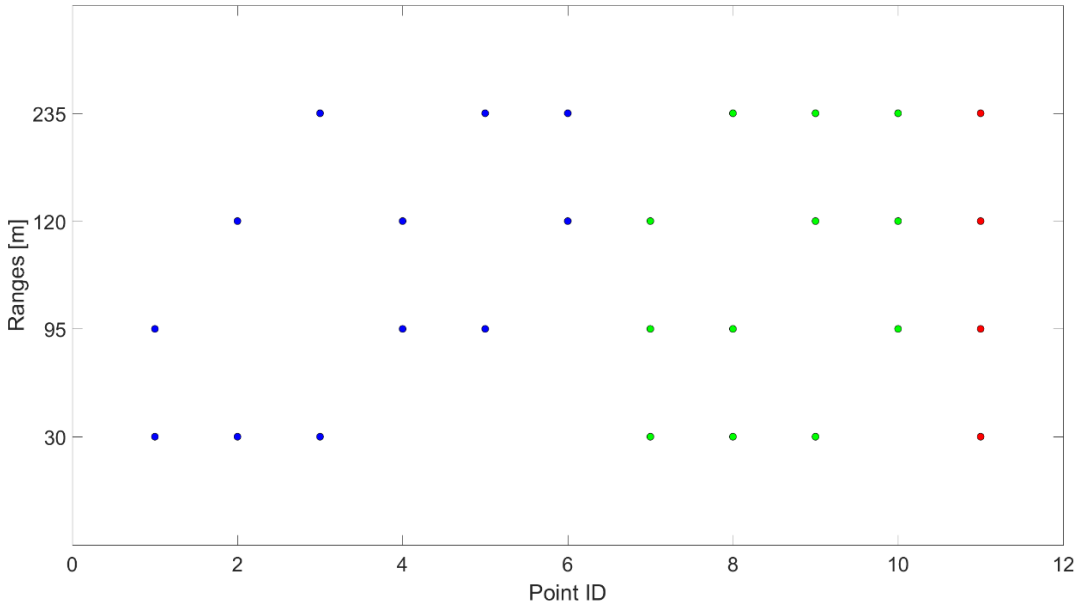

Figure 8. Range configurations of the ZDM using combinations of 2 (blue), 3 (green) and 4 (red) distances.

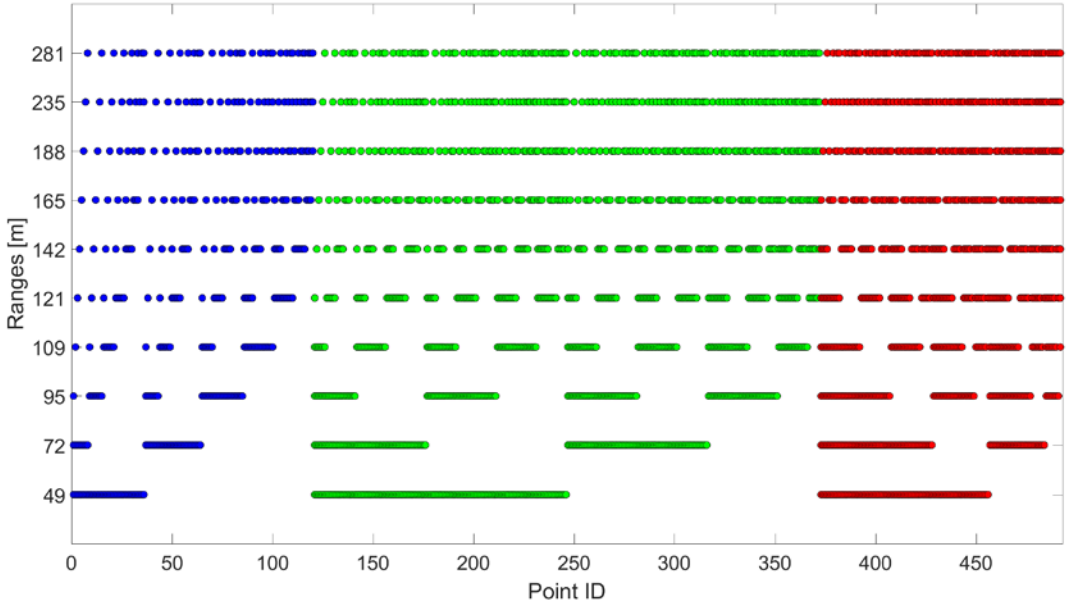

Figure 9. Range configurations of the 5B-Demo using combinations of 3 (blue), 5 (green) and 7 (red) distances.

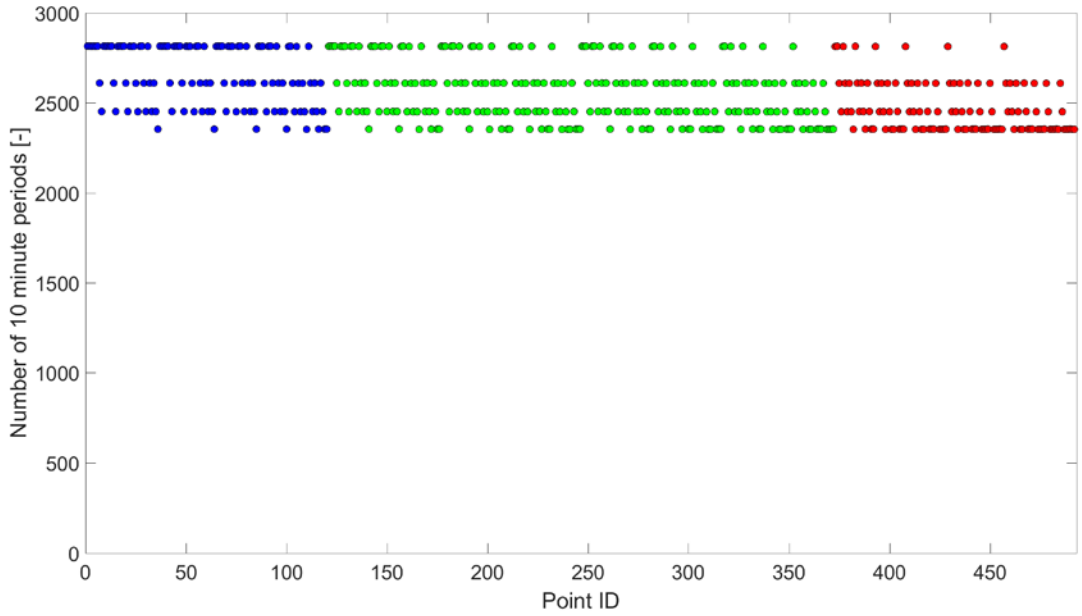

Figure 10. Number of valid 10-minute periods for each 5B-Demo range configuration (point ID).

4.2 Grouping range configurations

The sensitivity towards the range configurations is determined by calculating the average wind speed error and RMSE of configurations with similar characteristics. For example, when determining the sensitivity towards the minimum distance, an average wind speed error and RMSE is calculated for all configurations that contain the same minimum distance. The average wind speed error and RMSE obtained from configurations with different minimum distances can then be compared to determine the minimum distance that yields the most accurate reconstructions.

In this study, the range configurations are "grouped" according to minimum distance, maximum distance and number of ranges. It is not possible to group on the separation between ranges due to the fixed distances used in the NKE campaign. The number of range configurations (N_{conf}) included in each grouping is displayed in:

- Table 2 when grouping on the number of ranges.
- Table 3 and Table 4 when grouping on the minimum distance.
- Table 5 and Table 6 when grouping on the maximum distance.

4.3 Method used to determine the sensitivity

As described in Section 4.2, the wind speed error and RMSE are used to determine the sensitivity of the range configurations. In the NKE campaign, the wind speed error is computed as:

$$\Delta V_{hor} = V_{lidar} - V_{cup}.$$

Here, V_{cup} is the cup-measured horizontal wind speed and V_{lidar} is the lidar-reconstructed horizontal wind speed. Both refer to the horizontal wind speed $2.5D_{rot}$ upstream of the wind turbine at 80m above ground level (a.g.l.). In the CFD simulations, the wind speed error is computed as:

$$\Delta V_{\infty} = V_{\infty\ lidar} - V_{\infty\ CFD}.$$

Here, $V_{\infty\ CFD}$ is the free stream wind speed of the CFD simulations while $V_{\infty\ lidar}$ is the lidar-reconstructed free stream wind speed. In both approaches, the RMSE is calculated as:

$$RMSE = \sqrt{\frac{1}{N_{los}} \sum_{i=1}^{N_{los}} \left(V_{los,i} - \widehat{V}_{los,i}\right)^2}.$$

A wind speed error and RMSE is calculated for each point ID and 10-minute period (or CFD simulation). The wind speed errors and RMSEs are then grouped in $1ms^{-1}$ wide wind speed bins (cup-measured/CFD input) and 1° wide yaw misalignment bins (spinner-measured/CFD input) – unless otherwise stated. In each bin, the average wind speed error and RMSE is calculated for each group displayed in Table 2 to Table 6. In the NKE campaign, results are only displayed for bins containing at least $4*N_{conf}$ time periods. The reconstructions are based on both the 1D- and 2D-induction models to test the sensitivity towards the wind-induction model.

Table 2. Number of configurations when grouping on number of ranges (5B-Demo and ZDM).

	5B-Demo			ZDM		
Number of ranges	3	5	7	2	3	4
Number of configurations	120	252	120	6	4	1

Table 3. Number of configurations when grouping on minimum distance (5B-Demo).

Minimum distance [m]	49	72	95	109	121	142	165	188	235	281
All	246	126	63	31	15	7	3	1	0	0
3 ranges	36	28	21	15	10	6	3	1	0	0
5 ranges	126	70	35	15	5	1	0	0	0	0
7 ranges	84	28	7	1	0	0	0	0	0	0

Table 4. Number of configurations when grouping on minimum distance (ZDM).

Minimum distance [m]	30	95	120	235
All	7	3	1	0
2 ranges	3	2	1	0
3 ranges	3	1	0	0
4 ranges	1	0	0	0

Table 5. Number of configurations when grouping on maximum distance (5B-Demo).

Maximum distance [m]	49	72	95	109	121	142	165	188	235	281
All	0	0	1	3	7	15	31	63	126	246
3 ranges	0	0	1	3	6	10	15	21	28	36
5 ranges	0	0	0	0	1	5	15	35	70	126
7 ranges	0	0	0	0	0	0	1	7	28	84

Table 6. Number of configurations when grouping on maximum distance (ZDM).

Maximum distance [m]	30	95	120	235
All	0	1	3	7
2 ranges	0	1	2	3
3 ranges	0	0	1	3
4 ranges	0	0	0	1

5 Nørrekær Enge - sensitivity analysis results

This chapter contains the results of the sensitivity analysis when using the NKE data. It is structured such that it first presents the sensitivity to the induction model and lidar. With these results in mind, the sensitivity towards the minimum distance, maximum distance and number of ranges is investigated.

5.1 Induction model

To examine the influence of the induction model on the reconstructed wind speed, both the 1D- and 2D-induction models are used to reconstruct the horizontal wind speed for all 2815 time periods. For each model and time period, the difference between the lidar-reconstructed and cup-measured horizontal wind speed is calculated.

To ensure that the results are independent of range configuration and lidar type, the analysis is conducted using a similar configuration ([95m, 120/121m, 235m]) for both lidars, as well as by averaging over all range configurations. This means that the number of wind speed error values analysed is:

- N_{10min} when using the [95m, 120/121m, 235m] range configuration.
- $N_{10min}*N_{conf}$ when using all range configurations.

In both of the above cases, the mean error ΔV_{hor} (lidar-cup) is obtained by averaging the wind speed errors in $1ms^{-1}$ wide wind speed bins (cup-measured) and 2° wide yaw misalignment bins (spinner-measured). The result is displayed in Figure 11, where the circles and squares correspond to results obtained when using the 1D- and 2D-induction models, respectively. Results obtained for the 5B-Demo and ZDM are shown in the left and right column, respectively. The top row shows the result from the [95m, 120/121m, 235m] range configuration while the bottom row shows the average result of all configurations.

Observations:

From Figure 11, it can be seen that the 1D- and 2D-induction models allow to reconstruct nearly identical wind speeds regardless of the range configuration, wind speed and yaw misalignment. A similar figure including error bars (one standard deviation) is displayed in Figure A.1 (Annex A). The dispersion of errors is shown to be similar in magnitude for both induction models and both lidars.

The difference between the 1D- and 2D-induction models is also examined in terms of fitting residual statistics of RMSE in Figure A.2 (Annex A). No significant difference can be observed, neither in terms of magnitude of the mean RMSE nor in terms of its spread.

Conclusion:

The sensitivity of the reconstructed wind speed to the induction model is proved to be negligible. In the remainder of the chapter, the analysis will therefore only be based on the 1D-induction model. The results obtained from the 1D-induction model are assumed to also apply for the 2D-induction model.

A plausible argument for the similar behaviour of the 1D- and 2D-induction models is that the radial component in the 2D-induction model is small (see Section 3.4), with differences of less than 1% in the wind speed deficits for measurements taken within the rotor area (+/- $0.5D_{rot}$), as seen in Figure 7.

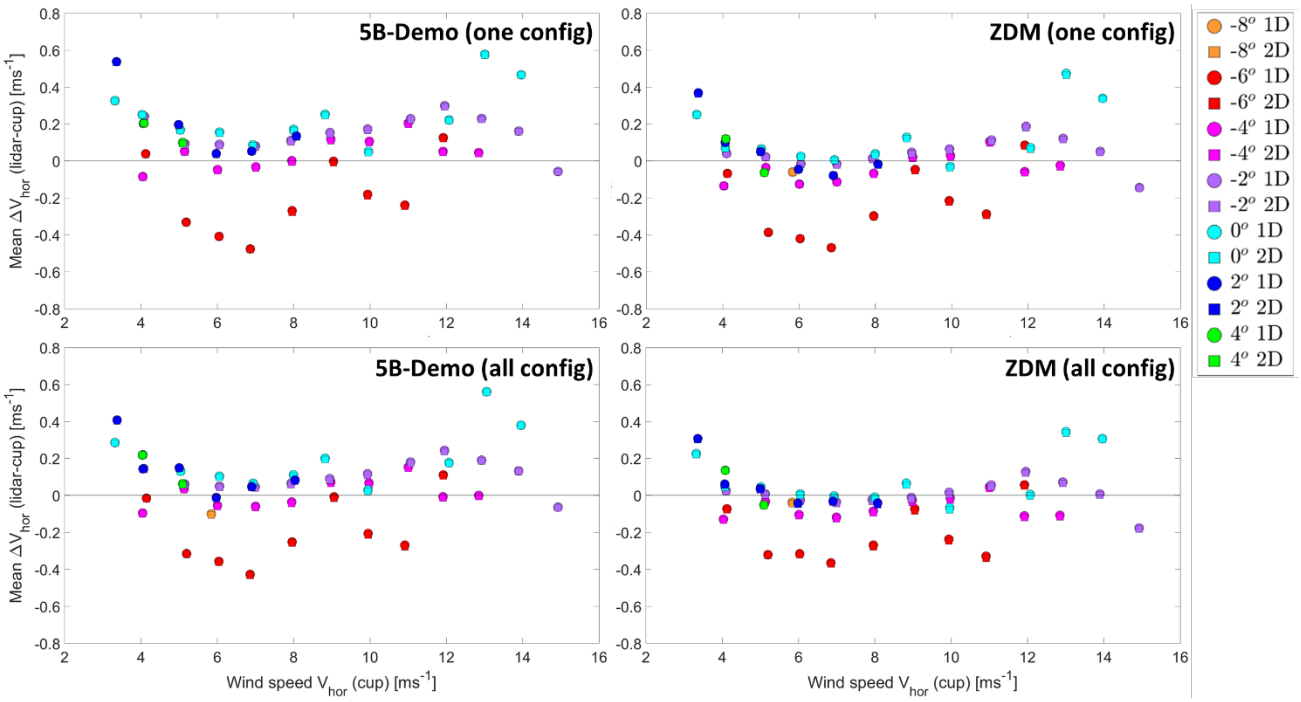

Figure 11. Influence of the induction model on the mean wind speed error when basing the reconstructions on the 5B-Demo (left column) and ZDM (right column) when using the [95m, 120/121m, 235m] range configuration (top row) and all available configurations (bottom row).

5.2 Lidar

In this section, the influence of the choice of lidar on the reconstructed wind speed is examined. The sensitivity to the lidar type is analysed in the same way as the sensitivity to the induction model was examined in Section 5.1. The only differences are that the analysis solely is based on the 1D-induction model and that the results obtained for the 5B-Demo and ZDM are plotted together. The wind speed error results are shown in Figure 12, where circles represent the 5B-Demo and squares the ZDM.

Observations:

From Figure 12, it can be seen that there is an almost constant offset between the two lidars. On average, the 5B-Demo estimates horizontal wind speeds that are 0.097±0.042ms^{-1} and 0.074±0.089ms^{-1} higher than the ZDM when using the [95m, 120/121m, 235m] configuration and all configurations, respectively. The trend is not seen at yaw misalignments of -6° and lower. It is not possible to determine if yaw misalignments of 6° and higher also differ from the trend due to the low number of measurements with yaw misalignments above 5° (see Figure 4).

The maximum ΔV_{hor} difference between the two lidars is:

- 0.201ms^{-1} for the [95m, 120/121m, 235m] configuration. This corresponds to the wind speed bin of 4ms^{-1} and yaw misalignment bin of -2°.
- 0.295ms^{-1} when using all configurations. This corresponds to the wind speed bin of 8ms^{-1} and yaw misalignment bin of +4°.

Figure A.3 (Annex B) shows the same results with error bars. In addition, Figure A.4 (Annex B) shows the comparison of RMSE residuals between both lidars for the [95m, 120/121m, 235m] configuration. For most wind speed and yaw misalignment bins, the mean RMSE is lower for the 5B-Demo than the ZDM.

Conclusion:

Although Figure 12 shows that, for the NKE campaign, the choice of lidar has a clear impact on the reconstructed wind speeds, the differences lay within the uncertainties of the reconstructed wind speed errors, as shown by Figure A.3 in Annex B.

The mean wind speed error (lidar-cup) is on average (± one standard deviation):

- 0.093±0.206ms^{-1} for the 5B-Demo when using the [95m, 121m, 235m] configuration.
- -0.005±0.177ms^{-1} for the ZDM when using the [95m, 120m, 235m] configuration.
- 0.027±0.240ms^{-1} for the 5B-Demo when using all configurations.
- -0.048±0.183ms^{-1} for the ZDM when using all configurations.

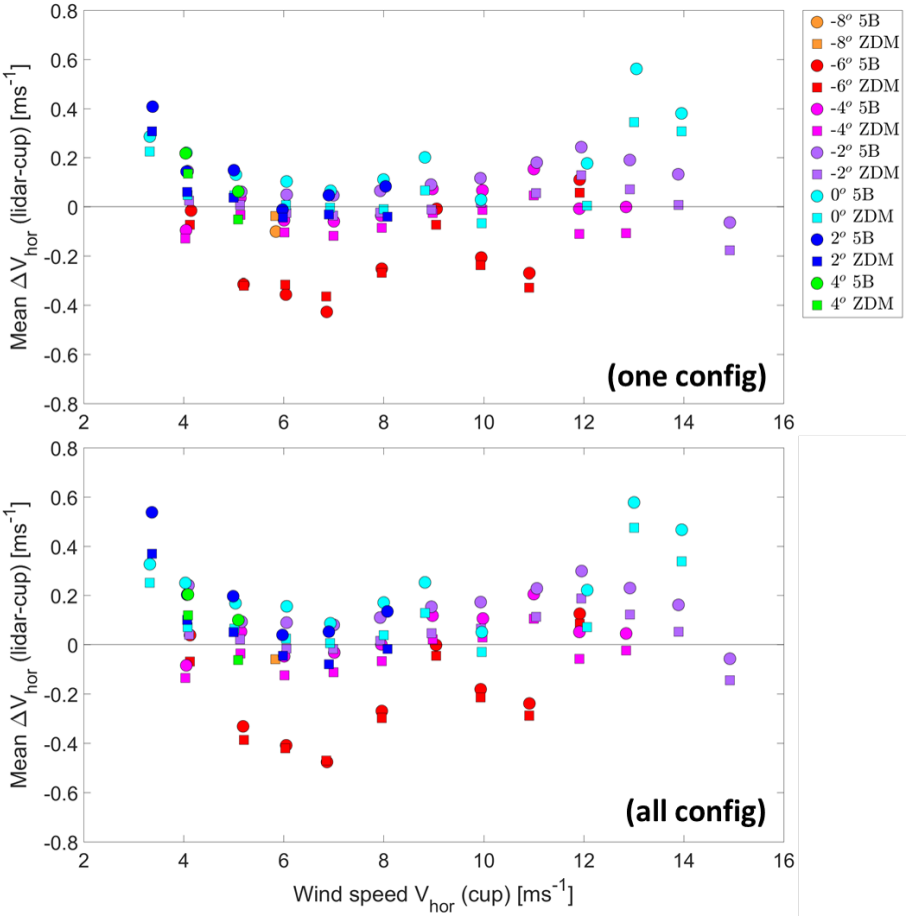

Figure 12. Influence of the lidar type on the mean wind speed bias when basing the reconstructions on the [95m, 120/121m, 235m] range configuration (top) and all available configurations (bottom).

5.3 Minimum distance

In this section, the sensitivity to the smallest configured distance is examined. The number of configurations containing the same minimum distance can be viewed in Table 3 and Table 4 for the 5B-Demo and ZDM, respectively. In both cases, we have not differentiated between configurations containing different number of ranges. Instead, all configurations containing the same minimum distance are considered. In addition, all reconstructions are based on the 1D-induction model.

The mean wind speed errors are shown as a function of cup-measured horizontal wind speed in Figure 13. The same figures are shown with error bars in Annex C, where Figure A.5 shows the result for the 5B-Demo while Figure A.9 shows the result for the ZDM. These figures also show the result for different number of ranges. The dependency on the number of ranges will first be discussed in Section 5.5.

The mean RMSEs are shown as a function of cup-measured horizontal wind speed in Figure 14. The same figures are shown with error bars in Annex C, where Figure A.6 shows the result for the 5B-Demo while Figure A.10 shows the result for the ZDM. These figures also show the result for different number of ranges. Again, these will first be considered in Section 5.5. In addition, Annex C also contains figures where the mean wind speed error and mean RMSEs are plotted as a function of spinner-measured yaw misalignment.

General observations:

The wind speed errors and RMSEs shown in Figure 13 and Figure 14 are on the order of 0.1ms^{-1}. Both figures demonstrate that the magnitude of the errors depend on the smallest configured range, where the errors generally become smaller with a decreasing minimum distance. Still, there are some exceptions to the overall trend. The figures are therefore described in greater detail beneath.

Observations in Figure 13 - left:

Figure 13 (left) reveals that the lowest wind speed errors generally are obtained when using 49m (blue) as the minimum distance. However, there are some exceptions. For wind speeds of 4ms^{-1} and 5ms^{-1}, the 72m range (green) results in the lowest wind speed errors. This is not completely unexpected, as the 72m range constitutes the second smallest distance. The result obtained at 7ms^{-1} is less expected. Here, the trend is completely reverse and the 188m range (orange) results in the smallest wind speed error. Furthermore, this result is not very significant as the wind speed errors obtained from the different configurations are very similar. Finally, at 15ms^{-1} the 109m range (pink) results in the smallest wind speed error. This could be an artifact of the limited number of measurements included in the comparison at 15ms^{-1}, as seen from Figure 3.

Observations in Figure 13 - right:

The wind speed errors resulting from the ZDM are also dependent on the minimum distance. Even though there is a clear “ordering” in the figure, the interpretation of the result is more ambiguous than for the 5B-Demo. It is difficult to determine an optimal minimum distance from the figure as all configurations result in the smallest wind speed error for various wind speeds:

- The 30m range results in the lowest wind speed error for 3, 4, 6, 11, 12, 13 and 14ms^{-1}.
- The 95m range results in the lowest wind speed error for 9 and 10ms^{-1}.
- The 120m range results in the lowest wind speed error for 5, 7, 8 and 15ms^{-1}.

Observations in Figure 14 - left:

Figure 14 (left) demonstrates that the RMSE is highly dependent on the minimum distance in the range configuration. When only considering the largest ranges (121m (turquoise), 142m (yellow), 165m (purple) and 188m (orange)), it is evident that the RMSE increases when the minimum distance is increased. Furthermore, this trend is not clear when considering the smallest ranges (49m (blue), 72m (green) and 95m (red)). In fact, the difference between these are very small and they result in the lowest RMSE for different wind speeds:

- The 49m range results in the lowest RMSE for 6, 7 and 8ms^{-1}.
- The 72m range results in the lowest RMSE for 4, 5, 9 and 10ms^{-1}.
- The 95m range results in the lowest RMSE for 3, 11, 12, 13, 14 and 15ms^{-1}.

It is therefore clear that the lowest RMSEs are obtained when using a small minimum distance. Furthermore, it is more difficult to determine the optimal minimum distance.

Observations in Figure 14 - right:

When observing the RMSEs for the ZDM, it is once again clear that the shortest ranges result in the lowest RMSEs. The 30m range (blue) results in the lowest RMSEs for all wind speeds except for wind speeds of 13ms^{-1} and 14ms^{-1}. At 13ms^{-1} and 14ms^{-1}, the 95m range (green) results in the lowest RMSE.

Observations in Annex C:

The wind speed error is shown as a function of yaw misalignment in Figure A.7 and Figure A.11 for the 5B-Demo and ZDM, respectively. The RMSEs are shown as a function of yaw misalignment for the 5B-Demo and ZDM in Figure A.8 and Figure A.12, respectively. Only the figures denoted 'All' are considered. The same trends that were observed in Figure 13 and Figure 14 are also observed in the figures in Annex C; the wind speed errors and RMSEs are (generally) reduced when basing the configurations on a small minimum distance. In addition, it can be seen that the error bars (one standard deviation) are similar for all configurations in the wind speed error plots. Furthermore, the size of the error bars increases with an increasing minimum distance in the RMSE plots.

Conclusions:

Figure 13 and Figure 14 demonstrate that the lowest wind speed errors and RMSEs (generally) are obtained when using range configurations where the minimum distance is located close to the wind turbine. It is therefore recommended to configure the lidar such that the minimum distance is located close to the turbine. However, the minimum distance should not be smaller than 0.3-0.5D_{rot} as the wind-induction model becomes invalid for such short distances (see [8]). Based on these results, we therefore recommend to use a minimum distance close to 0.5D_{rot}. In the NKE campaign, this corresponds to a minimum distance of 47m.

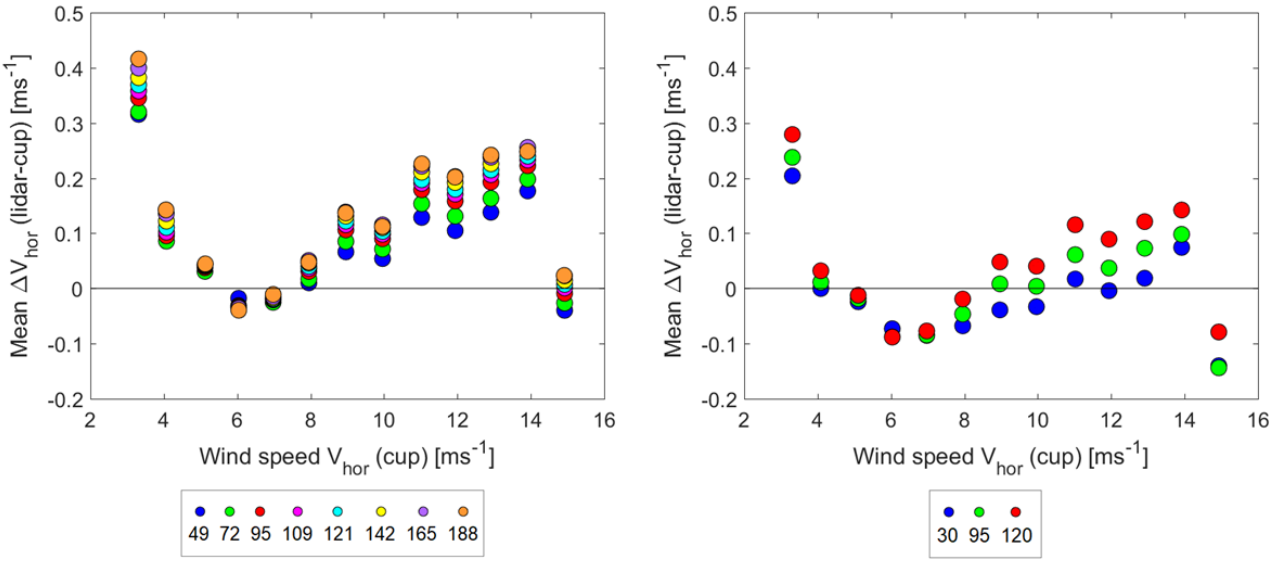

Figure 13. Mean wind speed error between the lidar reconstructed and cup measured horizontal wind speed for the 5B-Demo (left) and ZDM (right). Both reconstructions are obtained using the 1D-induction model. An average difference is calculated for configurations containing the same minimum distance (represented by the different colors). The mean differences are binned in intervals of 1ms^{-1} according to the horizontal wind speed measured by the met mast.

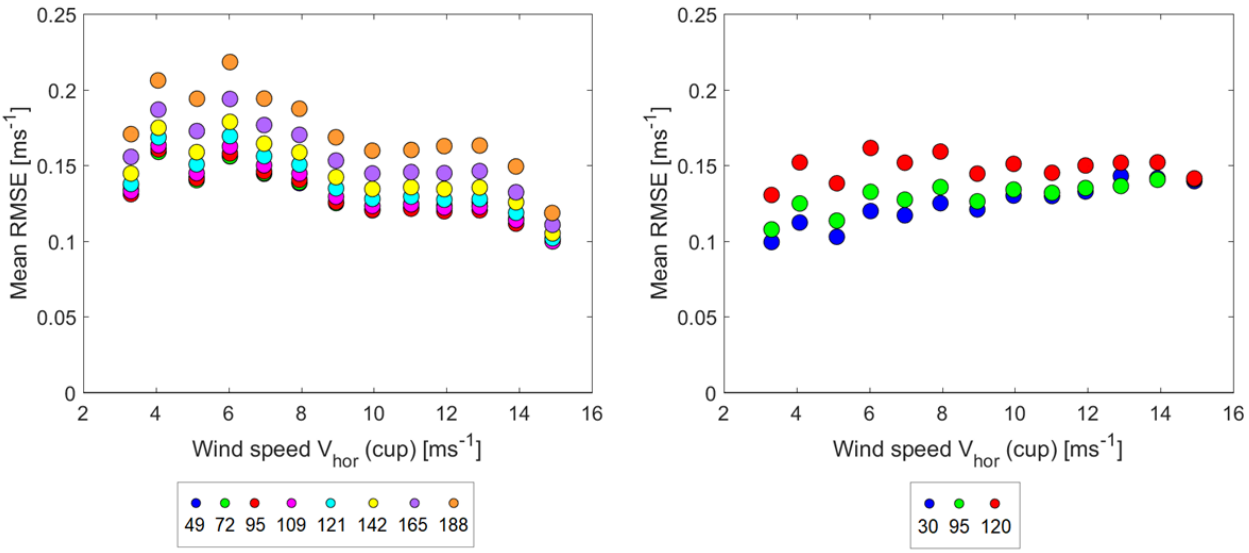

Figure 14. Mean RMSE between the modelled and lidar-measured V_{los} for the 5B-Demo (left) and ZDM (right). Both reconstructions are obtained using the 1D-induction model. An average RMSE is calculated for all configurations containing the same minimum distance (represented by the different colors). The mean differences are binned in intervals of 1ms^{-1} according to the horizontal wind speed measured by the met mast.

5.4 Maximum distance

In this section, the sensitivity to the largest configured distance is examined. The number of configurations containing the same maximum distance can be viewed in Table 5 and Table 6 for the 5B-Demo and ZDM, respectively. As in Section 5.3, we have not differentiated between configurations containing different number of ranges. Instead, all configurations containing the same maximum distance are considered. In addition, all reconstructions are based on the 1D-induction model.

The mean wind speed errors are shown as a function of cup-measured horizontal wind speed in Figure 15. The same figures are shown with error bars in Annex D, where Figure A.13 shows the result for the 5B-Demo while Figure A.17 show the result for the ZDM. These figures also show the result for different number of ranges. The dependency on the number of ranges will first be discussed in Section 5.5.

The mean RMSEs are shown as a function of cup-measured horizontal wind speed in Figure 16. The same figures are shown with error bars in Annex D, where Figure A.14 show the result for the 5B-Demo while Figure A.18 show the result for the ZDM. These figures also show the result for different number of ranges. Again, these will first be considered in Section 5.5. In addition, Annex D also contains figures where the mean wind speed error and mean RMSEs are plotted as a function of spinner-measured yaw misalignment.

General observations:

The wind speed errors and RMSEs shown in Figure 15 and Figure 16 are on the order of 0.1ms^{-1}. Both figures demonstrate that the magnitude of the errors depend on the largest configured range, where the errors generally become smaller with a decreasing maximum distance. In Figure 16, it can be seen that the RMSEs are ordered according to the maximum distance, where the smallest maximum distance results in the lowest RMSE. This is found for both the 5B-Demo and the ZDM, and for all horizontal wind speeds. The trend seen in Figure 15 is not as clear, especially for low wind speeds. This figure is therefore described in greater detail.

Observations in Figure 15 – left:

For wind speeds between 3ms^{-1} and 8ms^{-1}, the ordering of the configurations is rather random. It is therefore very difficult to determine an optimal maximum distance from these results. For wind speeds above 8ms^{-1}, the results are again ordered according to the maximum distance. Furthermore, the maximum distance that results in the lowest wind speed error varies between the wind speeds:

- The 95m range results in the lowest wind speed error for 11, 13 and 14 ms^{-1}.
- The 109m range results in the lowest wind speed error for 12ms^{-1}.
- The 121m range results in the lowest wind speed error for 9 and 10ms^{-1}.
- The 281m range results in the lowest wind speed error for 15ms^{-1}.

The three smallest maximum distances are hereby shown to generally result in the smallest wind speed errors. The result obtained for 15ms^{-1} is not believed to be significant due to the limited number of measurements included in the comparison, as seen from Figure 3.

Observations in Figure 15 – right:

The wind speed errors resulting from the ZDM are also found to be dependent on the maximum distance. Just like in the case of the 5B-Demo, it is difficult to determine an optimal maximum distance from the figure as all configurations result in the smallest wind speed error for various wind speeds:

- The 95m range results in the lowest wind speed error for 3 and 6 ms^{-1}.
- The 120m range results in the lowest wind speed error for 4, 11, 12, 13 and 14ms^{-1}.
- The 235m range results in the lowest wind speed error for 5, 7, 8, 9, 10 and 15ms^{-1}.

Observations in Annex D:

The wind speed errors are shown as a function of yaw misalignment in Figure A.15 and Figure A.19 for the 5B-Demo and ZDM, respectively. The RMSEs are shown as a function of yaw misalignment for the 5B-Demo and ZDM in Figure A.16 and Figure A.20, respectively. Only the figures denoted 'All' are considered. The same trends that were observed in Figure 15 and Figure 16 are also observed in the figures in Annex D; the lowest RMSEs are found for configurations containing the smallest maximum distance, while the wind speed error results are more ambiguous. In addition, it can be seen that the error bars (one standard deviation) are similar for all configurations in the wind speed error plots. Furthermore, the size of the error bars increases with an increasing maximum distance in the RMSE plots.

Conclusions:

Figure 15 and Figure 16 demonstrate that the lowest wind speed errors and RMSEs (generally) are obtained when using range configurations where the maximum distance is located close to the wind turbine. Based on these results, it is therefore recommended to configure the lidar such that the maximum distance is located approximately 1.0-1.5D_{rot} from the wind turbine. In the NKE campaign, this corresponds to a maximum distance of 90m-140m.

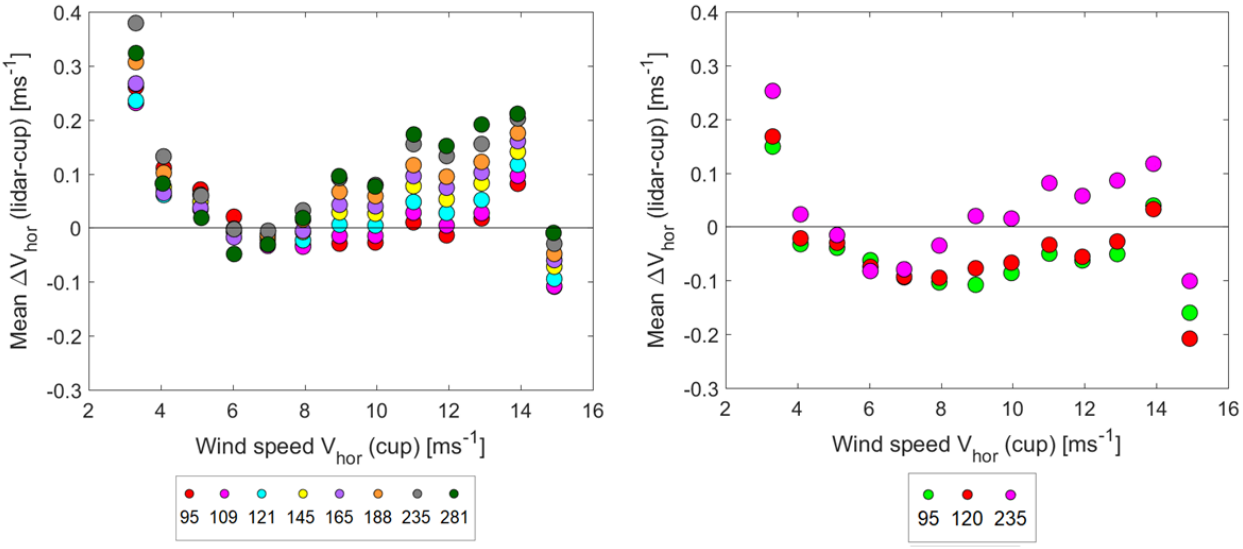

Figure 15. Mean wind speed error between the lidar reconstructed and cup measured horizontal wind speed for the 5B-Demo (left) and ZDM (right). Both reconstructions are obtained using the 1D-induction model. An average difference is calculated for configurations containing the same maximum distance (represented by the different colors). The mean differences are binned in intervals of 1ms^{-1} according to the horizontal wind speed measured by the met mast.

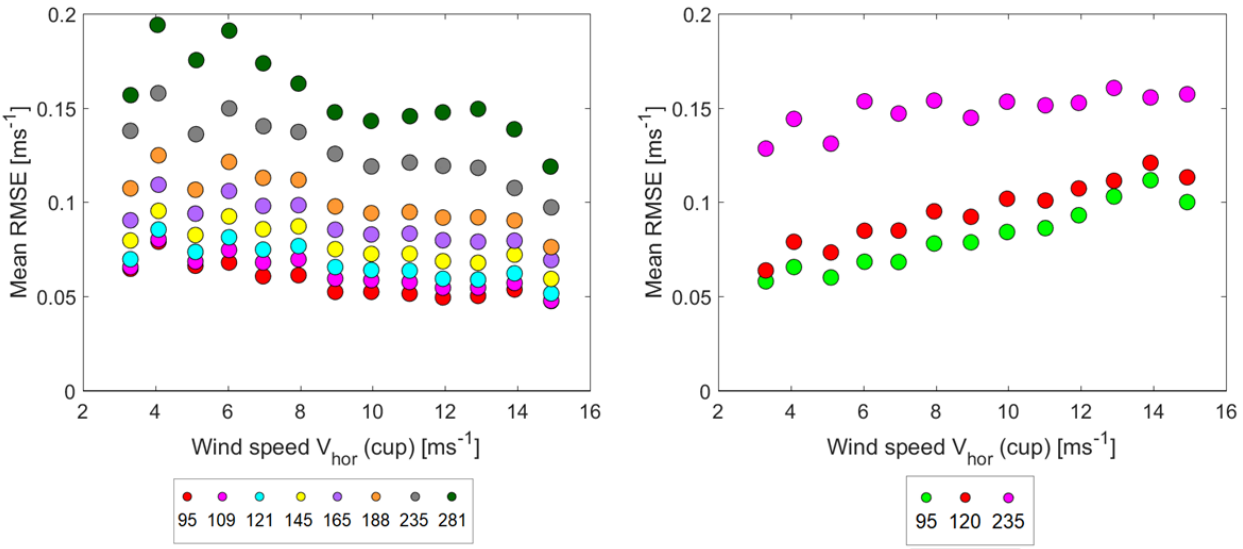

Figure 16. Mean RMSE between the modelled and lidar-measured V_{los} for the 5B-Demo (left) and ZDM (right). Both reconstructions are obtained using the 1D-induction model. An average RMSE is calculated for all configurations containing the same maximum distance (represented by the different colors). The mean differences are binned in intervals of 1ms^{-1} according to the horizontal wind speed measured by the met mast.

5.5 Number of ranges

The sensitivity to the number of ranges can be determined from any figure in Annex C and Annex D. The figures in Annex C show the sensitivity to the minimum distance when considering all configurations, as well as configurations based on specific number of ranges. The number of configurations considered in each figure is shown in Table 3 and Table 4 for the 5B-Demo and ZDM, respectively.

Similarly, the figures in Annex D show the sensitivity to the maximum distance when considering all configurations, as well as configurations based on specific number of ranges. The number of configurations considered in each figure can be deduced from Table 5 and Table 6 for the 5B-Demo and ZDM, respectively.

The results shown for all configurations in Annex C and Annex D have already been described in Section 5.3 and Section 5.4, respectively. The focus of this section is to examine if the results presented in Section 5.3 and Section 5.4 change when basing the analysis on specific number of ranges.

Observations:

In general, there seems to be very small differences in the wind speed errors when basing the analysis on different number of ranges. The positions of the colored dots seem to be nearly identical in figures based on different number of ranges. This can for example be seen when comparing the different rows in Figure A.5 and Figure A.13. Furthermore, the RMSEs shown in Annex C seem to increase slightly when basing the analysis on a greater number of ranges. This can for example be seen when comparing the different rows in Figure A.6 and Figure A.10. This trend is not seen in Annex D.

Conclusions:

When a configuration includes the same minimum range (Annex C) or maximum range (Annex D), the influence of the number of ranges on the wind speed error and RMSE is limited. As the results are nearly independent of the number of configured ranges, it is recommended to use a limited number of ranges in the range configurations. Based on this study, 3-5 ranges is considered appropriate.

6 CFD-based sensitivity analysis results

This chapter contains the results of the sensitivity analysis when using the CFD simulated data. It is structured such that it first presents the sensitivity to the induction model and the lidar. With these results in mind, the sensitivity towards the minimum distance, maximum distance and number of ranges is investigated.

6.1 Induction model

The influence of the induction model is examined by reconstructing the free stream wind speed using both the 1D- and 2D-induction model for all 48 CFD simulations. For each model and CFD simulation, the difference between the lidar-reconstructed and CFD-based free stream wind speed is calculated.

Similarly to the case of the NKE campaign, the analysis is made for both lidars using a similar configuration ([95m, 120/121m, 235m]), as well as by averaging over all range configurations. This ensures that the result is independent of range configuration and lidar type. The number of wind speed errors to analyse is:

- N_{CFD} when using the [95m, 120/121m, 235m] range configuration.
- $N_{CFD}*N_{conf}$ when using all range configurations.

In both of the above mentioned cases, the mean free stream wind speed error ΔV_∞ (lidar-CFD) is calculated for each CFD simulation (wind speed and yaw misalignment condition). The result is displayed in Figure 17, where circle and square markers correspond to results obtained using the 1D- and 2D-induction models, respectively. Results obtained from the 5B-Demo are shown in the left column while results obtained from the ZDM are shown in the right column. The top row shows the result from the [95m, 120/121m, 235m] range configuration while the bottom row shows the average result of all configurations.

Observations:

From Figure 17, it can be seen that the 1D- and 2D-induction models allow to reconstruct nearly identical wind speeds regardless of the range configuration, wind speed and yaw misalignment. A similar figure including error bars (one standard deviation) is displayed in Figure A.21 (Annex E). The difference between the 1D- and 2D-induction models is also examined in terms of fitting residual statistics of RMSE in Figure A.22 (Annex E). No significant difference can be observed, neither in terms of magnitude of the mean RMSE nor in terms of its spread.

For both induction models, it can be observed that the wind speed biases are the largest at wind speeds where the thrust exerted by the wind on the turbine is maximal, i.e. approximately 8-10ms^{-1}. At these speeds, the RMSE values are also maximal. For both lidars, the wind speed biases are slightly larger using the 2D-induction model instead of using the 1D-induction model.

The wind speed biases and RMSEs are on the order of 0.01ms^{-1}. These values are an order of magnitude smaller than the results presented for the NKE campaign (see Chapter 5).

Conclusion:

The sensitivity of the reconstructed wind speed to the induction model is proved to be negligible. In the remainder of the chapter, the analysis will therefore only be based on the 1D-induction model. The results obtained from the 1D-induction model are assumed to also apply for the 2D-induction model.

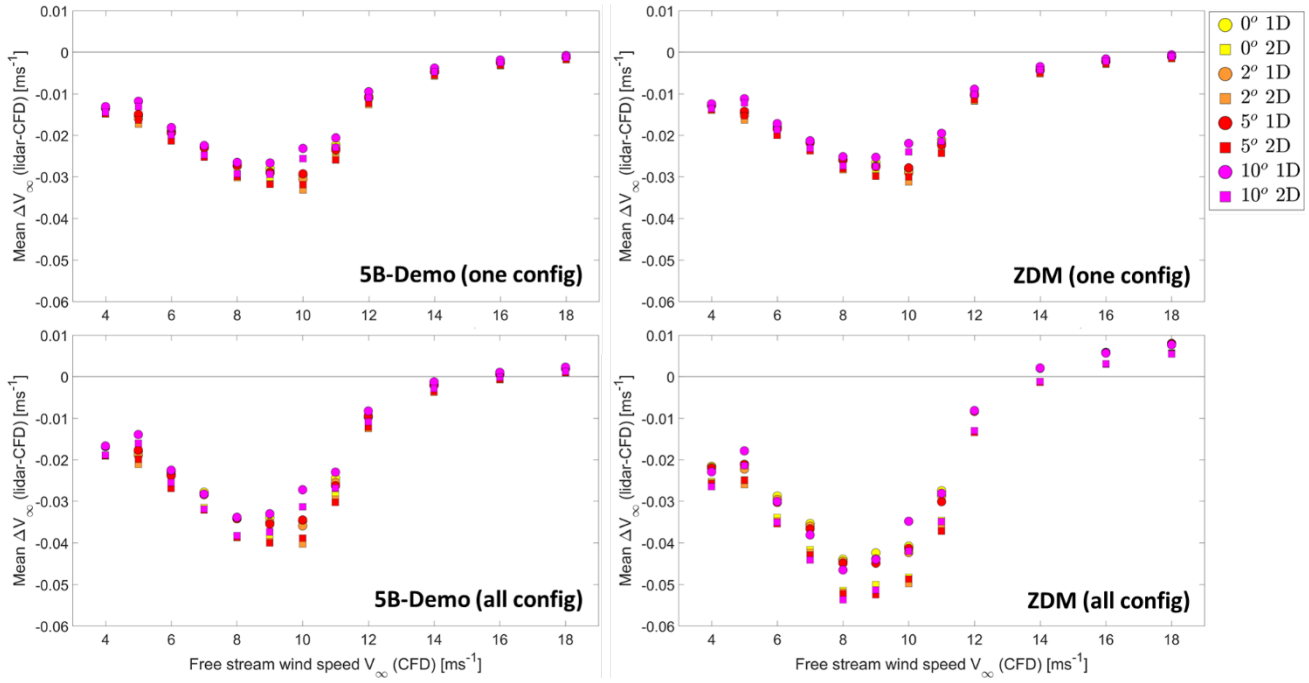

Figure 17. Influence of the induction model on the mean free stream wind speed bias when basing the reconstructions on the 5B-Demo (left column) or ZDM (right column) and using the [95m, 120/121m, 235m] range configuration (top row) or all available configurations (bottom row).

6.2 Lidar

In this section, the influence of the lidar trajectories on the reconstructed wind speed is examined (the only difference between the simulated 5B-Demo data and simulated ZDM data is the lidar trajectories). The sensitivity to the lidar trajectories is analysed in the same way as the sensitivity to the induction model was examined in Section 6.1. Here however the analysis is solely based on the 1D-induction model and the results obtained from the 5B-Demo (five LOS used) and ZDM (six LOS used) are plotted together. The wind speed error results are shown in Figure 18, where circles represent the 5B-Demo and squares the ZDM.

Observations:

The “one config” plot in Figure 18 shows that the results are almost identical for the ZDM and 5B-Demo when using a similar range configuration. With this range configuration, the central beam of the 5B-Demo has a negligible influence on the reconstructed free stream wind speed. The same figure is shown with error bars in Figure A.23 (Annex F).

The wind speed biases are slightly larger for the ZDM than for the 5B-Demo in the “all config” case. This is believed to be caused by the greater number of configurations over which the results are averaged for the 5B-Demo than for the ZDM.

In Figure A.24 (Annex F), the RMSE results are shown. The RMSE values are slightly larger for the 5B-Demo than for the ZDM. This is likely explained by the fact that the 1D-induction model was used and that the corner beams of the 5B-Demo are at different radial positions than the central beam, whereas all beams are located at similar radial positions in the ZDM.

Conclusion:

The sensitivity of the reconstructed wind speed to the studied lidar trajectories (5B-Demo and ZDM) is negligible.

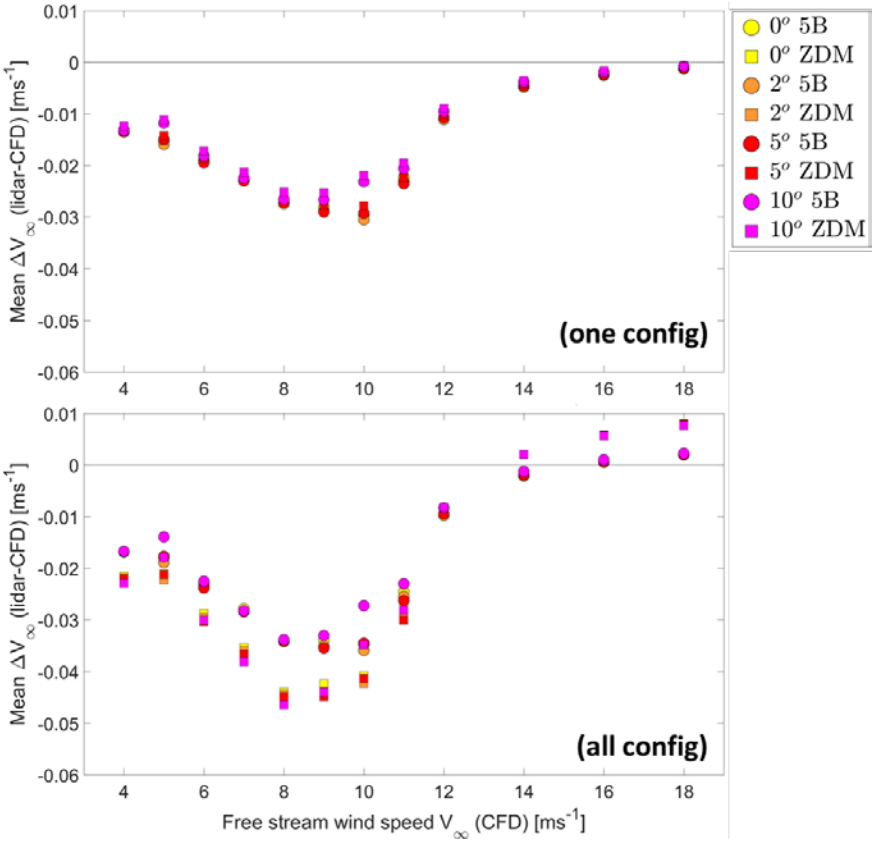

Figure 18. Influence of the lidar trajectory on the mean free stream wind speed bias when the reconstructions use the [95m, 120/121m, 235m] range configuration (top row) and all available configurations (bottom row).

6.3 Minimum distance

This section examines the sensitivity of the lidar-reconstructed free stream wind speed to the minimum distance in the configured ranges. Results are shown without differentiating between range configurations containing different number of ranges (“all” configurations in Table 3 and Table 4).

The mean wind speed errors are shown as a function of free stream wind speed (CFD input) in Figure 19. The same figures are shown with error bars in Annex G, where Figure A.25 shows the result for the 5B-Demo while Figure A.29 shows the result for the ZDM.

The mean RMSEs are shown as a function of free stream wind speed (CFD input) in Figure 20. The same figures are shown with error bars in Annex G, where Figure A.26 shows the result for the 5B-Demo while Figure A.30 shows the result for the ZDM. In addition, Annex G also contains figures where the mean wind speed error and mean RMSEs are plotted as a function of yaw misalignment (CFD input).

Observations:

The free stream wind speed errors shown in Figure 19 are found to decrease with increasing minimum distance. The magnitude of the errors is similar for both lidars when using the same minimum range (e.g. 95m). The RMSEs shown in Figure 20 are also found to decrease with increasing minimum range.

In Annex G (from Figure A.25 to Figure A.32), the investigations are conducted both as a function of free stream wind speed and as a function of yaw misalignment. As previously observed, the free stream wind speed biases and RMSE values are the highest close to the maximum thrust wind speeds. There is no sensitivity of the results to the yaw misalignment (see e.g. Figure A.27).

Conclusion:

Based on the CFD simulations, the smallest wind speed errors and RMSEs are found when using range configurations with large minimum distances. The larger the minimum distance is, the better the results become. Although this may be counter-intuitive – and is contradictory to the UniTTe approach – this is physically consistent; as the CFD does not include wind field evolution, the observed errors essentially represent the inadequacy of the simple induction model, which nominally decreases as we move further upstream. When lidar measurements are simulated at distances further away from the rotor, the wind flow can more and more correctly be assumed to be representative of the “free stream”.

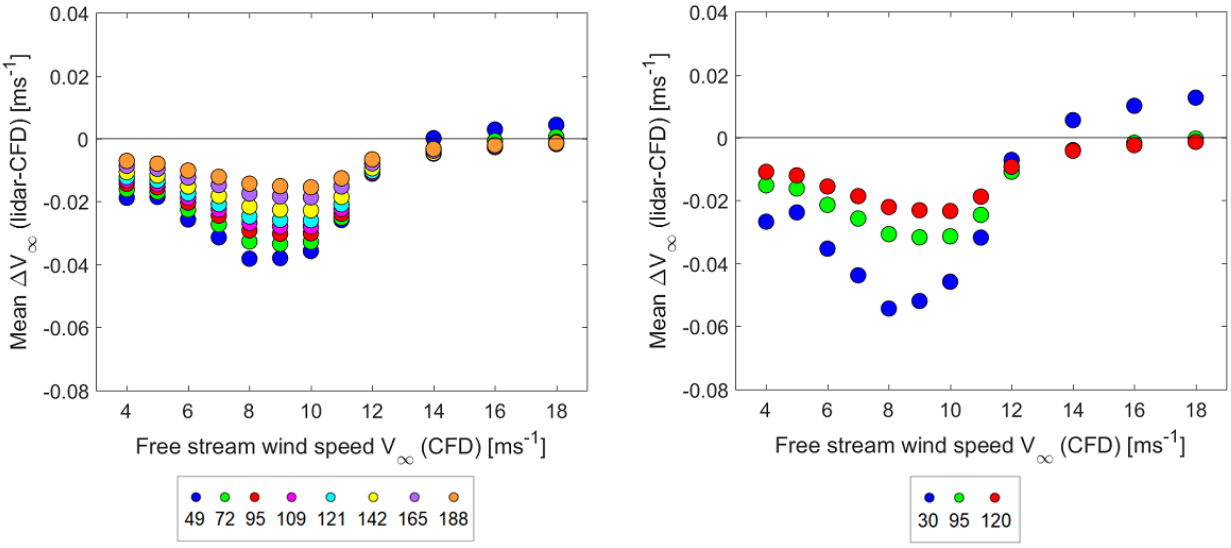

Figure 19. Mean wind speed error between the lidar reconstructed V_∞ and the V_∞ used in the CFD simulations for the 5B-Demo (left) and ZDM (right). Both reconstructions are obtained using the 1D-induction model. An average difference is calculated for configurations containing the same minimum distance (represented by the different colors). The mean differences are binned in intervals of $1ms^{-1}$ according to the free stream wind speed in the CFD simulations.

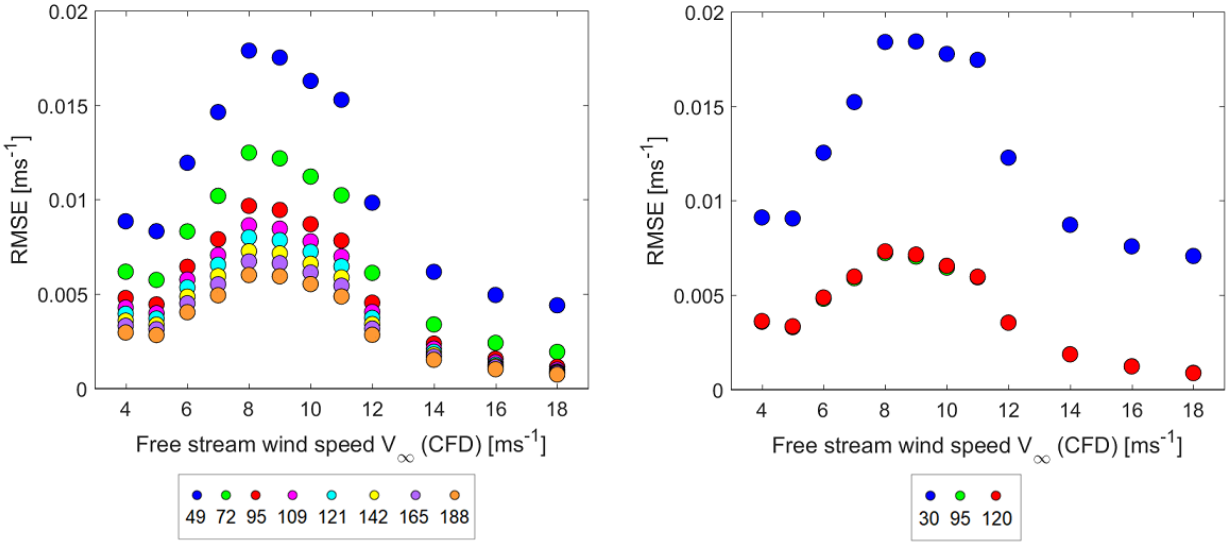

Figure 20. Mean RMSE between the modelled and lidar-simulated V_{los} for the 5B-Demo (left) and ZDM (right). Both reconstructions are obtained using the 1D-induction model. An average RMSE is calculated for all configurations containing the same minimum distance (represented by the different colors). The mean differences are binned in intervals of $1ms^{-1}$ according to the free stream wind speed in the CFD simulations.

6.4 Maximum distance

This section examines the sensitivity of the lidar-reconstructed free stream wind speed to the maximum distance in the configured ranges. Results are shown without differentiating between range configurations containing different number of ranges ("all" configurations in Table 5 and Table 6).

The mean wind speed errors are shown as a function of free stream wind speed (CFD input) in Figure 21. The same figures are shown with error bars in Annex H, where Figure A.33 shows the result for the 5B-Demo while Figure A.37 shows the result for the ZDM.

The mean RMSEs are shown as a function of free stream wind speed (CFD input) in Figure 22. The same figures are shown with error bars in Annex H, where Figure A.34 shows the result for the 5B-Demo while Figure A.38 shows the result for the ZDM. In addition, Annex H also contains figures where the mean wind speed error and mean RMSEs are plotted as a function of yaw misalignment (CFD input).

Observations:

The free stream wind speed errors shown in Figure 21 become smaller when the maximum distance becomes greater. The trend shown by the RMSEs (Figure 22) is more ambiguous. The ranges that yield the smallest RMSEs when using the 5B-Demo are:

- The 121m at 4, 7, 8, 16 and 18ms^{-1}.
- The 145m at 5, 6, 9, 10, 11, 12 and 14ms^{-1}.

For the ZDM, the 120m range results in the lowest RMSE for all wind speeds. Moving either closer or further from the turbine results in greater RMSEs.

In Annex H (from Figure A.33 to Figure A.40), the results are displayed both as a function of free stream wind speed and yaw misalignment. Similar observations are made as in Section 6.3: there is no sensitivity of the results to the yaw misalignment (see e.g. Figure A.39).

Conclusion:

The smallest wind speed errors are found when using range configurations with large maximum distances. The explanation for this phenomena is completely identical to the explanation made in Section 6.3 (minimum distance). Furthermore, the CFD results also demonstrate that a maximum distance of approximately 1.25-2D_{rot} results in the lowest RMSEs. In this study, 1.25-2D_{rot} corresponds to approximately 116-188m.

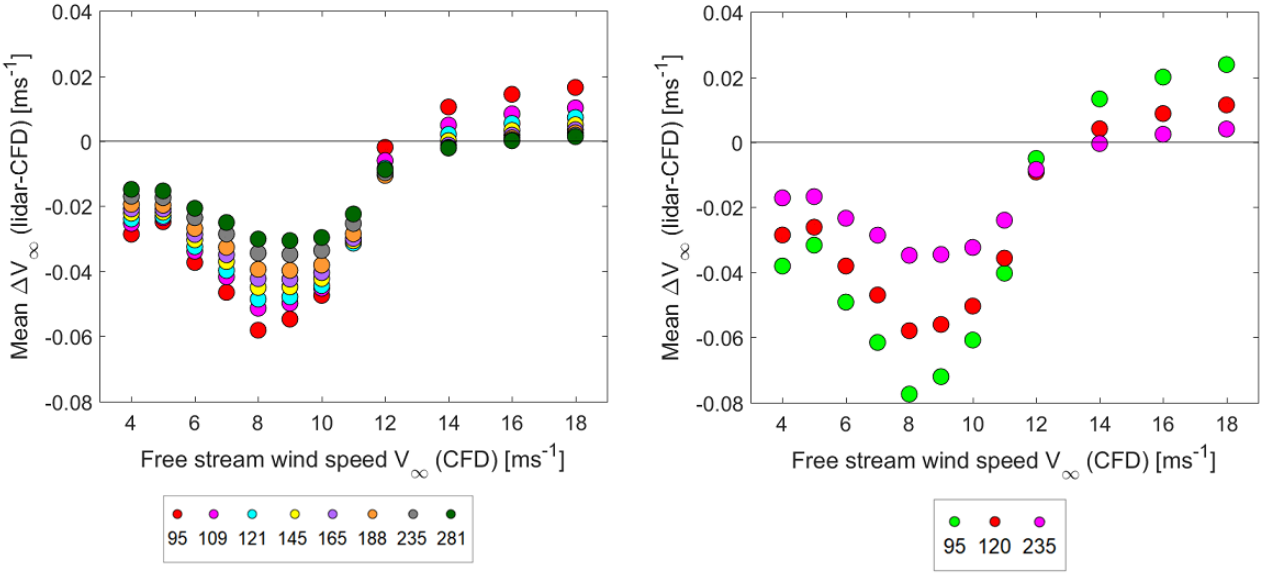

Figure 21. Mean wind speed error between the lidar reconstructed V_∞ and the V_∞ used in the CFD simulations for the 5B-Demo (left) and ZDM (right). Both reconstructions are obtained using the 1D-induction model. An average difference is calculated for configurations containing the same maximum distance (represented by the different colors). The mean differences are binned in intervals of $1ms^{-1}$ according to the free stream wind speed in the CFD simulations.

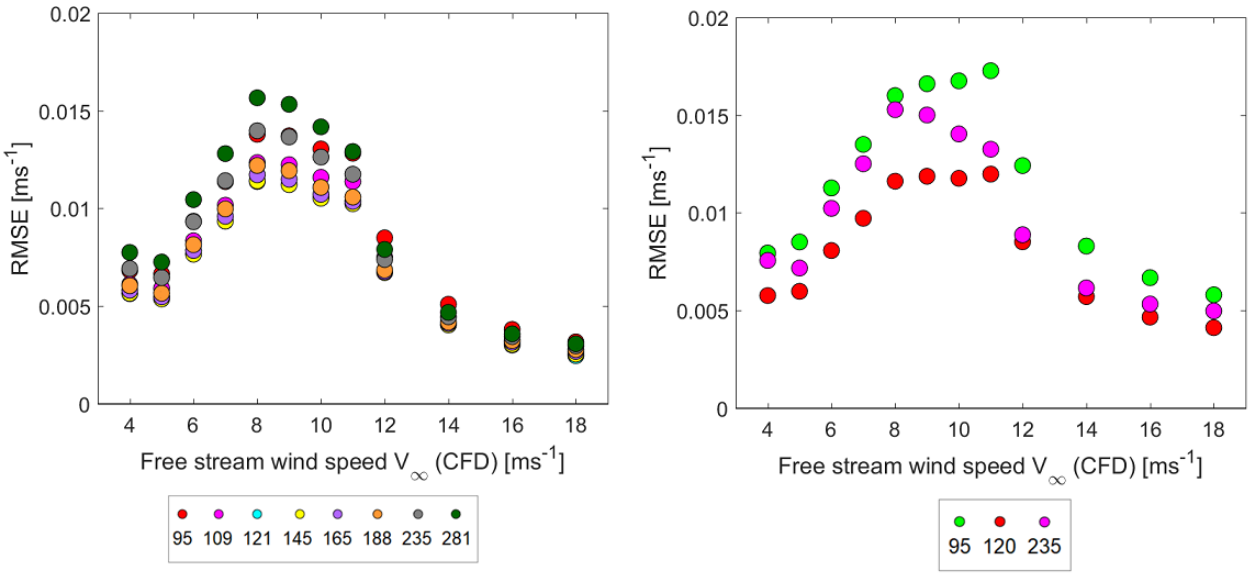

Figure 22. Mean RMSE between the modelled and lidar-simulated V_{los} for the 5B-Demo (left) and ZDM (right). Both reconstructions are obtained using the 1D-induction model. An average RMSE is calculated for all configurations containing the same maximum distance (represented by the different colors). The mean differences are binned in intervals of $1ms^{-1}$ according to the free stream wind speed in the CFD simulations.

6.5 Number of ranges

In this section, we investigate the sensitivity of the lidar-reconstructed free stream wind speed to the number of lidar measurement ranges used as inputs to the wind field reconstruction.

The mean wind speed errors are shown as a function of free stream wind speed (CFD input) in Figure 23. The same figures are shown with error bars in Annex I, where Figure A.41 shows the result for the 5B-Demo while Figure A.43 shows the result for the ZDM.

The mean RMSEs are shown as a function of free stream wind speed (CFD input) in Figure 24. The same figures are shown with error bars in Annex I, where Figure A.41 shows the result for the 5B-Demo while Figure A.43 shows the result for the ZDM. In addition, Annex I also contains figures where the mean wind speed error and mean RMSEs are plotted as a function of yaw misalignment (CFD input).

Observations:

The free stream wind speed errors shown in Figure 23 are nearly identical when basing the reconstructions on different number of ranges. In the case of the ZDM, the differences between the 2-range cases and 4-range case are due to the limited number of configurations included in the analysis (see Table 2). Consequently, the 4-range case includes measurement ranges close to the rotor that were shown to impact the fitting negatively (see Sections 6.3 and 6.4).

In terms of RMSE residuals (Figure 24), it can be observed that the RMSE increases with the number of ranges, which may be imputed to the higher difficulty of fitting many ranges than a few.

In Annex I, the results are displayed both as a function of free stream wind speed and yaw misalignment. The influence on the number of ranges is also negligible when grouping data by yaw misalignment instead of wind speeds.

Conclusion:

Based on the CFD simulations, the free stream wind speed error is shown to be independent of the number of ranges, while the RMSE statistics increase.

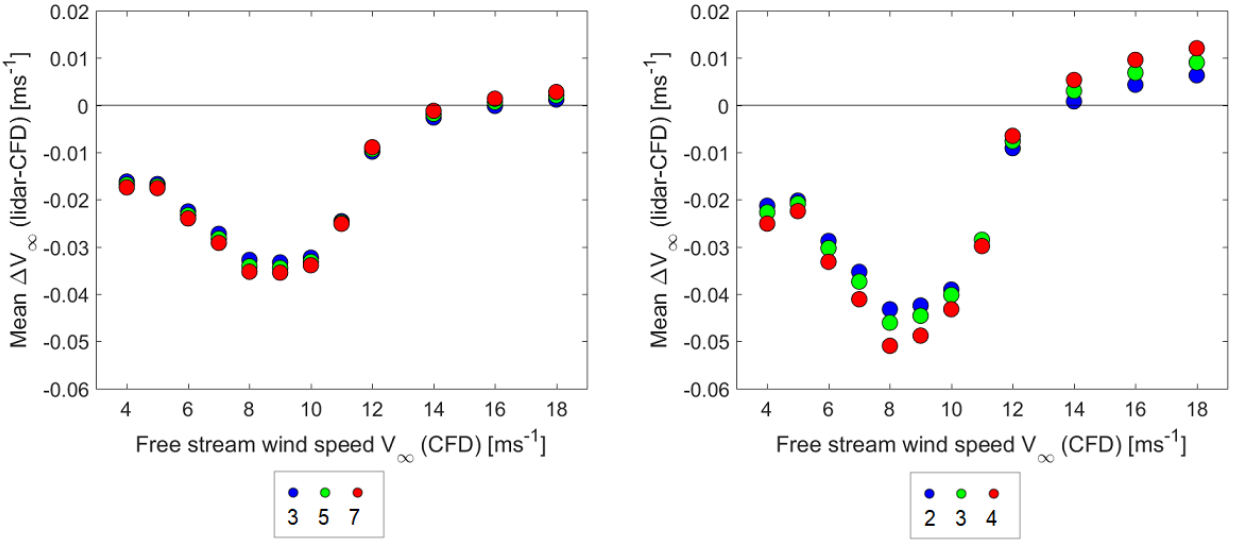

Figure 23. Mean wind speed error between the lidar reconstructed V_∞ and the V_∞ used in the CFD simulations for the 5B-Demo (left) and ZDM (right). Both reconstructions are obtained using the 1D-induction model. An average difference is calculated for configurations containing the same number of ranges (represented by the different colors). The mean differences are binned in intervals of $1ms^{-1}$ according to the free stream wind speed in the CFD simulations.

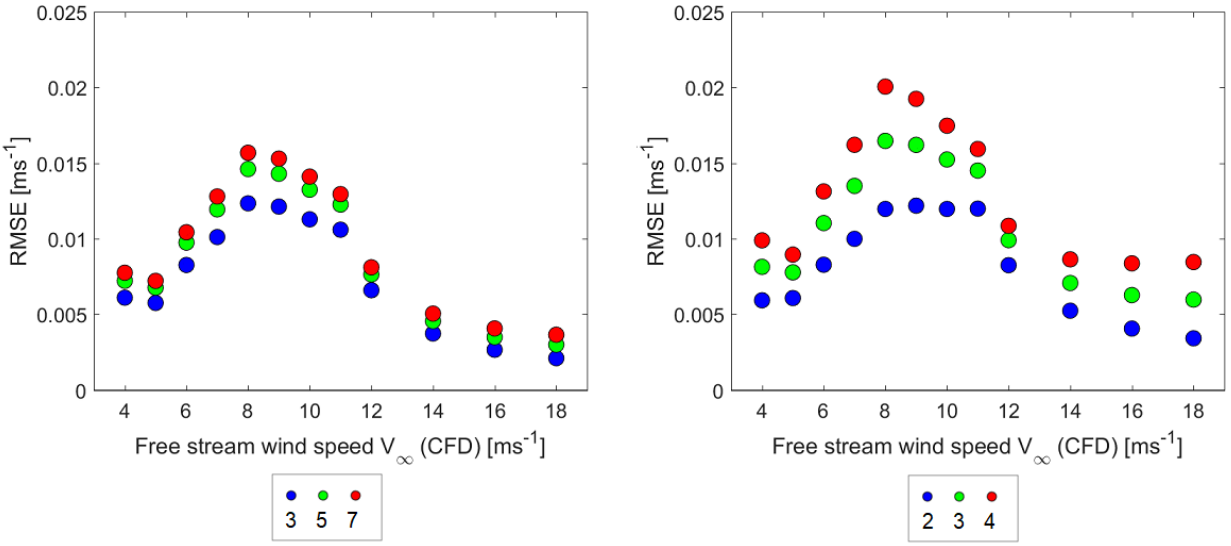

Figure 24. Mean RMSE between the modelled and lidar-simulated V_{los} for the 5B-Demo (left) and ZDM (right). Both reconstructions are obtained using the 1D-induction model. An average RMSE is calculated for all configurations containing the same number of ranges (represented by the different colors). The mean differences are binned in intervals of $1ms^{-1}$ according to the free stream wind speed in the CFD simulations.

7 Discussion

7.1 Adequacy of the simple induction model for the NKE turbine

Originally, it was planned to only use CFD simulations and corresponding lidar-simulated data for the sensitivity analysis. However, it has been demonstrated that the wind speed errors and RMSEs are an order of magnitude (factor of 10) smaller for the CFD simulations than for the experimental data of the NKE campaign. The focus of the sensitivity analysis has therefore been moved to the NKE data set. Due to the fixed range configurations used in the NKE campaign, it was not possible to examine the sensitivity of the reconstructed wind speeds to the separation between the ranges.

As described in Chapter 4 of [2], the errors in lidar-reconstructed wind field characteristics (estimated using the model-fitting reconstruction technique) can be split into two sources:

1) **The uncertainty due to the model inadequacy**. The inadequacy is mainly related to the (in)correctness of the assumptions inherent to the wind model, and eventually related to potential inaccuracies of the implementation.
2) **The (measurement) uncertainties of the wind field reconstruction inputs**. This is essentially the uncertainty of the lidar LOS velocities.

In the CFD approach, the second term is non-existent as the lidar simulations correspond to "perfect measurements" of the CFD simulated wind field. Consequently, the results presented in Chapter 6 simply show the (in)adequacy of the simple induction model compared to the CFD RANS simulations of the NKE turbine model. The negative biases identified on the free stream wind speed errors (see e.g. Figure 17) using the simulated data set can therefore be understood as characteristic of the NKE turbine aerodynamic model.

Moreover, in [8] (Fig. 2, reproduced in Figure 25), N. Troldborg and A.R.M. Forsting showed that the thrust coefficient curve of the SWT-2.3MW turbine was the most peculiar of the pitch-regulated turbines simulated using the same CFD RANS simulation setup, especially at low speeds. The SWT-2.3MW turbine shows in particular the highest local thrust (see plot on the right) resulting in the highest induction (see Fig. 4 in [8]).

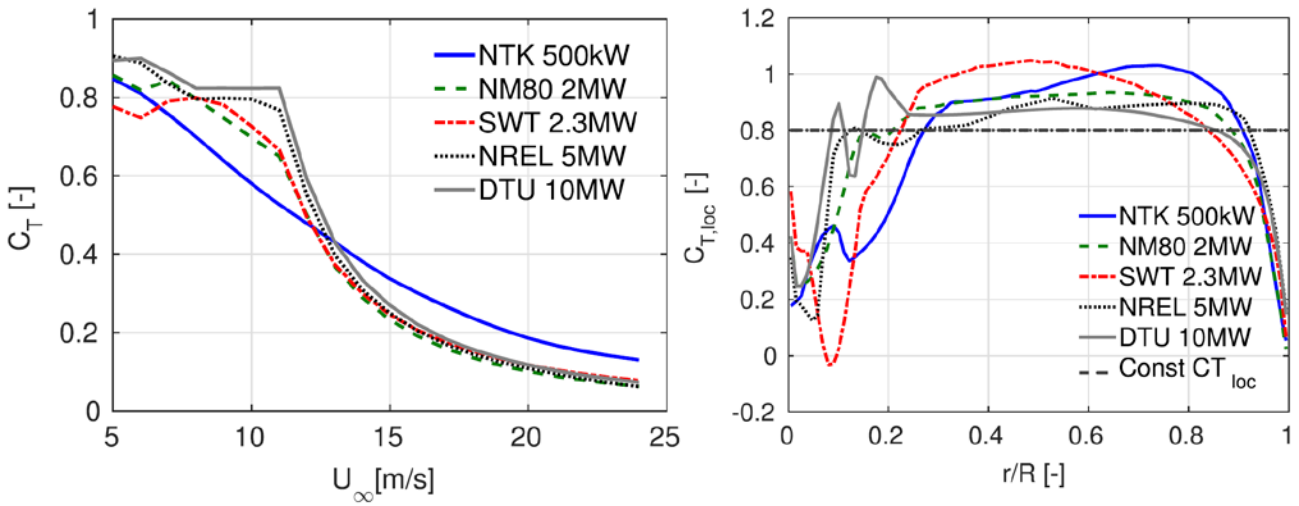

Figure 25. Computed C_T curves for all simulated wind turbines (left) and radial variation of $C_{T,\,loc}$ at C_T =0.8 (right). Reproduced from Troldborg and Meyer Forsting (2017), [8].

7.2 Lidar simulator using unsteady numerical flow fields

The sensitivity analysis based on the steady-state (RANS) CFD simulations showed that this approach was unable to capture the sensitivity of lidar estimates of the free stream wind speed to range configuration and wind-induction model. Even more, the CFD approach yielded contradictory conclusions to the ones made using the NKE experimental data set.

When sitting on a turbine's nacelle, a lidar probes the wind at different locations in space and time. The time sampling process at a given measurement location is fundamentally different from the regular sampling performed by data acquisition units of meteorological masts for instruments such as cup or sonic anemometers, wind vanes, pressure and temperature sensors, etc. Along (one of) its LOS, a lidar probes the wind during a short time. For example, in the NKE campaign:

- The 5B-Demo used an accumulation time of one second per LOS. Consequently, the wind was probed for one second at the specific measurement locations (configured ranges) along a LOS. During the next four seconds, no measurements were made along the same LOS as this corresponds to the time in which the lidar measures along the other four LOS.
- The ZDM continuously measured in one azimuthal sector for 20ms, at a given distance. After about three revolutions (1s/rev.), the ZDM refocused its laser beam to the next distance. For example, the 95m distance (about $1D_{rot}$) was probed for 10 seconds and then not at all during 40 seconds.

On one hand, inherent to the measurement process, time series obtained by single Doppler lidars contain "data gaps". This may be a source of uncertainty in the 10-minute statistics, which is a disadvantage compared to time series obtained by masts. On the other hand, wind lidars have the ability to probe the wind at many different locations. This means that lidar measurements can be used to retrieve wind characteristics that are representative of the entire flow field affecting a wind turbine. This is a great advantage compared to masts, which only make measurements at one location.

A realistic lidar simulator – i.e. a lidar simulator that provides inputs with uncertainties that are representative of experimental measurement uncertainties – needs to reproduce the exact time and space sampling of the lidars. Such simulator must additionally be based on numerical flow fields generated by unsteady CFD simulations, such as:

- Large Eddy Simulations (LES). This approach is however computationally expensive, which may be unnecessary.
- Constrained turbulence fields as demonstrated by N. Dimitrov in [13], using a so-called turbulence box.

Additionally, random noise characterising the lidar LOS velocity measurement uncertainties should be added. This would make the real-time lidar simulator even more representative of experimental lidar measurement processes.

7.3 IEC standard and “lidar classification”

The power curve measurement standard, the IEC 61400-12-1, was revised in 2017 [3]. In the next couple of years, the standard is planned to be split in several documents, where the individual wind measurement systems will be considered independently.

The project and work on the document related to the use of nacelle-based wind lidar systems (IEC 61400-50-3) has started in 2017, under the responsibility of Technical Committee 88. There, discussions on the so-called “lidar classification” were undertaken.

The terminology of classification has so far been introduced in order to quantify the sensitivity of the measuring instruments to external conditions. For example, the cup anemometer classification attempts to quantify the operational uncertainties due to the cup sensitivity to turbulence intensity, inflow angles, temperature, etc.

Lidar classification must be carefully studied. In terms of first principles, lidar measurements are not expected to be sensitive to the same variables as other instruments; it could for instance be expected that lidars are sensitive to aerosol concentration, but not to temperature and pressure.

Additionally, the assumptions made on the flow field in order to retrieve wind field characteristics will add sensitivity to wind parameters violating these assumptions. Examples of common assumptions are given hereafter:

- **Horizontal homogeneity**
  This assumption is reasonably valid for 10-minute averages obtained by two-beam nacelle-based wind lidars as long as the physical distance between the two measurement locations remains small. Furthermore, there is an ongoing trend in growing turbine rotor sizes, especially for offshore applications. For a rotor diameter of 150m and a half-opening angle of 15°, the separation between the two beams will be about 200m when measuring at $2.5D_{rot}$. The demonstrated benefits of two-beam nacelle lidars for power curve measurement (see e.g. [1]) will be drastically lowered in such situations due to flow inhomogeneities. Measuring at shorter ranges is an advantage since the flow homogeneity assumption is more acceptable.

- **Wind shear**
  If a nacelle lidar probes the wind at several heights – such as the 5B-Demo, ZDM and other commercially available systems – the wind shear can be estimated and accounted for in the retrieval of the wind speed at the heights of interest. However, the assumptions made on the shear profile will remain a source of uncertainty.
  For the two-beam nacelle lidar technique, wind shear is an even larger source of uncertainty as the two lidar beams probe different heights in real-time due to the dynamic motion (tilting and rolling) of the wind turbine. At large measurement ranges, the lidar beams will most of the time be outside the range of 1% to hub height, which is required by the IEC 61400-12-1, even on a 10-minute time basis.

7.4 Recommendations on lidar configurations for WFR

The future of power performance testing and wind measurements based on forward-looking nacelle lidars is likely to move towards the use of lidar measurement ranges configured close to the turbine rotor. This makes it possible to bypass the challenges presented in Section 7.3 and other challenges such as the range capabilities of the current nacelle lidar technologies.

The ultimate goal of this report was to provide practical recommendations for the optimal range configurations when using forward-looking nacelle lidars. In addition, we wanted to specify the minimal requirements to ensure that the short-range nacelle lidar measurement technique – where the induction is accounted for and free stream wind speed estimated using simple combined wind-induction models – performs the best.

Based on the studies and results reported in Chapter 5 and in [8], the authors' recommendations on the lidar range configurations are:

1) To use a minimum of three distances, separated by a distance of approximately 0.1 to 0.2 rotor diameter. Moreover, it was shown – via the RMSE statistics – that using a large number of measurement ranges can yield higher fitting residuals. There is currently no evidence for a need of using more than five measurement ranges.
2) The minimum range should be configured so that the lidar probes the wind at a distance of 0.5 rotor diameters upstream the turbine. Measuring closer to the turbine would mean risking that the probed flow field is directly influenced by the aerodynamics of the blades and the presence of the nacelle, which effects are turbine specific. In order to accept the assumption of "self-similarity" of the induction zone of a wind turbine, $0.5D_{rot}$ was identified as a reasonable minimum.
3) The maximum distance should be configured to approximately 1-1.5 rotor diameter.

8 Conclusion

A sensitivity analysis has been conducted with the aim of determining the sensitivity of nacelle lidar reconstructed wind speeds to wind-induction model and lidar range configuration. Based on the results, recommendations on the optimal range configurations have been provided. The recommendations apply for forward-looking nacelle lidars that are used for the primary purpose of power performance testing.

The sensitivity analysis was conducted using both experimental data from the Nørrekær Enge (NKE) campaign and simulated lidar data from steady-state computational fluid dynamics (CFD) simulations. The study used two different nacelle lidar types: a five-beam Demonstrator (5B-Demo) unit developed by *Avent Lidar Technology* and a ZephIR Dual-Mode (ZDM) unit developed by *Zephir Lidar*. The lidar wind field reconstruction was performed using the so-called model-fitting technique.

The wind speed errors and residual root mean squared errors (RMSEs) obtained from the NKE data were on the order of $0.1ms^{-1}$ while the wind speed errors and RMSEs obtained from the CFD simulations were on the order of $0.01ms^{-1}$. It was hereby concluded that the results obtained from the CFD study could not be used to determine the sensitivity of nacelle lidar wind speed measurements to wind-induction reconstruction model and lidar range configuration in a real experiment. Instead, the CFD results allowed to quantify the inadequacy of the simple induction model compared to the CFD RANS simulations of the NKE turbine model. The recommendations provided in this report are therefore based on the results of the NKE campaign. Due to the fixed range configurations used in the NKE campaign, it was not possible to examine the sensitivity of the reconstructed wind speeds to the separation between the ranges.

The results of the NKE campaign demonstrate that the nacelle lidar free stream wind speed measurements are insensitive to the wind-induction reconstruction model (either the one- or two-dimensional models). Furthermore, the choice of lidar is shown to have an impact on the reconstructed wind speeds. However, the differences between the lidars lay within the uncertainties of the reconstructed wind speed errors.

Based on the NKE results, it is recommended to configure nacelle lidars to measure at approximately 3-5 ranges. The minimum distance should be configured to measure at approximately $0.5D_{rot}$ while the maximum range should measure at approximately $1\text{-}1.5D_{rot}$.

References

[1] Wagner R., Pedersen T.F., Courtney M., Antoniou I., Davoust S., Rivera R.L.: "*Power curve measurement with a nacelle mounted lidar*", [2014], Wind Energy, vol: 17, issue: 9, pages 1441–1453 (http://dx.doi.org/10.1002/we.1643).

[2] Borraccino A.: "*Remotely measuring the wind using turbine-mounted lidars: Application to power performance testing*", [2017], Ph.D. thesis, DTU Wind Energy, Roskilde, Denmark. (http://dx.doi.org/10.11581/DTU:00000021).

[3] IEC 61400-12-1 (edition 2), [2017], "*Power performance measurements of electricity producing wind turbines*", International Electrotechnical Commission.

[4] IEC 61400-12-2, [2013], "*Power performance measurements of electricity producing wind turbines based on nacelle anemometry*", International Electrotechnical Commission.

[5] Borraccino A. et al.: "*Wind field reconstruction from nacelle-mounted lidar short-range measurements*", [2017], Wind Energy Science, vol: 2, issue: 1, pages 269–283 (http://dx.doi.org/10.5194/wes-2-269-2017).

[6] Vignaroli A., Weber Kock C.: "*UniTTe MC2 Nørrekær Enge Measurement System & Calibration report*", [2016], Technical Report, DTU Wind Energy, Roskilde, Denmark.

[7] Meyer Forsting A.R., Troldborg N., Gaunaa M.: "*The flow upstream of a row of aligned wind turbine rotors and its effect on power production*", [2017], Wind Energy, vol: 20, issue: 1, pages: 63–77 (http://dx.doi.org/10.1002/we.1991).

[8] Troldborg N., Meyer Forsting A.R.: "*A simple model of the wind turbine induction zone derived from numerical simulations*", [2017], Wind Energy, 1–10, (http://dx.doi.org/10.1002/we.2137).

[9] Schlipf D. et al.: "Model Based Wind Vector Field Reconstruction from Lidar Data", [2012,]in proceedings of the German Wind Energy Conference DEWEK, Bremen, Germany (http://dx.doi.org/10.18419/opus-8136).

[10] Borraccino A. and Courtney M.: "*Calibration report for ZephIR Dual Mode lidar (unit 351)*", [2016], Technical Report, DTU Wind Energy, Roskilde, Denmark (DTU Wind Energy E; No. 0088) (http://orbit.dtu.dk/files/123699869/Calibration_report_for_ZephIR.pdf).

[11] Borraccino A. and Courtney M.: "*Calibration report for Avent 5-beam Demonstrator lidar*", [2016], Technical Report, DTU Wind Energy, Roskilde, Denmark (DTU Wind Energy E; No. 0087) (http://orbit.dtu.dk/files/123699807/Calibration_report_for_Avent.pdf).

[12] Medici D., Ivanell S., Dahlberg J., and Alfredsson P. H.: "*The upstream flow of a wind turbine: blockage effect*", [2011], Wind Energy, 14, 691–697 (http://dx.doi.org/10.1002/we.451).

[13] Dimitrov N. and Natarajan A.: "*Application of simulated lidar scanning patterns to constrained Gaussian turbulence fields for load validation*", [2017], Wind Energy, vol: 20, issue: 1, pages: 79–95 (http://dx.doi.org/10.1002/we.1992).

Annexes

Annex A. Sensitivity to wind-induction model (NKE)

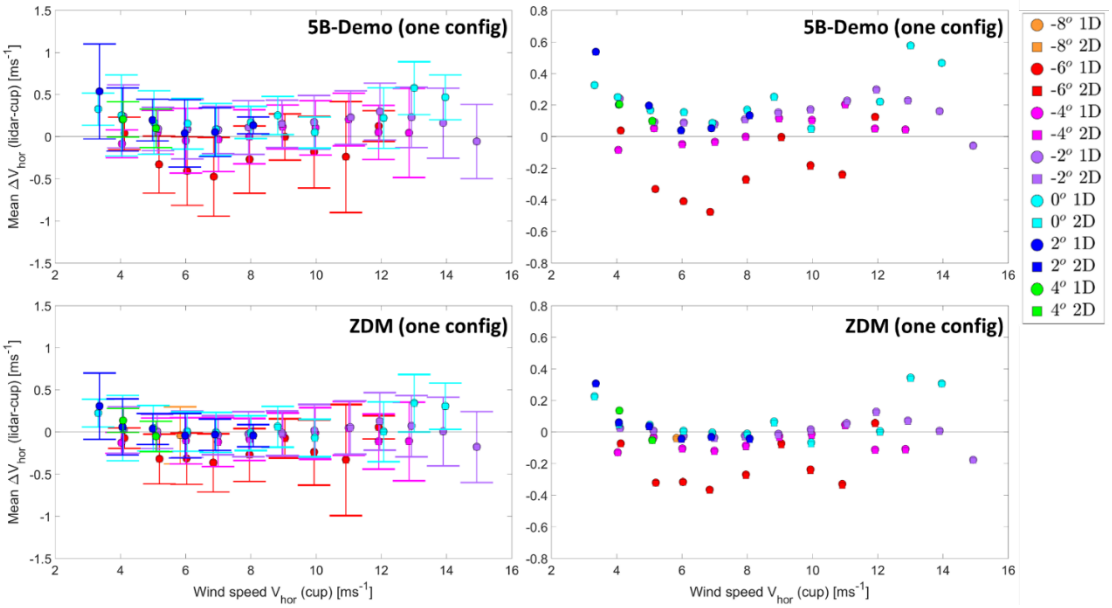

Figure A.1. Wind speed error as a function of horizontal wind speed (cup) and yaw misalignment (spinner). The figures correspond to the [95m, 120/121m, 235m] configuration. The right column is the same as the left, but without error bars.

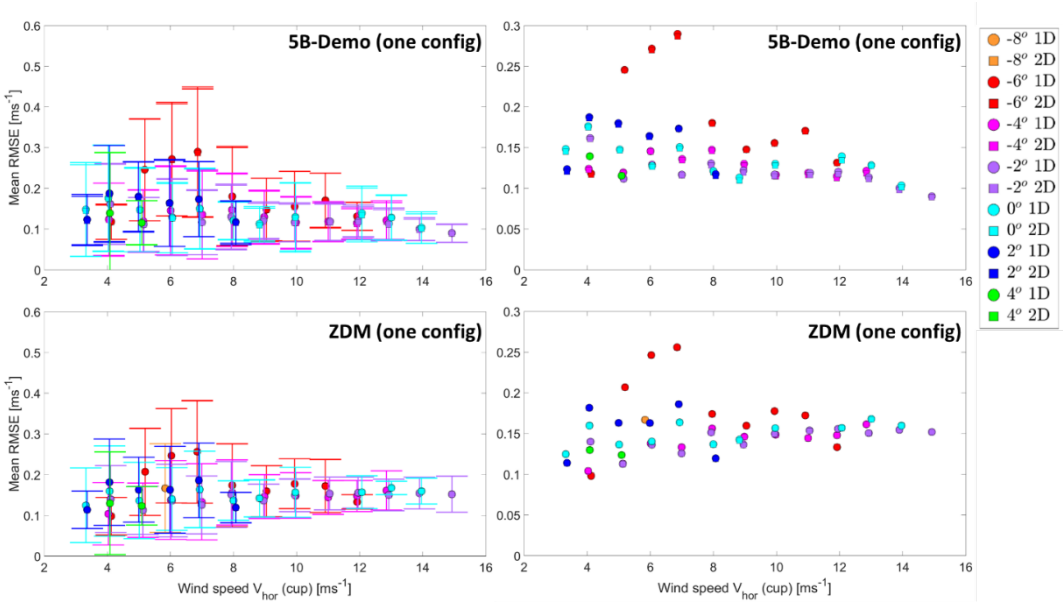

Figure A.2. RMSE as a function of horizontal wind speed (cup) and yaw misalignment (spinner). The figures correspond to the [95m, 120/121m, 235m] configuration. The right column is the same as the left, but without error bars.

Annex B. Sensitivity to lidar type and trajectory (NKE)

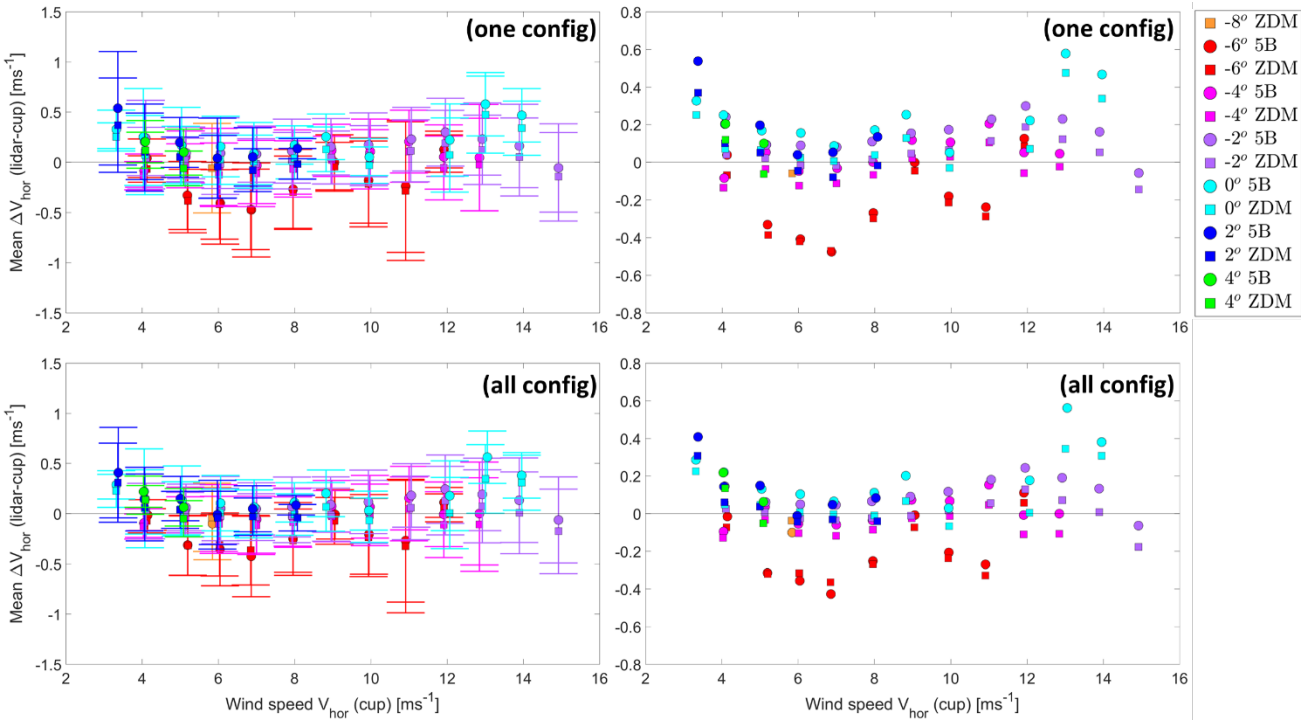

Figure A.3. Wind speed error as a function of horizontal wind speed (cup) and yaw misalignment (spinner). The top row corresponds to the [95m, 120/121m, 235m] configuration while the bottom row correspond to all configurations. The right column is the same as the left, but without error bars.

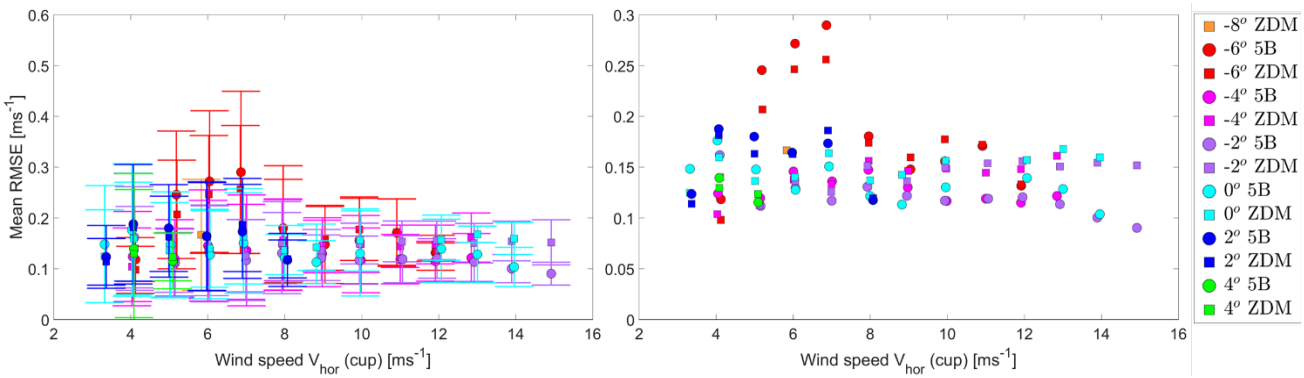

Figure A.4. RMSE as a function of horizontal wind speed (cup) and yaw misalignment (spinner). The figures correspond to the [95m, 120/121m, 235m] configuration. The right column is the same as the left, but without error bars.

Annex C. Sensitivity to minimum distance (NKE)

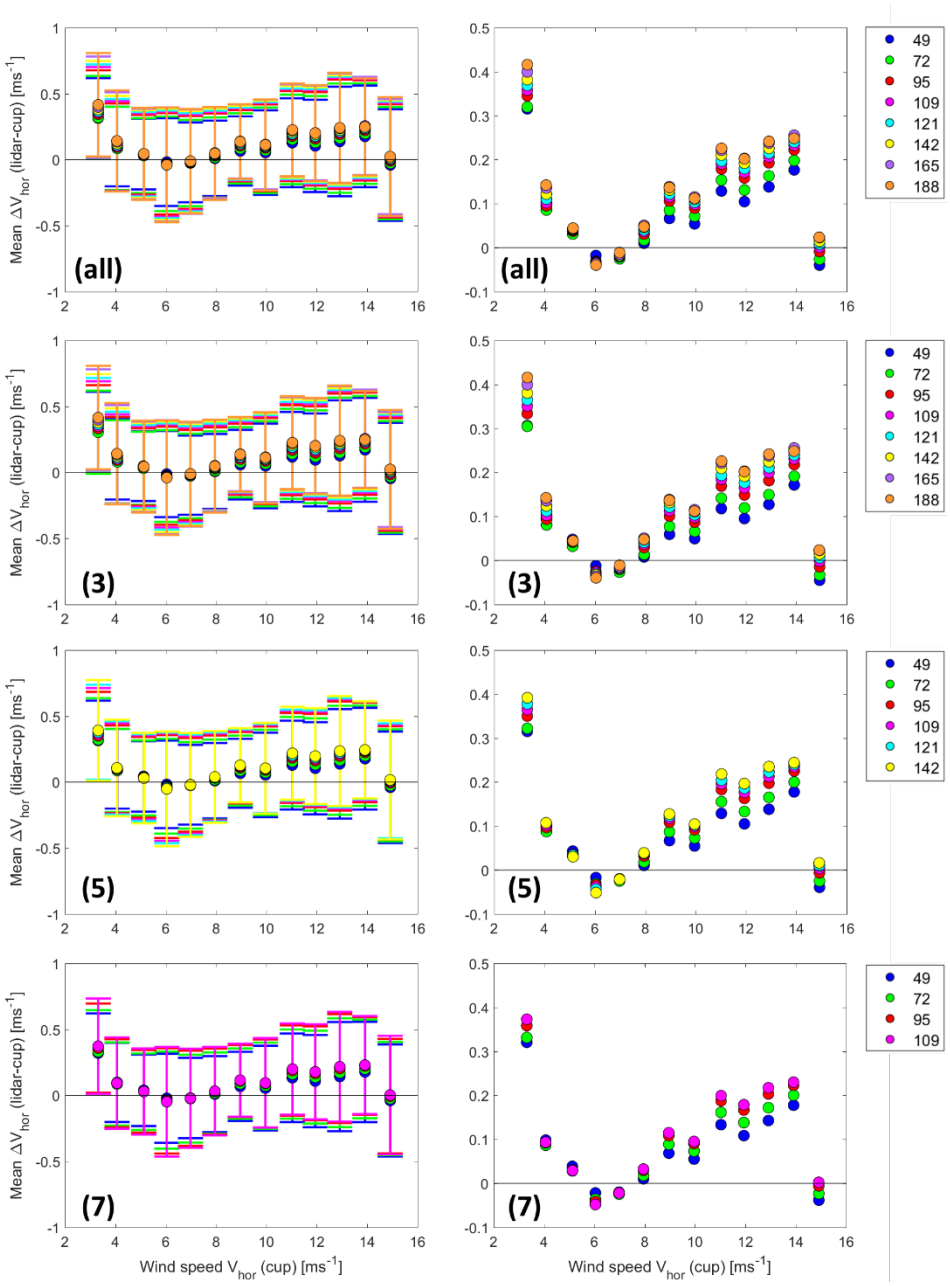

Figure A.5. Wind speed error as a function of horizontal wind speed (cup-measured). The different colors represent different minimum distances. The different rows represent different number of ranges. The right column is the same as the left, but without error bars. Results correspond to the 5B-Demo and 1D induction model.

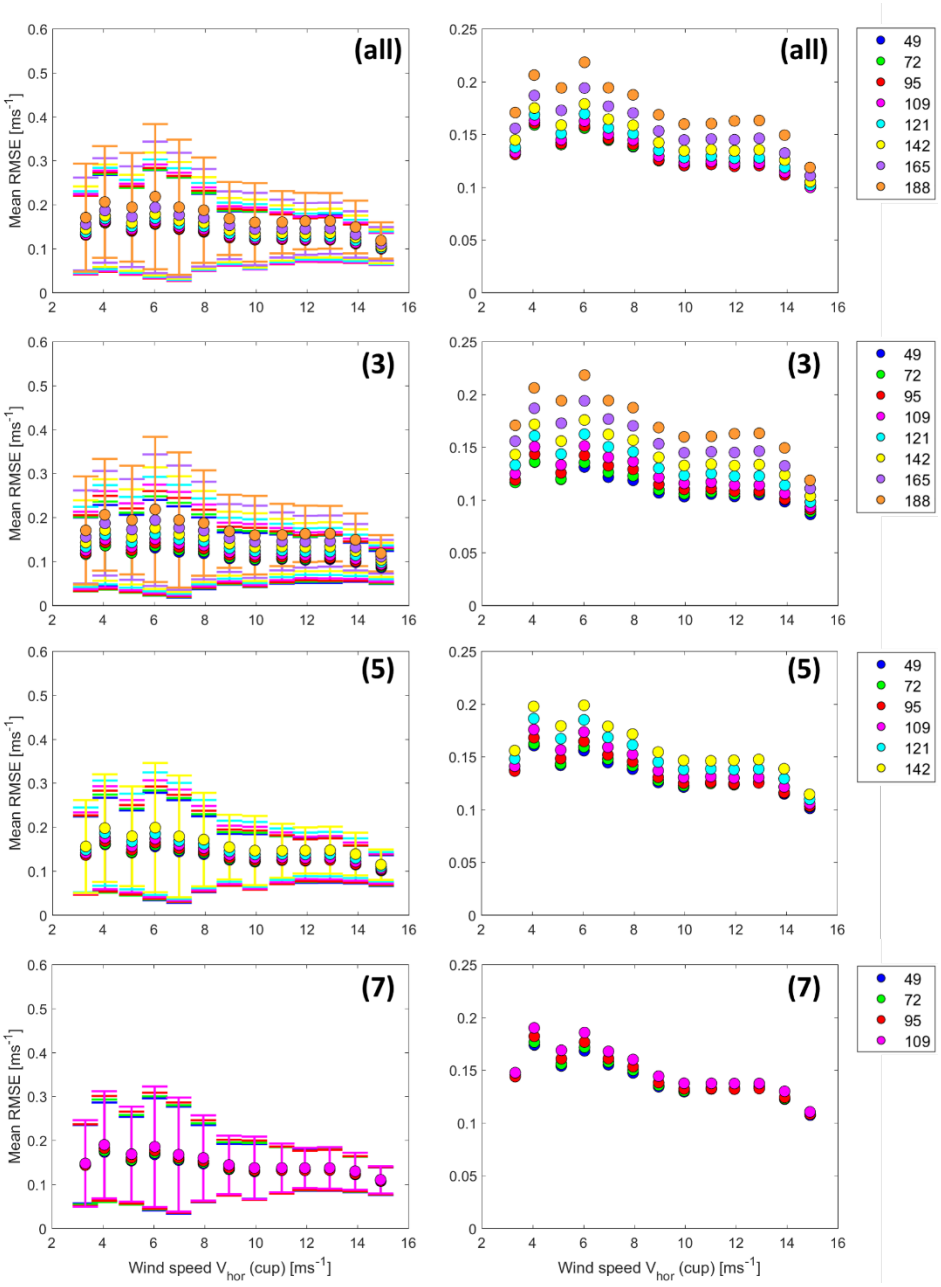

Figure A.6. RMSE as a function of horizontal wind speed (cup-measured). The different colors represent different minimum distances. The different rows represent different number of ranges. The right column is the same as the left, but without error bars. Results correspond to the 5B-Demo and 1D induction model.

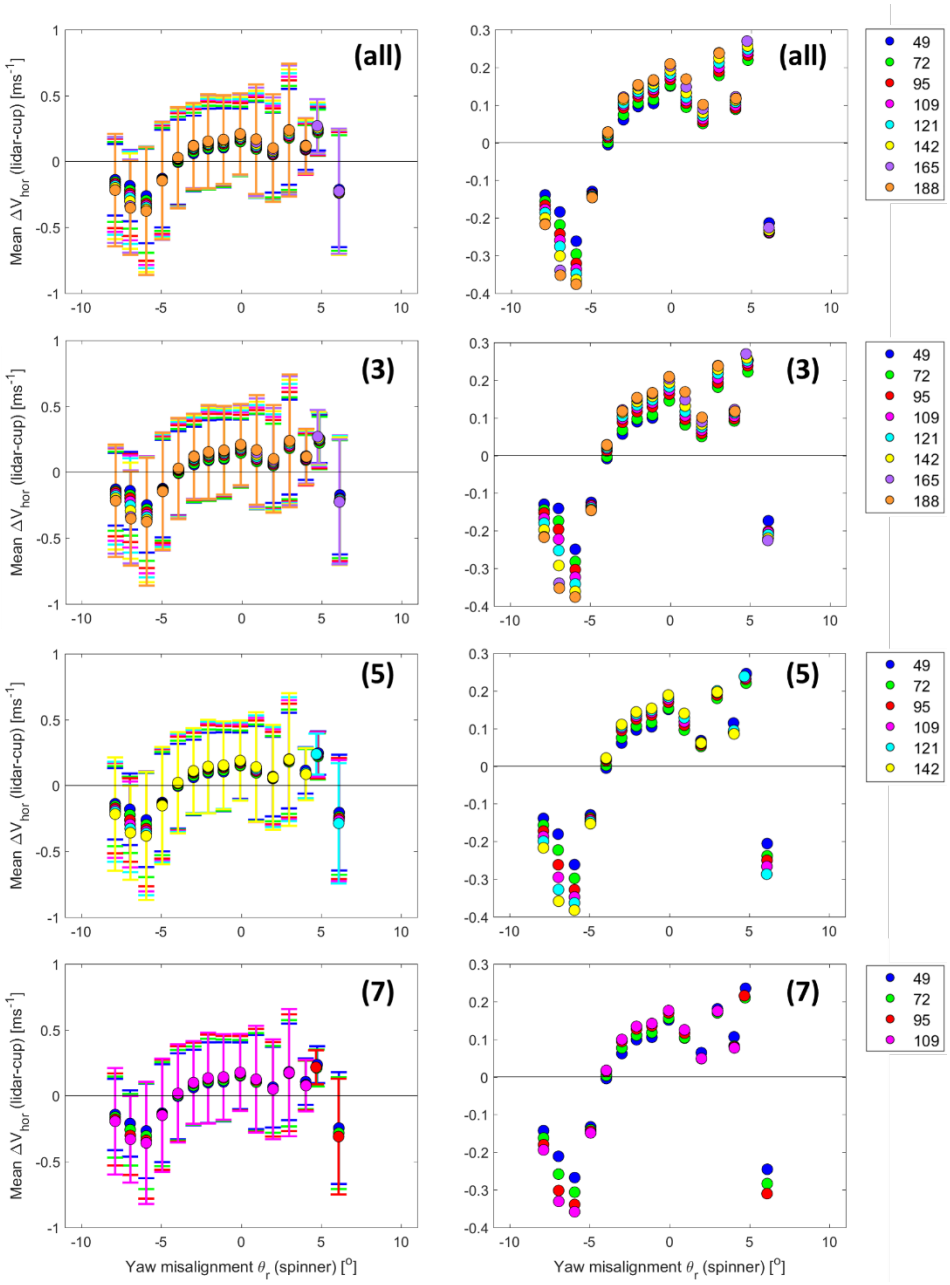

Figure A.7. Wind speed error as a function of yaw misalignment (spinner-measured). The different colors represent different minimum distances. The different rows represent different number of ranges. The right column is the same as the left, but without error bars. Results correspond to the 5B-Demo and 1D induction model.

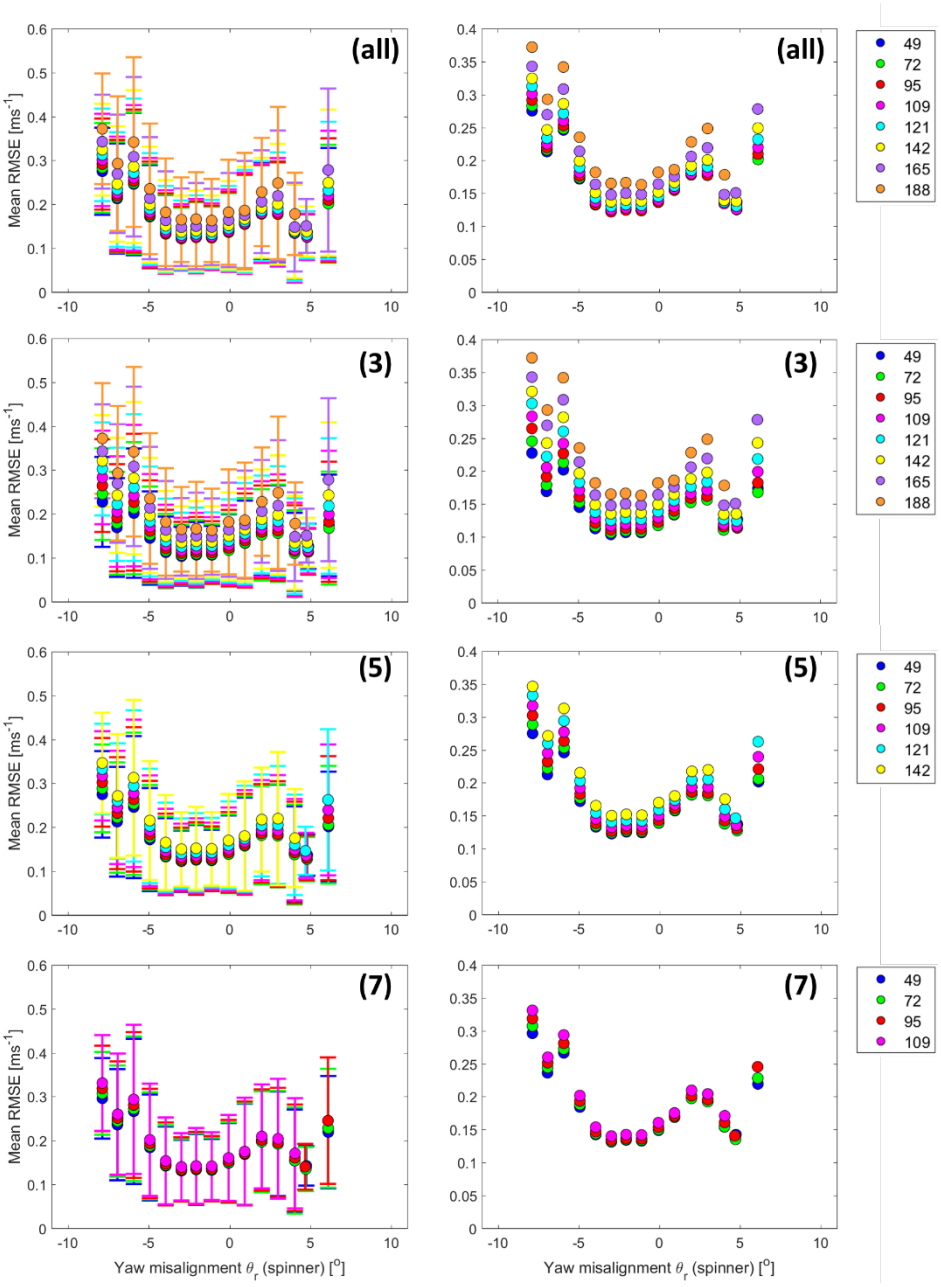

Figure A.8. RMSE as a function of yaw misalignment (spinner-measured). The different colors represent different minimum distances. The different rows represent different number of ranges. The right column is the same as the left, but without error bars. Results correspond to the 5B-Demo and 1D induction model.

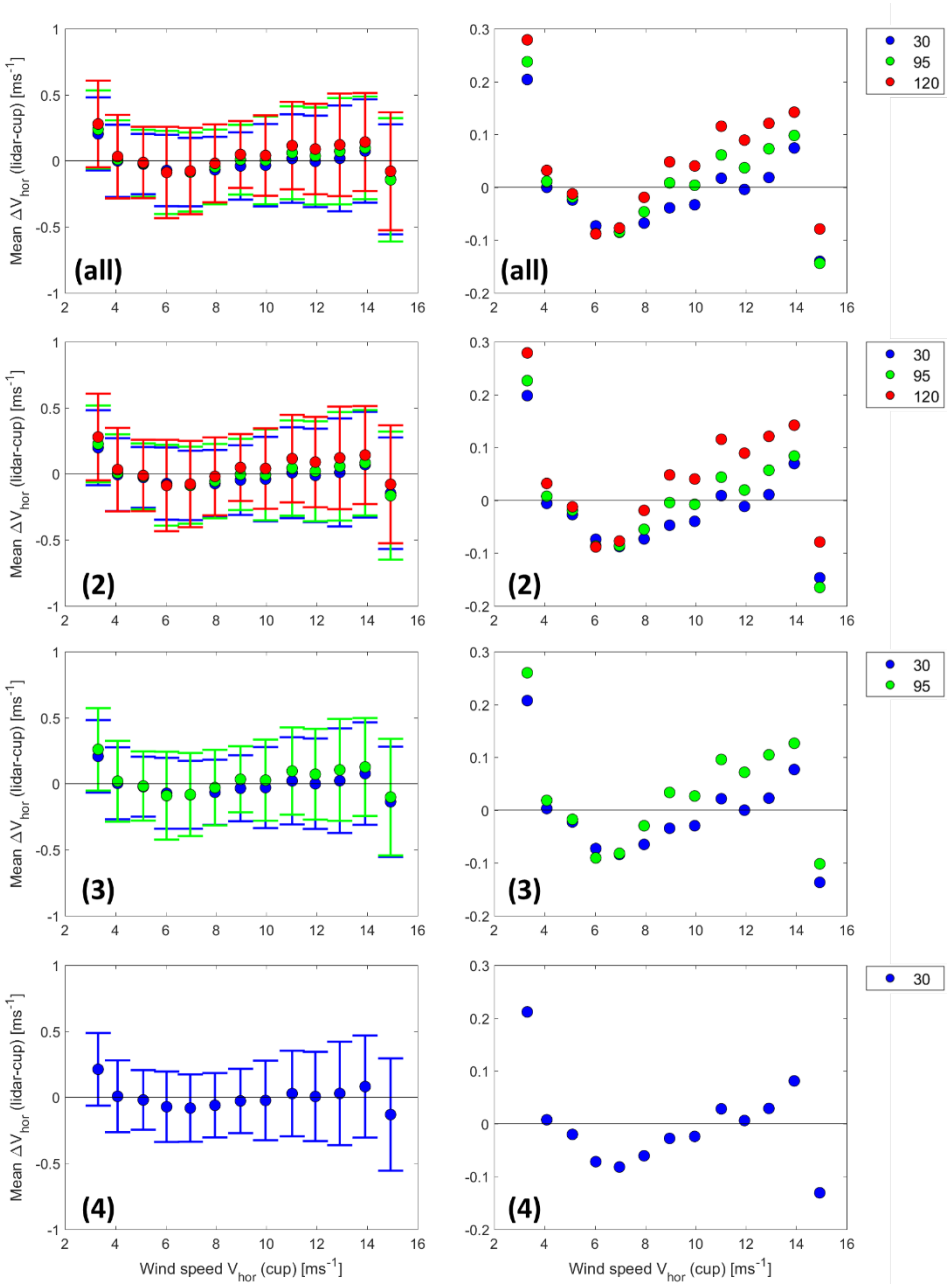

Figure A.9. Wind speed error as a function of horizontal wind speed (cup-measured). The different colors represent different minimum distances. The different rows represent different number of ranges. The right column is the same as the left, but without error bars. Results correspond to the ZDM and 1D induction model.

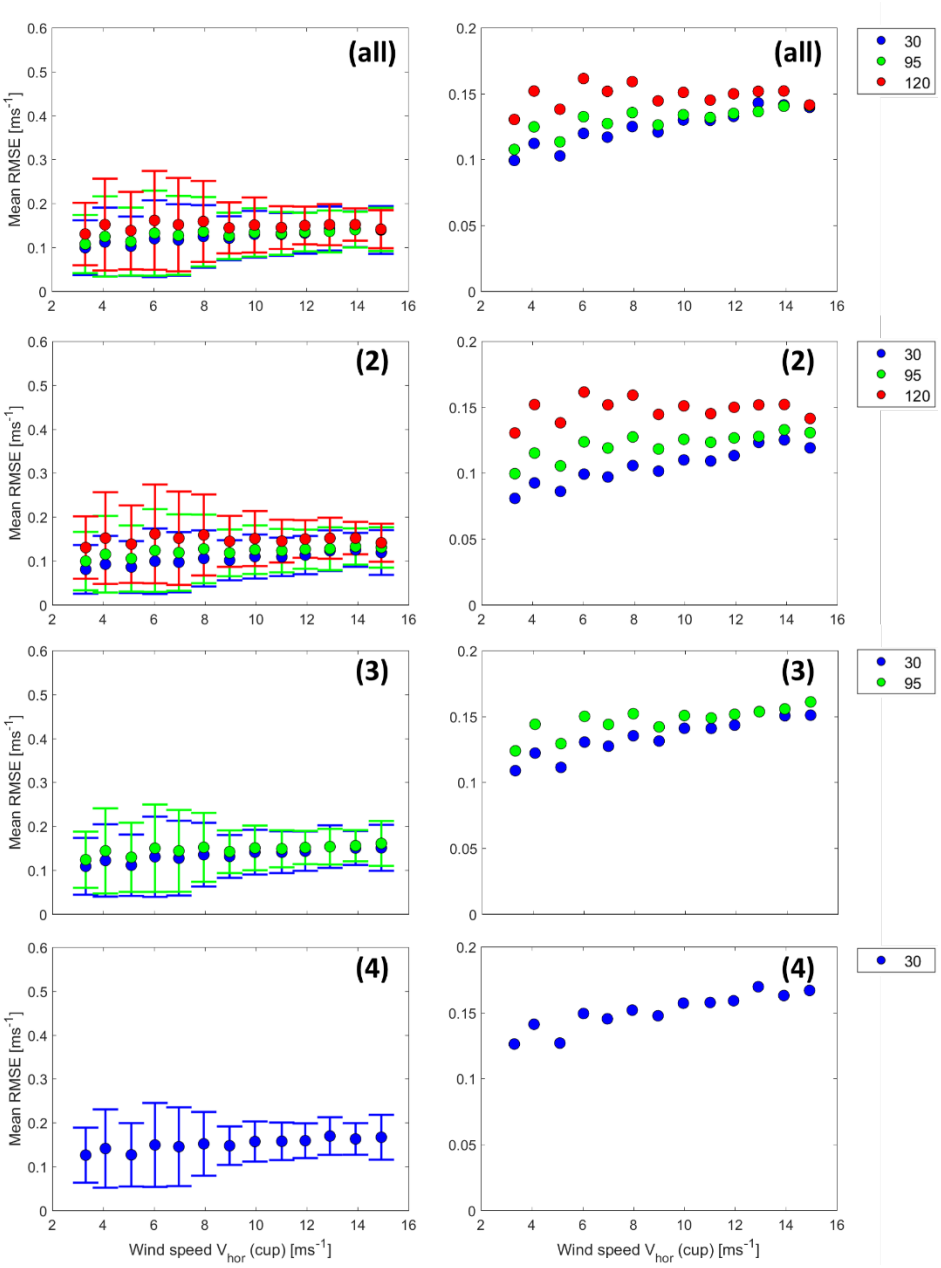

Figure A.10. RMSE as a function of horizontal wind speed (cup-measured). The different colors represent different minimum distances. The different rows represent different number of ranges. The right column is the same as the left, but without error bars. Results correspond to the ZDM and 1D induction model.

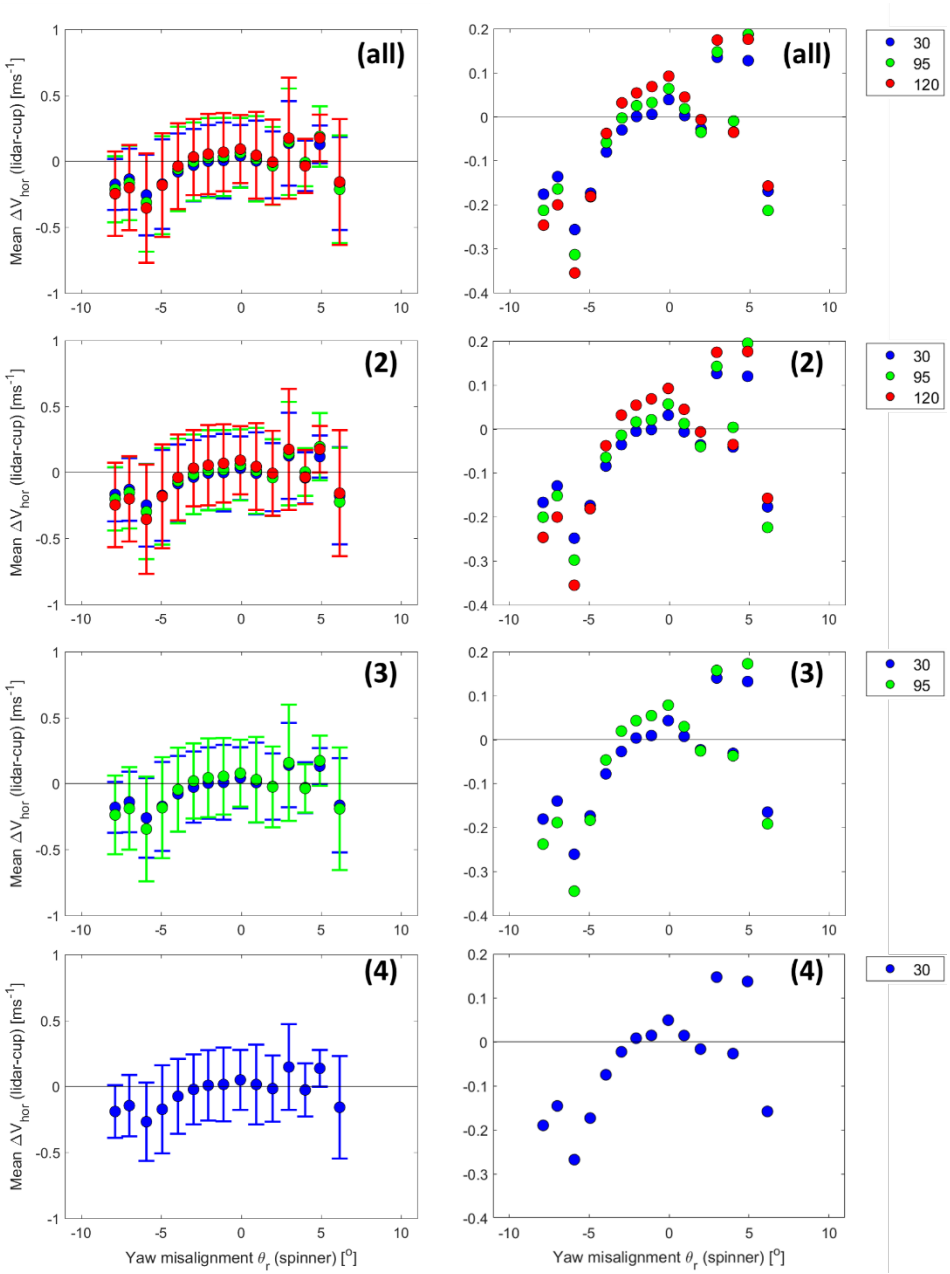

Figure A.11. Wind speed error as a function of yaw misalignment (spinner-measured). The different colors represent different minimum distances. The different rows represent different number of ranges. The right column is the same as the left, but without error bars. Results correspond to the ZDM and 1D induction model.

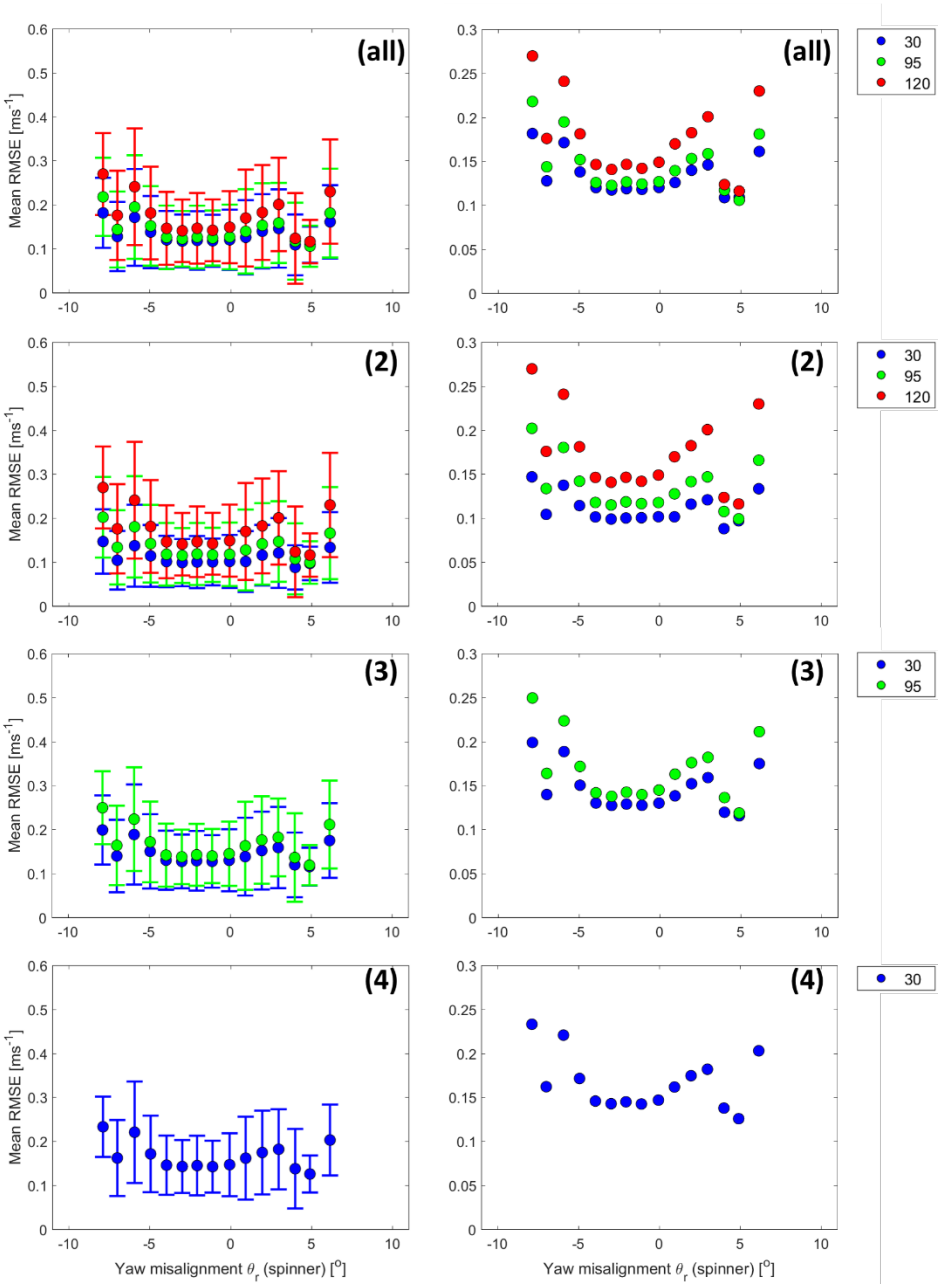

Figure A.12. RMSE as a function of yaw misalignment (spinner-measured). The different colors represent different minimum distances. The different rows represent different number of ranges. The right column is the same as the left, but without error bars. Results correspond to the ZDM and 1D induction model.

Annex D. Sensitivity to maximum distance (NKE)

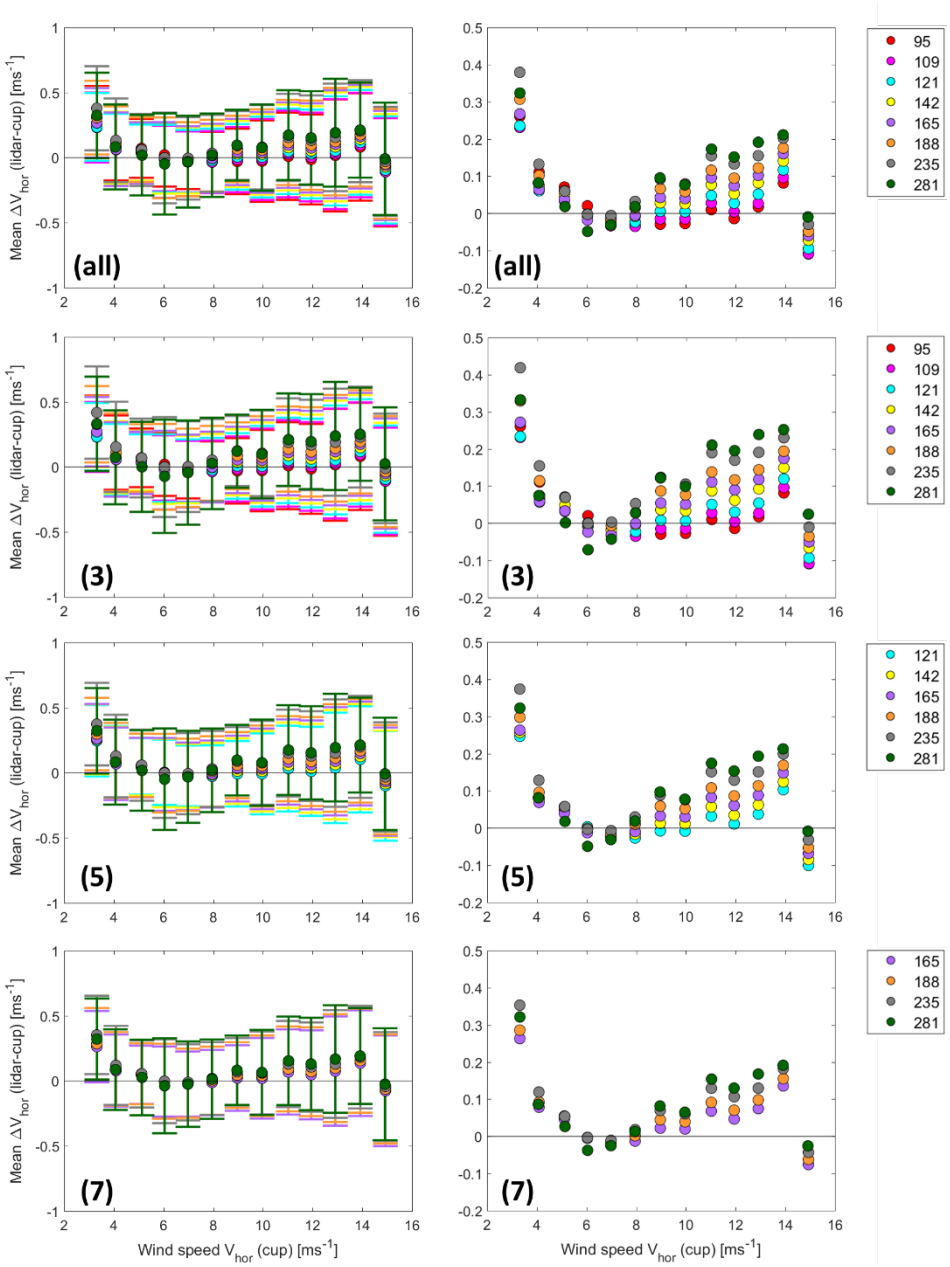

Figure A.13. Wind speed error as a function of horizontal wind speed (cup-measured). The different colors represent different maximum distances. The different rows represent different number of ranges. The right column is the same as the left, but without error bars. Results correspond to the 5B-Demo and 1D induction model.

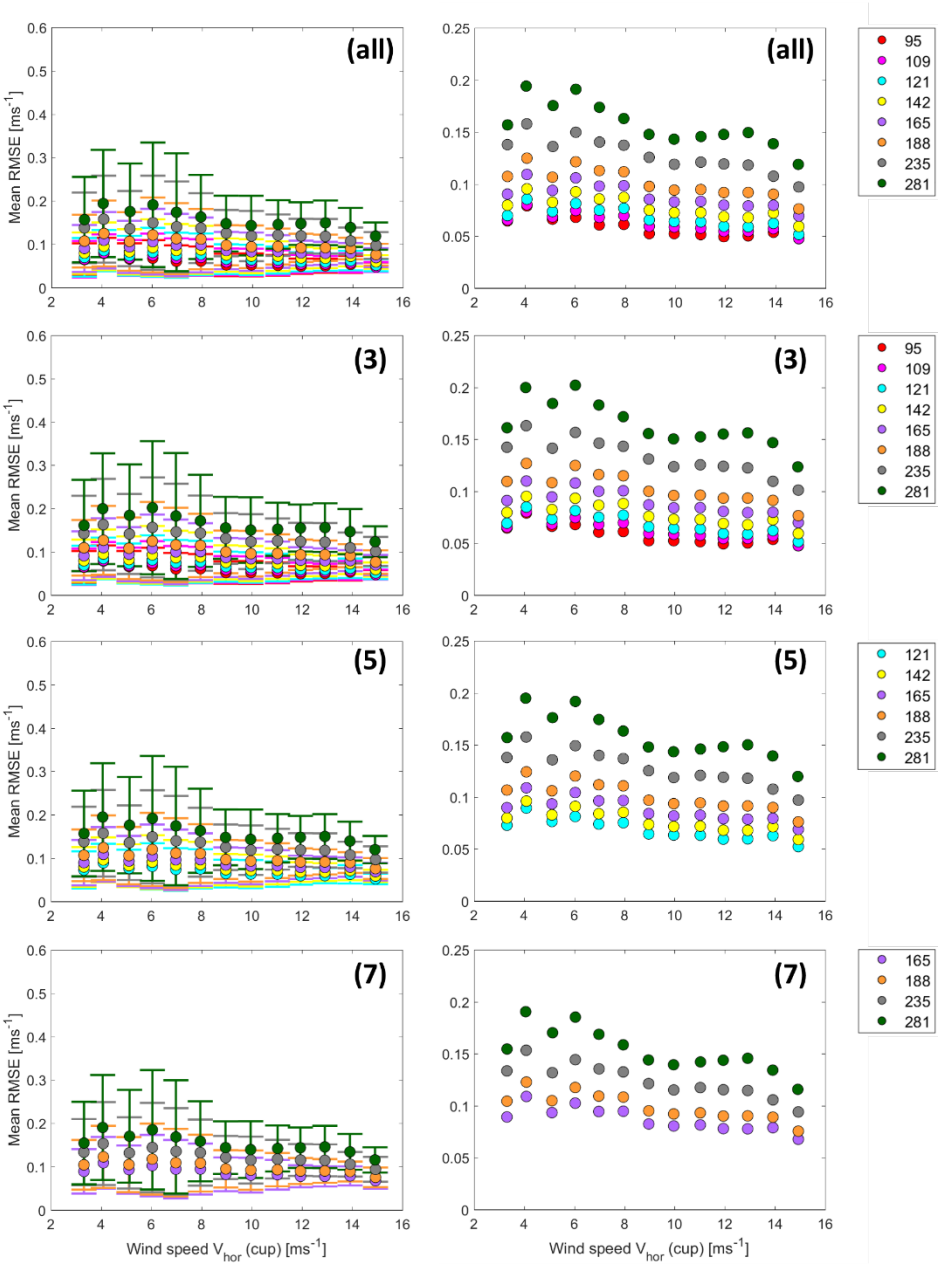

Figure A.14. RMSE as a function of horizontal wind speed (cup-measured). The different colors represent different maximum distances. The different rows represent different number of ranges. The right column is the same as the left, but without error bars. Results correspond to the 5B-Demo and 1D induction model.

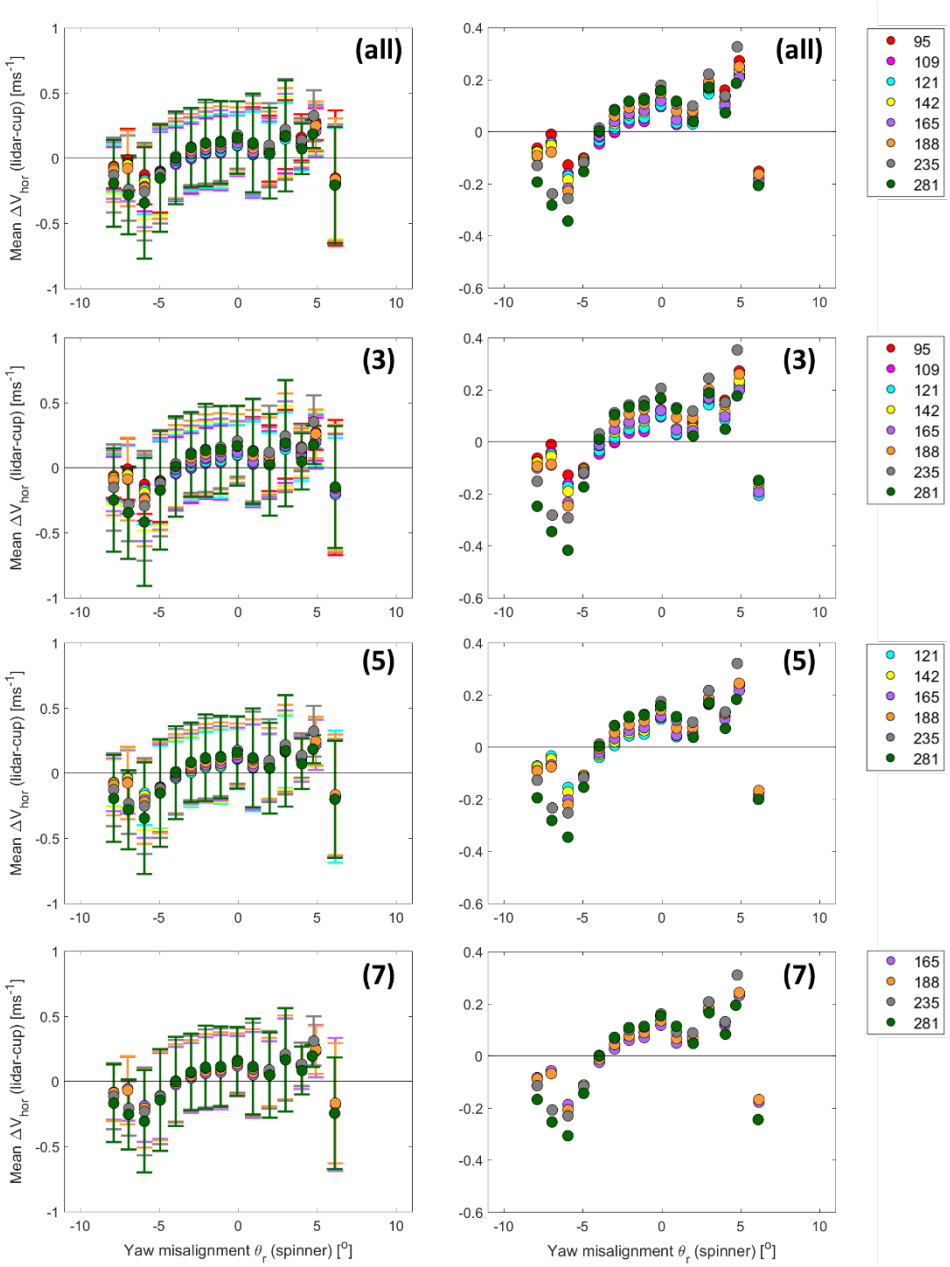

Figure A.15. Wind speed error as a function of yaw misalignment (spinner-measured). The different colors represent different maximum distances. The different rows represent different number of ranges. The right column is the same as the left, but without error bars. Results correspond to the 5B-Demo and 1D induction model.

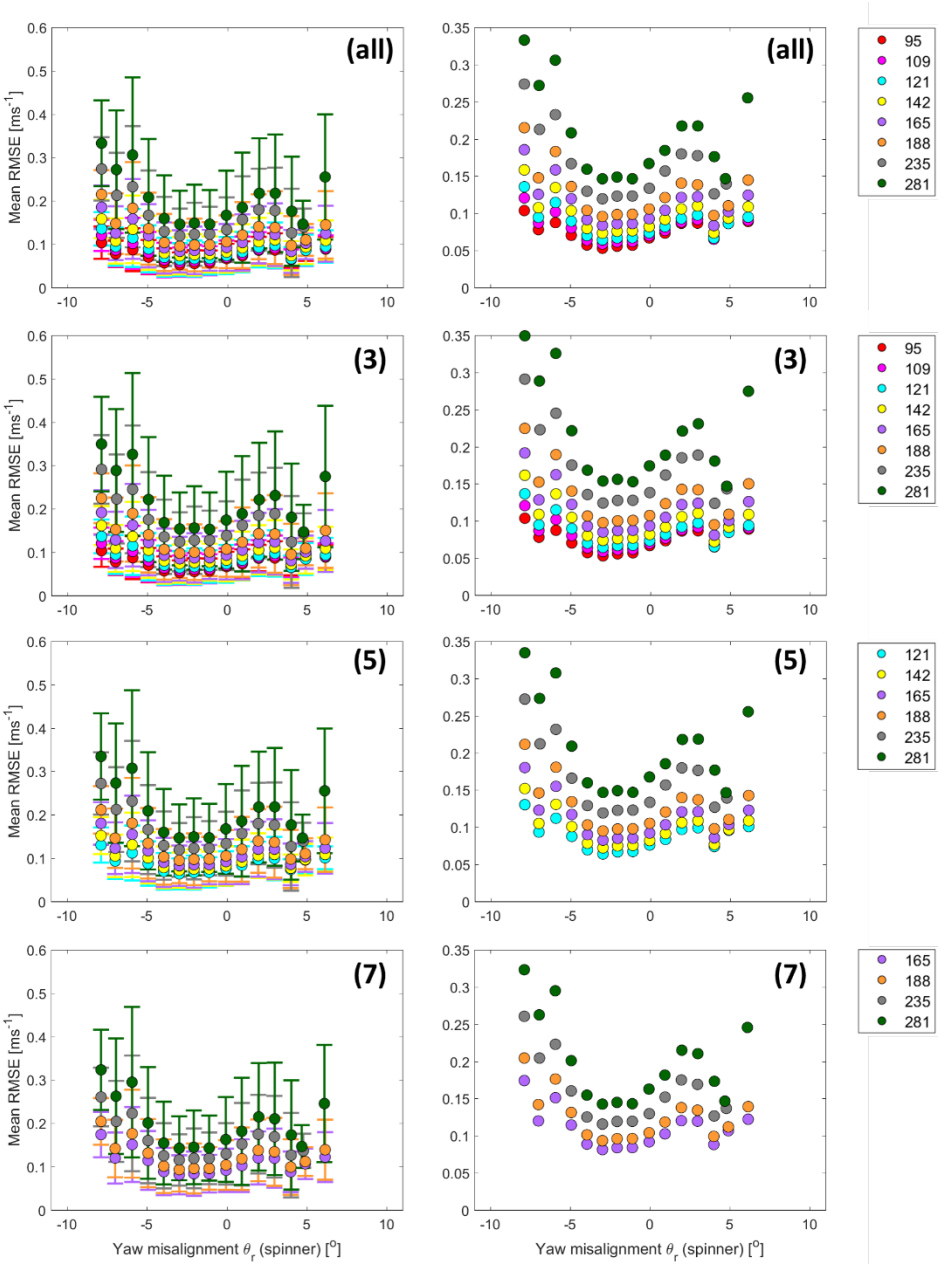

Figure A.16. RMSE as a function of yaw misalignment (spinner-measured). The different colors represent different maximum distances. The different rows represent different number of ranges. The right column is the same as the left, but without error bars. Results correspond to the 5B-Demo and 1D induction model.

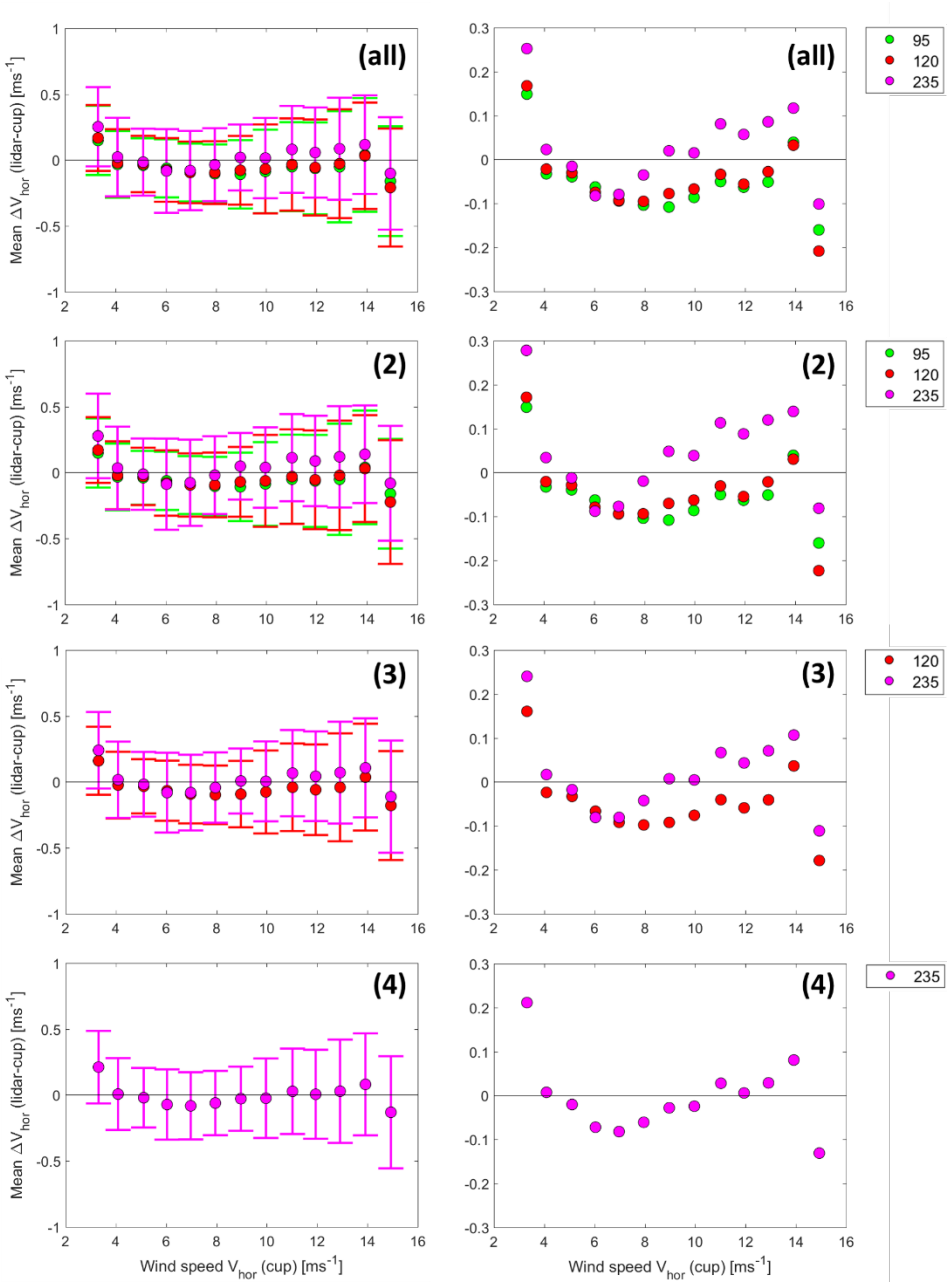

Figure A.17. Wind speed error as a function of horizontal wind speed (cup-measured). The different colors represent different maximum distances. The different rows represent different number of ranges. The right column is the same as the left, but without error bars. Results correspond to the ZDM and 1D induction model.

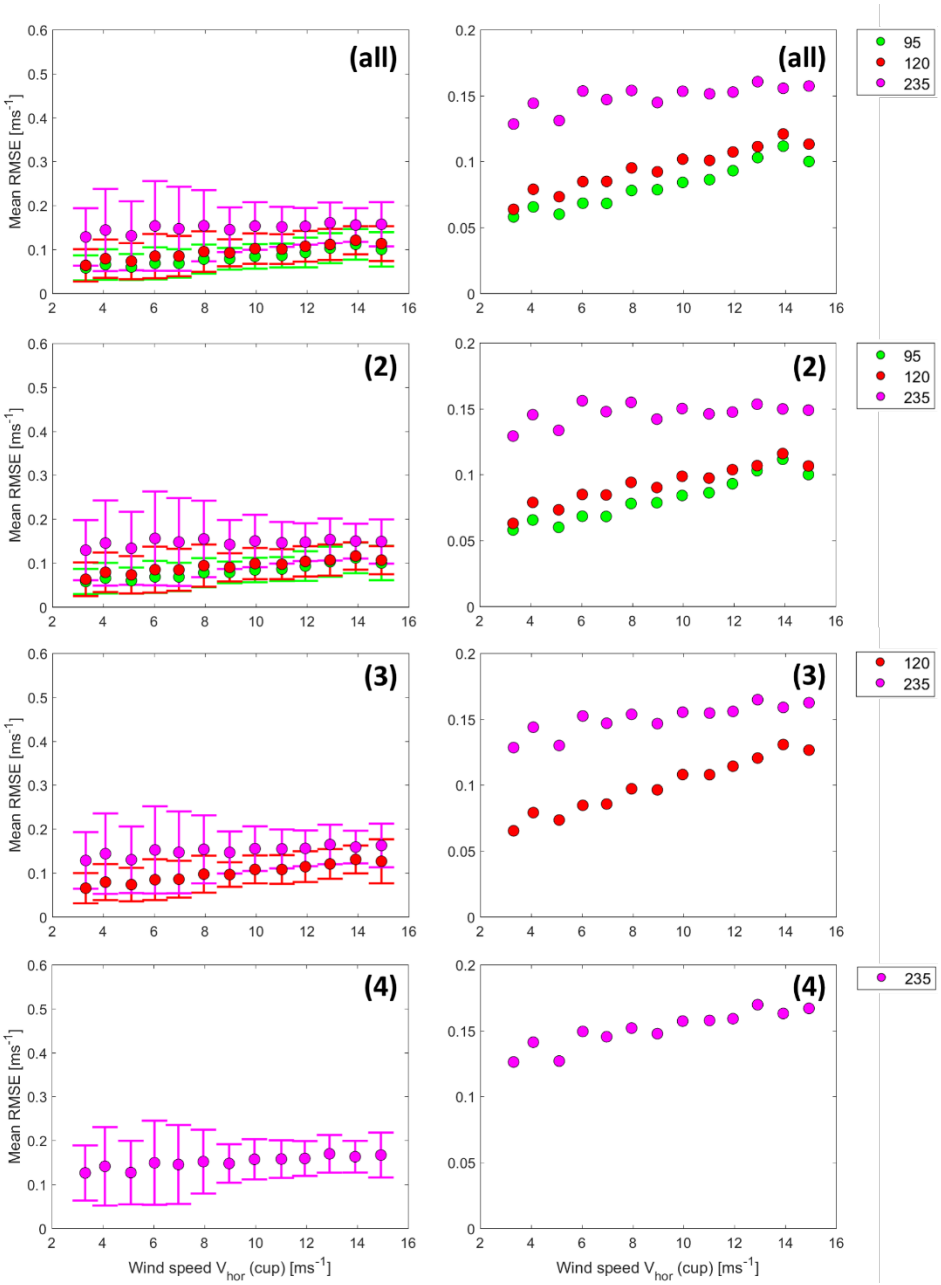

Figure A.18. RMSE as a function of horizontal wind speed (cup-measured). The different colors represent different maximum distances. The different rows represent different number of ranges. The right column is the same as the left, but without error bars. Results correspond to the ZDM and 1D induction model.

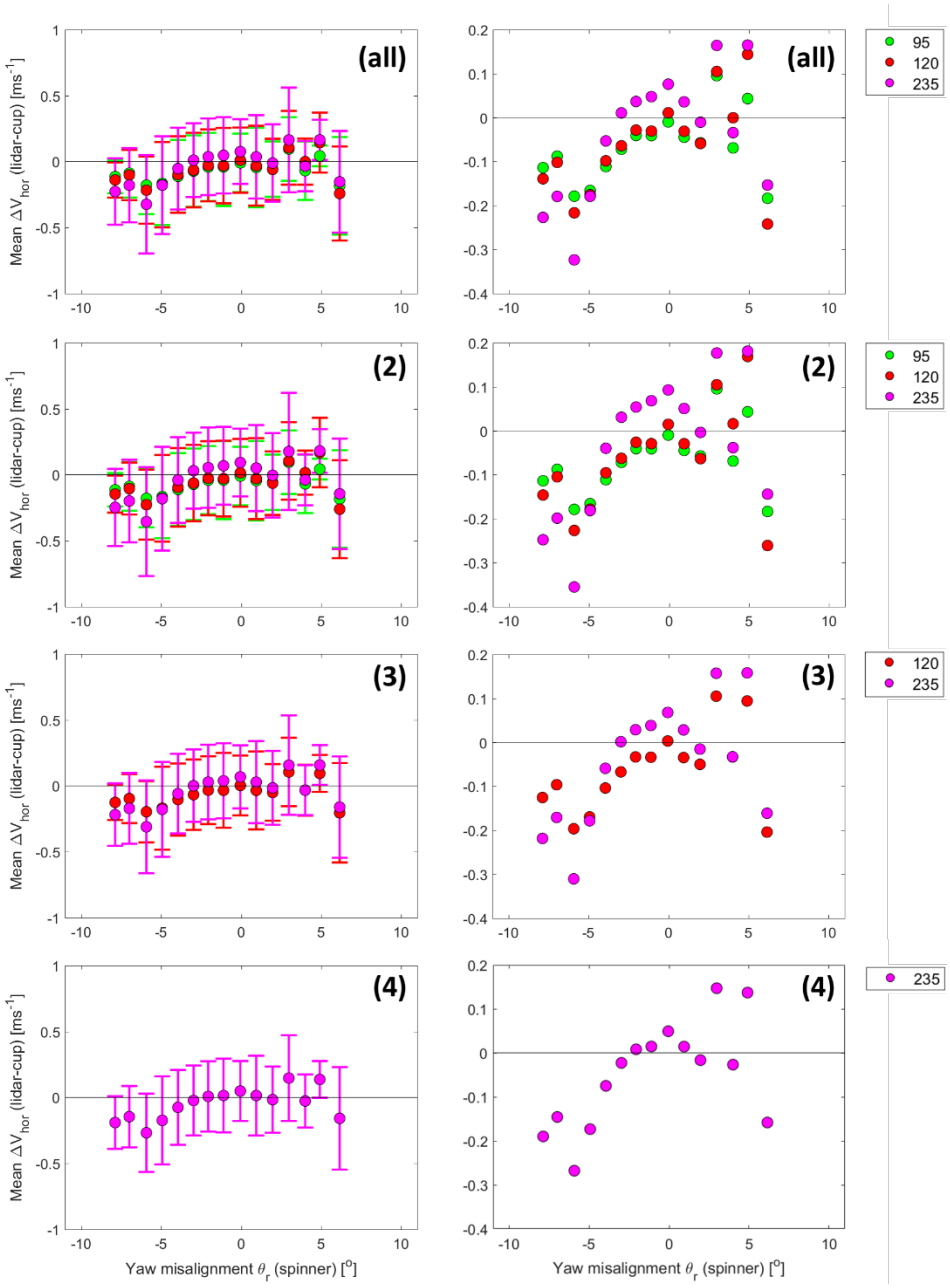

Figure A.19. Wind speed error as a function of yaw misalignment (spinner-measured). The different colors represent different maximum distances. The different rows represent different number of ranges. The right column is the same as the left, but without error bars. Results correspond to the ZDM and 1D induction model.

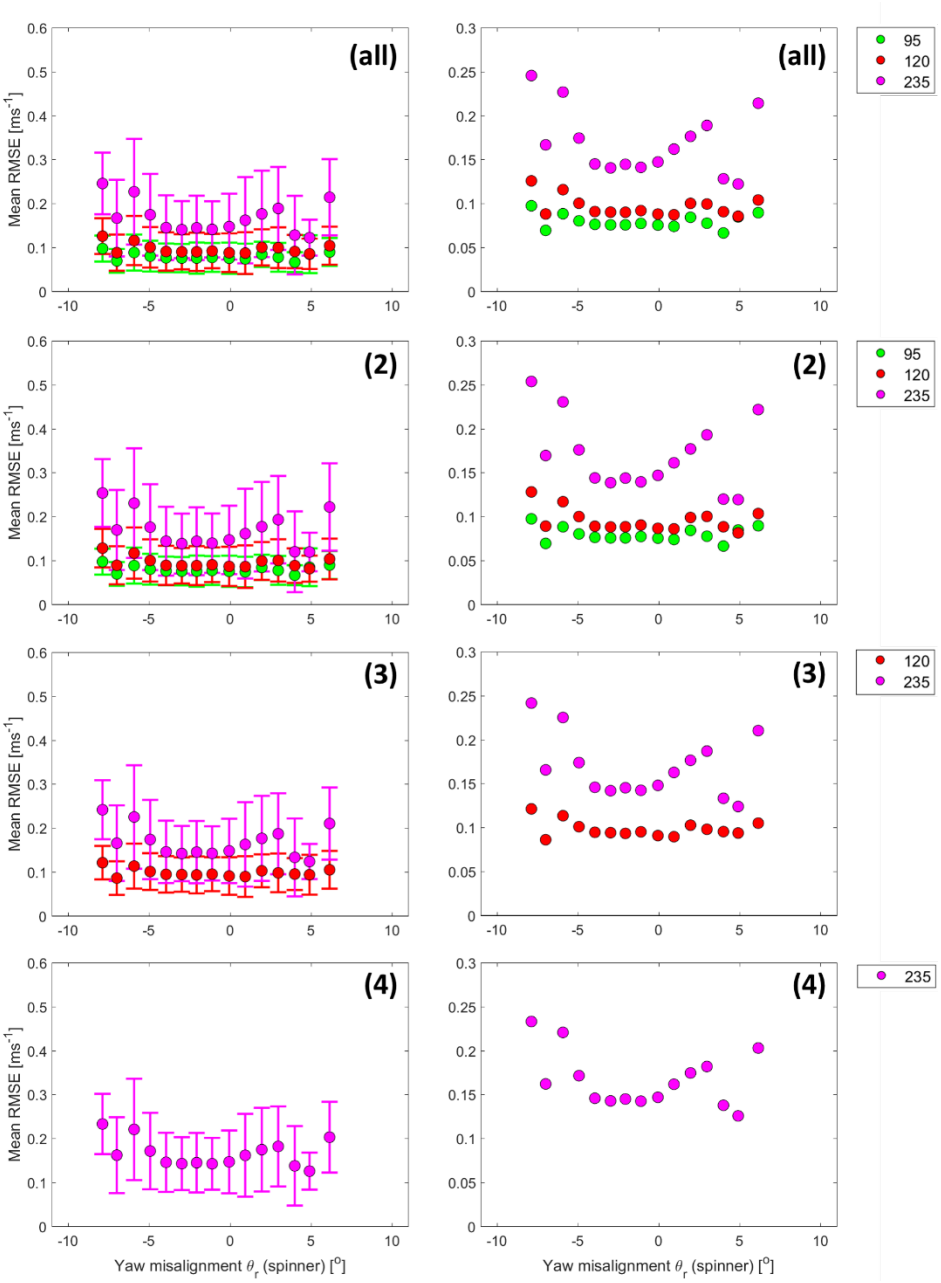

Figure A.20. RMSE as a function of yaw misalignment (spinner-measured). The different colors represent different maximum distances. The different rows represent different number of ranges. The right column is the same as the left, but without error bars. Results correspond to the ZDM and 1D induction model.

Annex E. Sensitivity to wind-induction model (CFD)

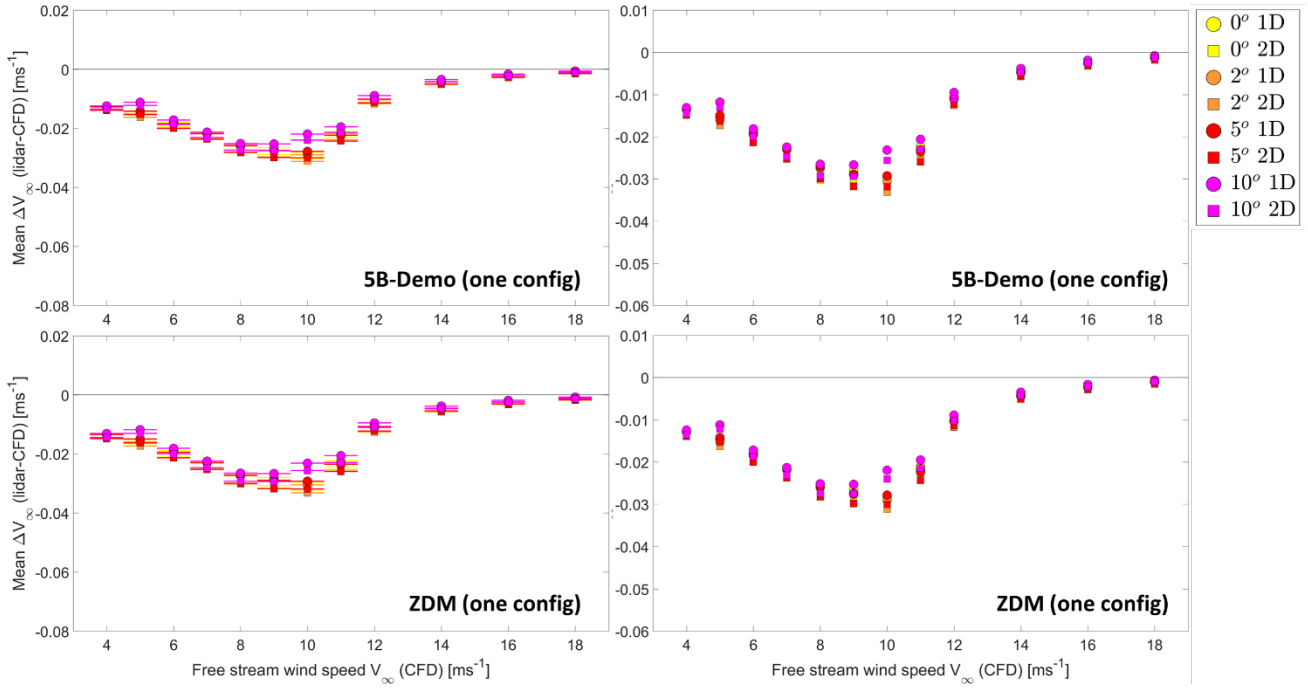

Figure A.21. Free stream wind speed error as a function of the wind speed (CFD input) and yaw misalignment (CFD input). The figures correspond to the [95m, 120/121m, 235m] configuration. The right column is the same as the left, but without error bars.

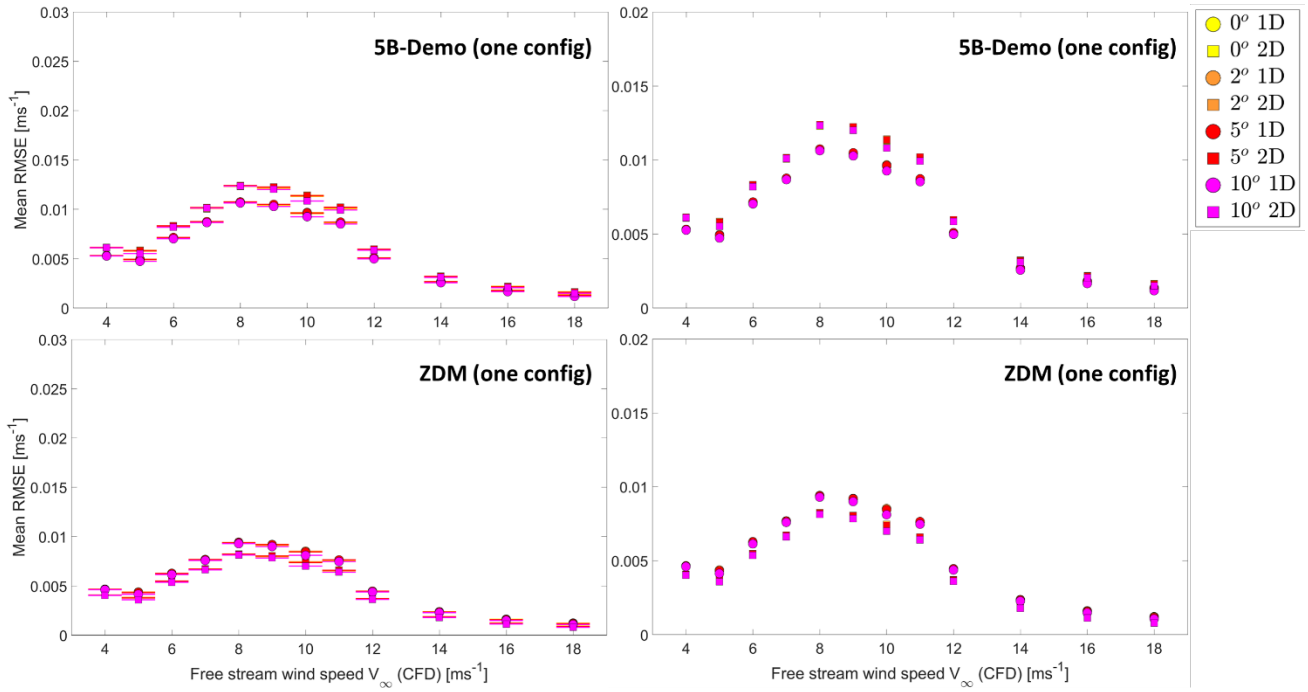

Figure A.22. RMSE as a function of free stream wind speed (CFD input) and yaw misalignment (CFD input). The figures correspond to the [95m, 120/121m, 235m] configuration. The right column is the same as the left, but without error bars.

Annex F. Sensitivity to lidar type and trajectory (CFD)

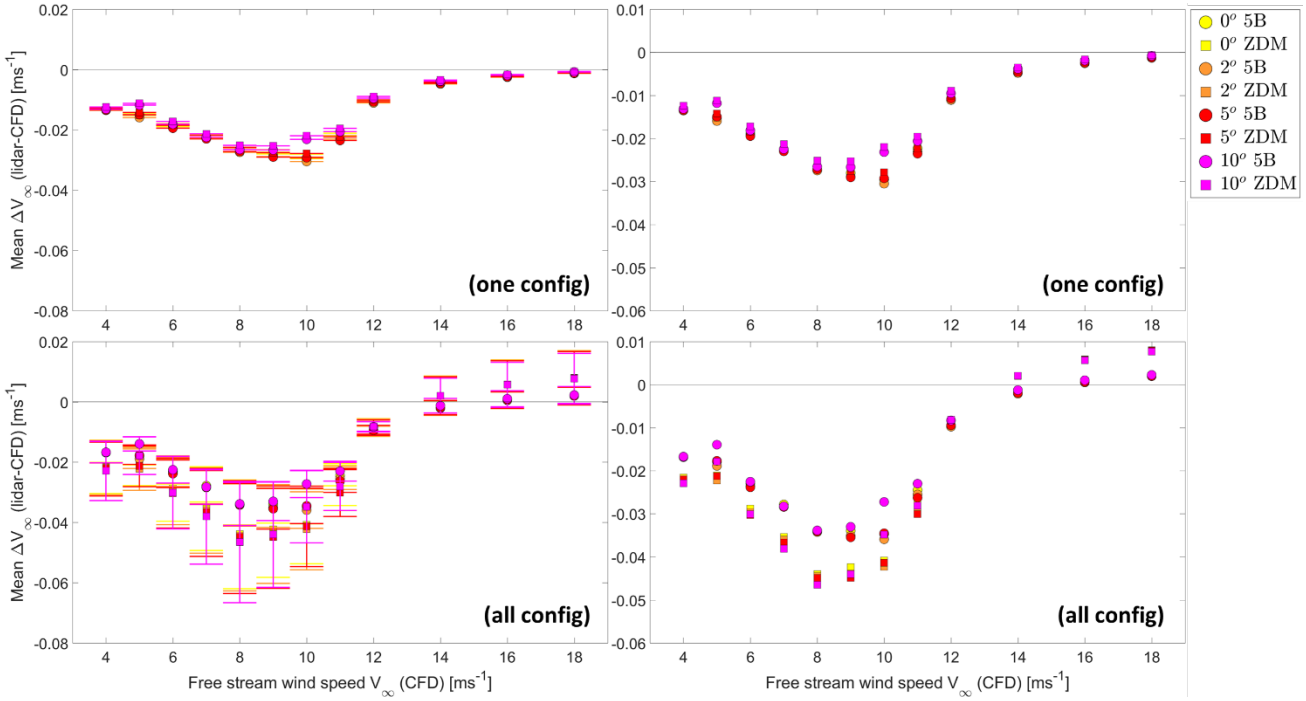

Figure A.23. Free stream wind speed error as a function of the wind speed (CFD input) and yaw misalignment (CFD input). The top row corresponds to the [95m, 120/121m, 235m] configuration while the bottom row corresponds to all configurations. The right column is the same as the left, but without error bars.

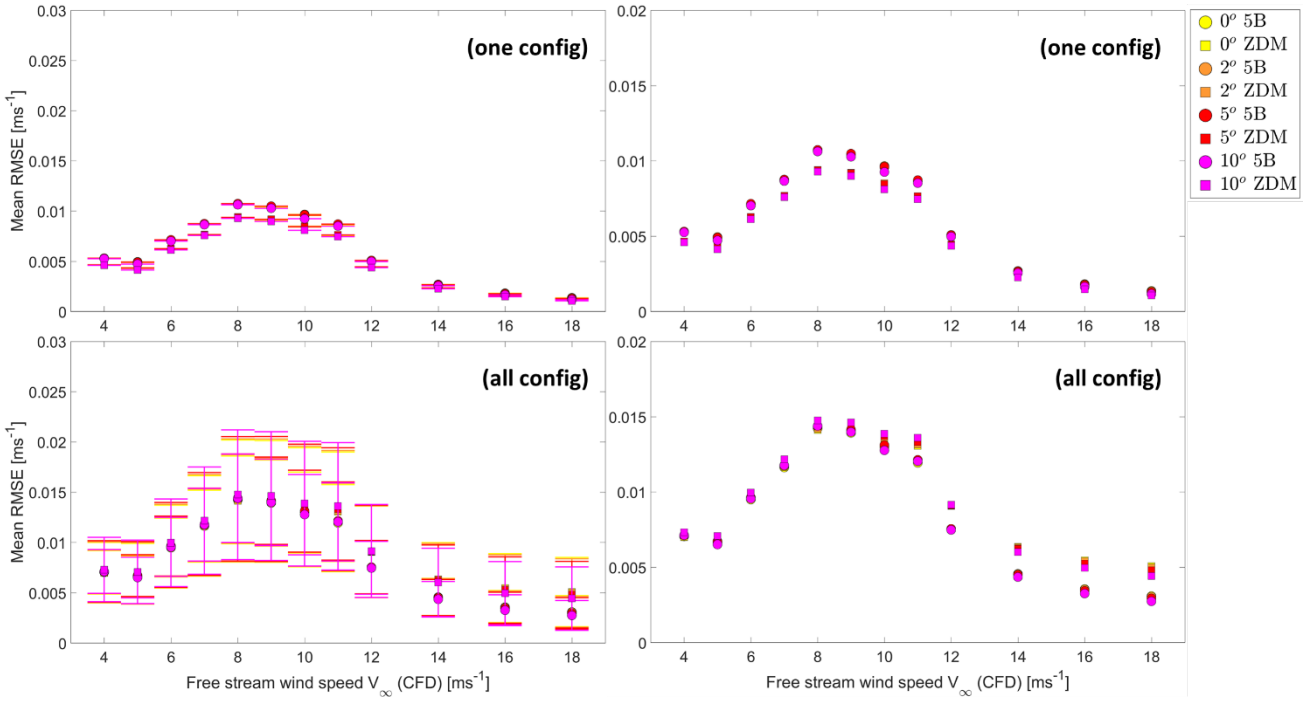

Figure A.24. RMSE as a function of free stream wind speed (CFD input) and yaw misalignment (CFD input). The top row corresponds to the [95m, 120/121m, 235m] configuration while the bottom row corresponds to all configurations. The right column is the same as the left, but without error bars.

Annex G. Sensitivity to minimum distance (CFD)

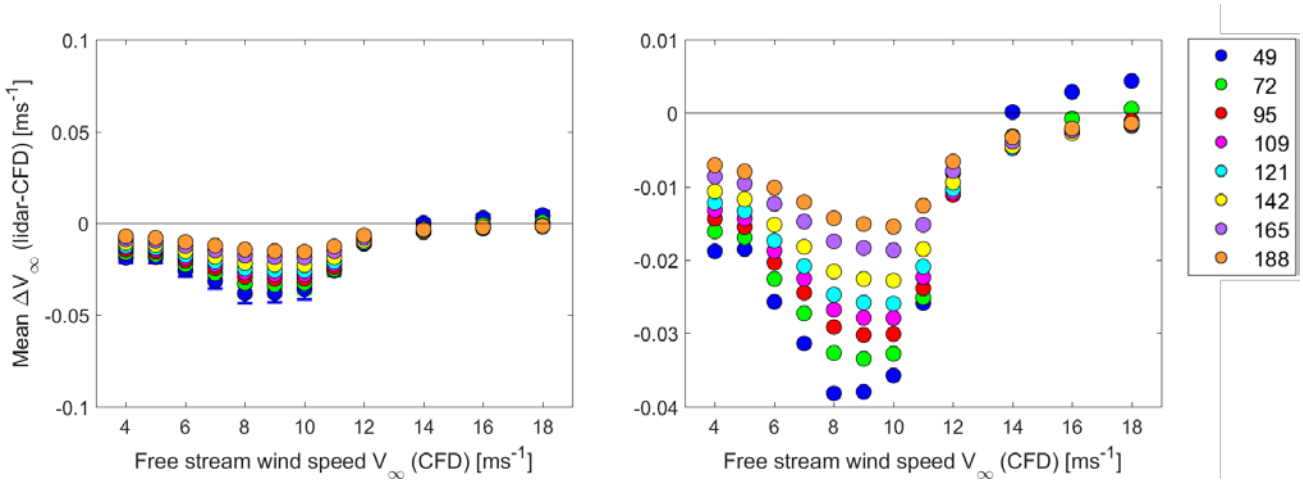

Figure A.25. Free stream wind speed error as a function of free stream wind speed (CFD input). The different colors represent different minimum distances. The right column is the same as the left, but without error bars. Results correspond to the 5B-Demo, 1D induction model and all configurations.

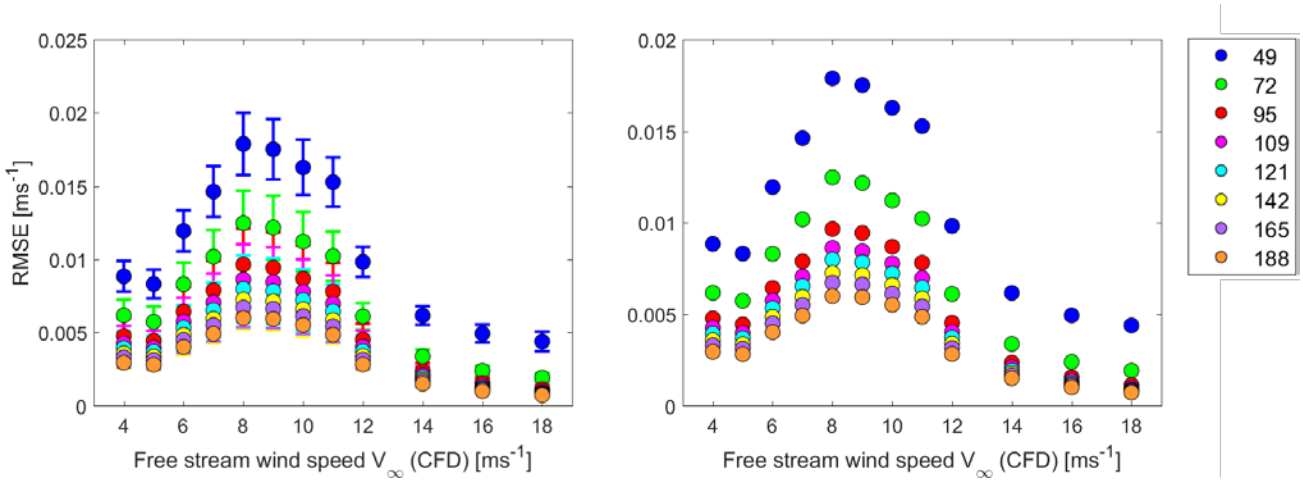

Figure A.26. RMSE as a function of free stream wind speed (CFD input). The different colors represent different minimum distances. The right column is the same as the left, but without error bars. Results correspond to the 5B-Demo, 1D induction model and all configurations.

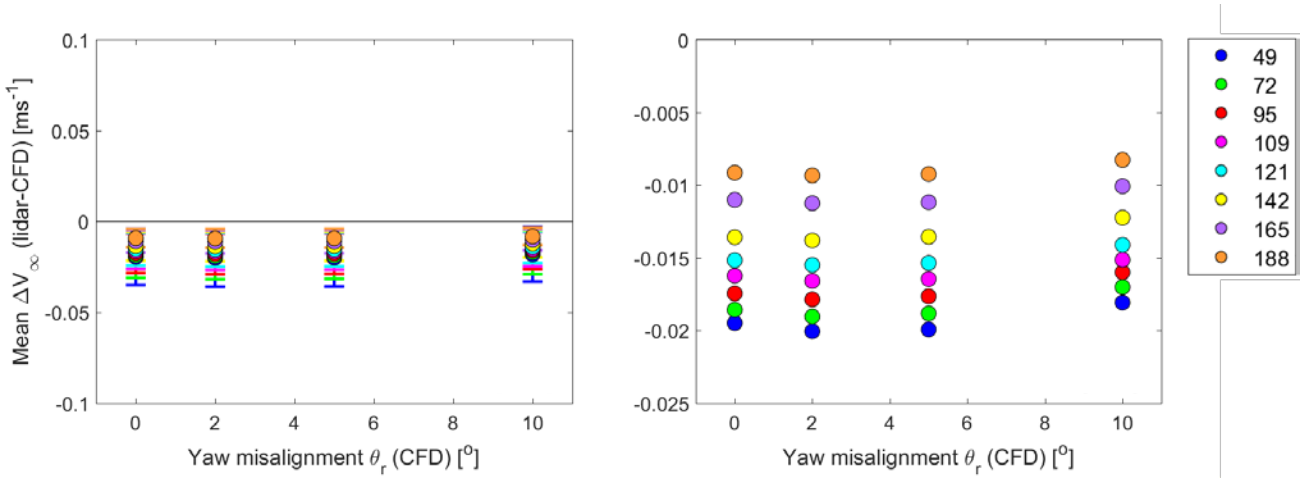

Figure A.27. Free stream wind speed error as a function of yaw misalignment (CFD input). The different colors represent different minimum distances. The right column is the same as the left, but without error bars. Results correspond to the 5B-Demo, 1D induction model and all configurations.

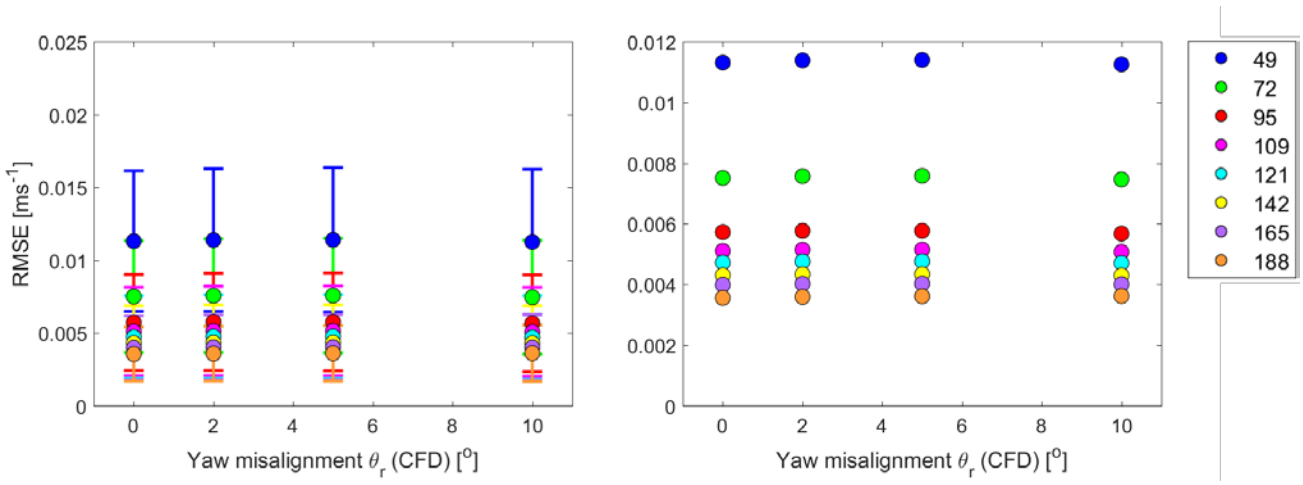

Figure A.28. RMSE as a function of yaw misalignment (CFD input). The different colors represent different minimum distances. The right column is the same as the left, but without error bars. Results correspond to the 5B-Demo, 1D induction model and all configurations.

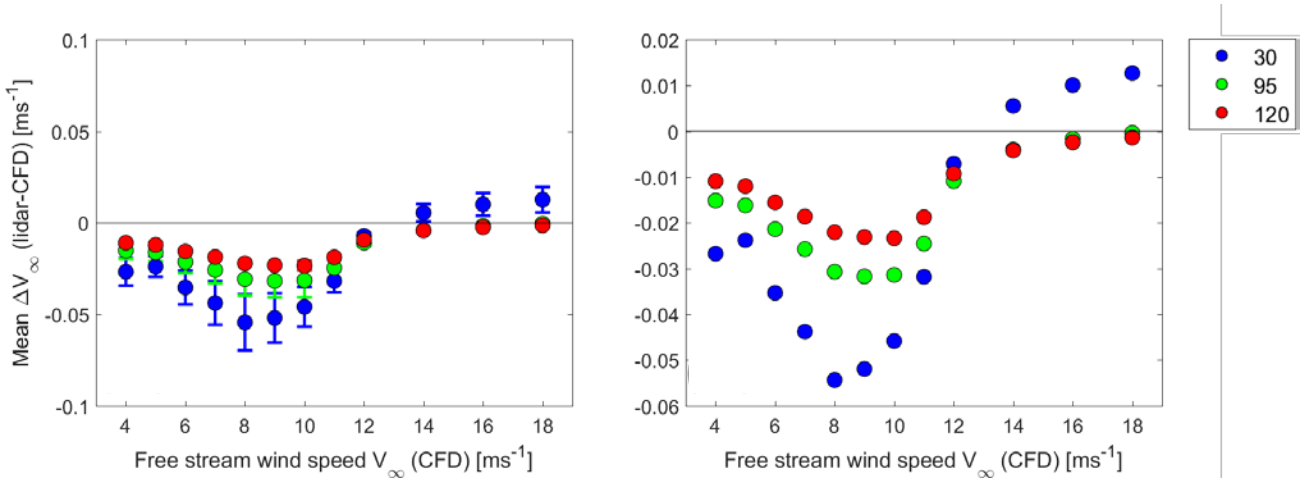

Figure A.29. Free stream wind speed error as a function of free stream wind speed (CFD input). The different colors represent different minimum distances. The right column is the same as the left, but without error bars. Results correspond to the ZDM, 1D induction model and all configurations.

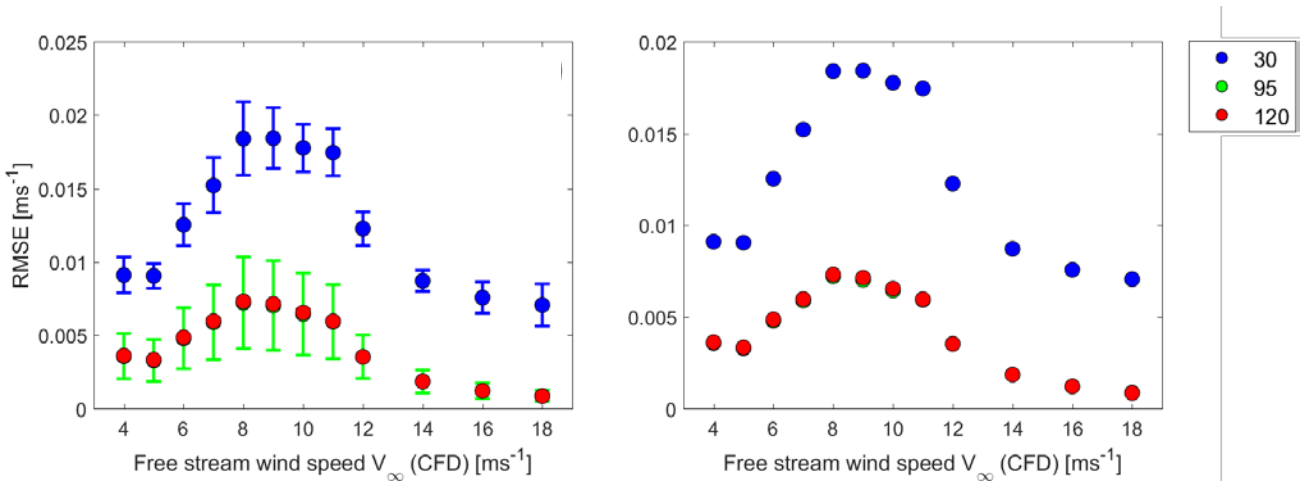

Figure A.30. RMSE as a function of free stream wind speed (CFD input). The different colors represent different minimum distances. The right column is the same as the left, but without error bars. Results correspond to the ZDM, 1D induction model and all configurations.

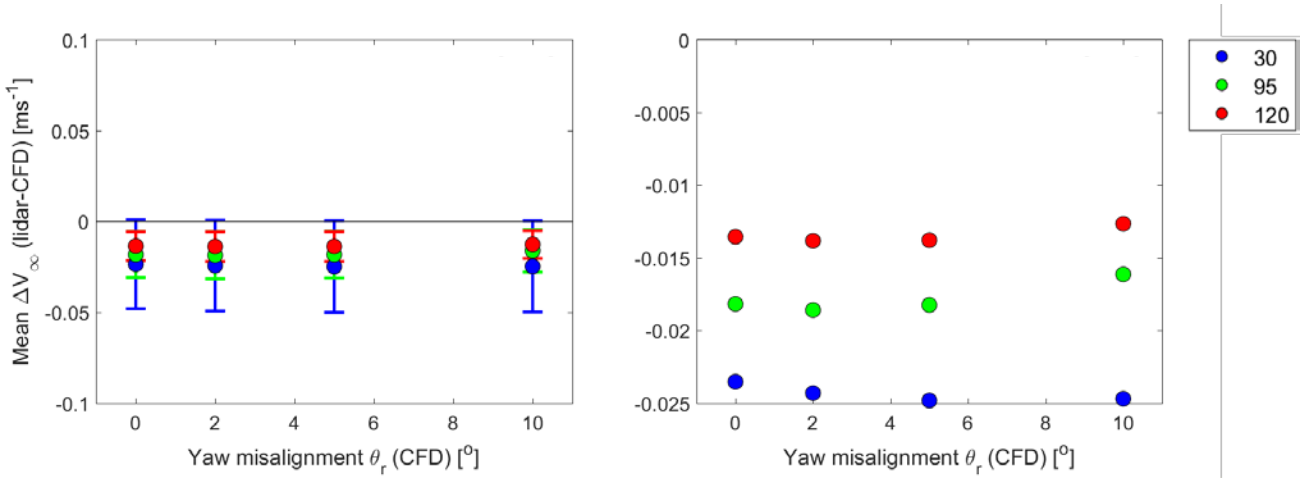

Figure A.31. Free stream wind speed error as a function of yaw misalignment (CFD input). The different colors represent different minimum distances. The right column is the same as the left, but without error bars. Results correspond to the ZDM, 1D induction model and all configurations.

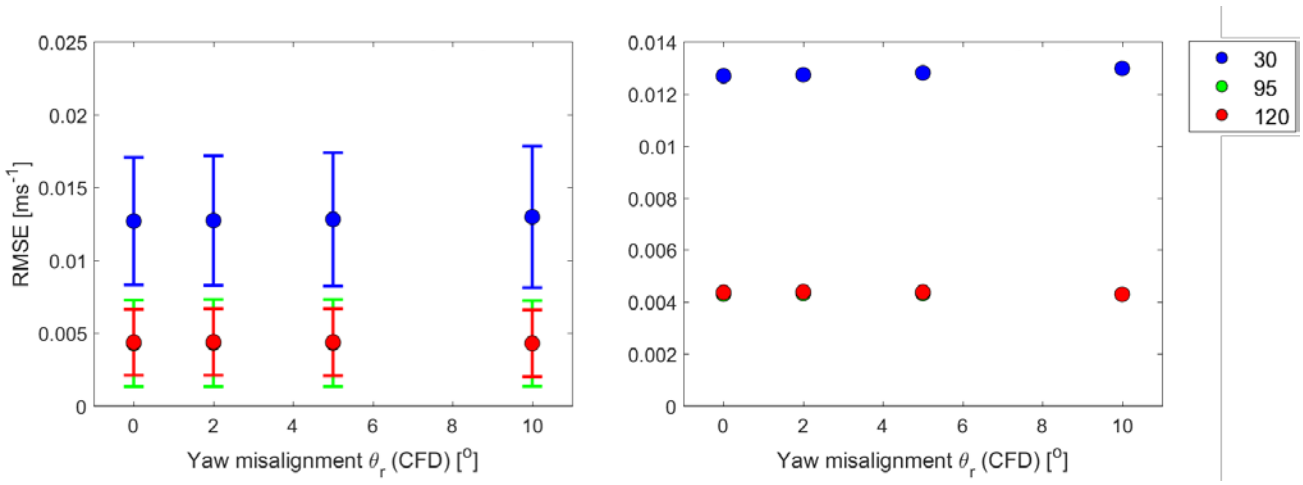

Figure A.32. RMSE as a function of yaw misalignment (CFD input). The different colors represent different minimum distances. The right column is the same as the left, but without error bars. Results correspond to the ZDM, 1D induction model and all configurations.

Annex H. Sensitivity to maximum distance (CFD)

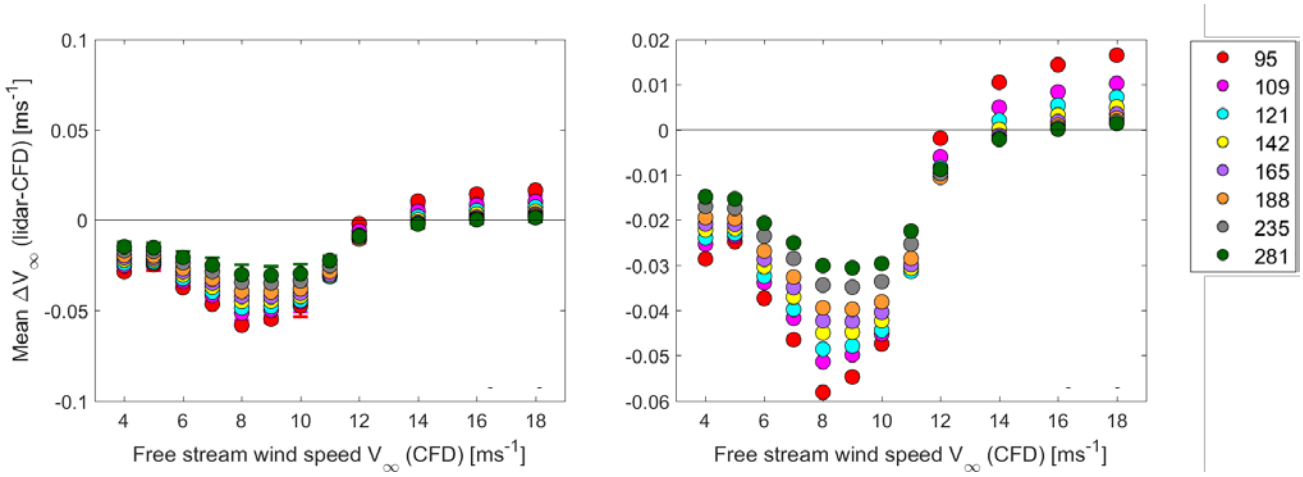

Figure A.33. Free stream wind speed error as a function of free stream wind speed (CFD input). The different colors represent different maximum distances. The right column is the same as the left, but without error bars. Results correspond to the 5B-Demo, 1D induction model and all configurations.

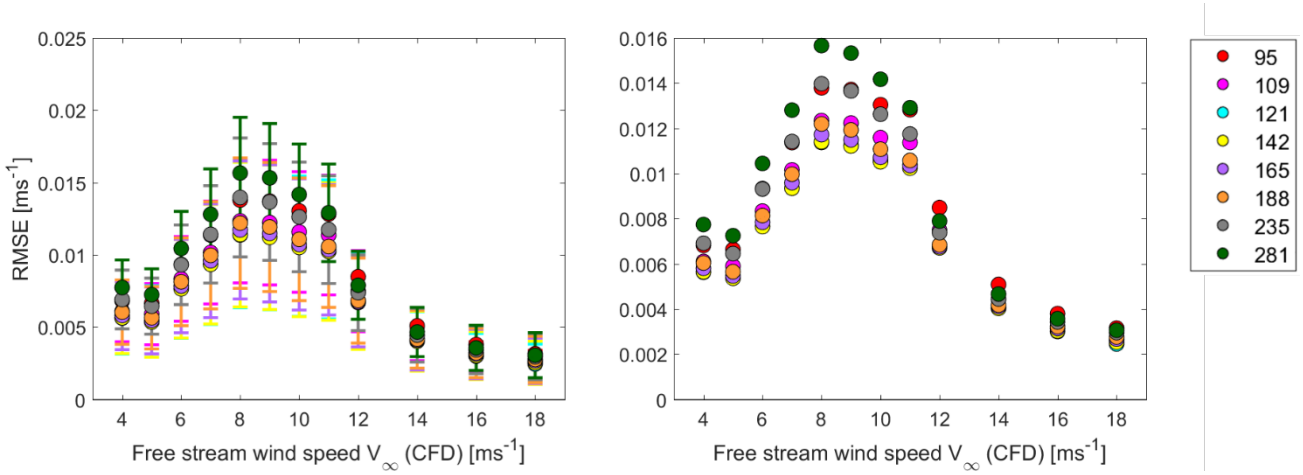

Figure A.34. RMSE as a function of free stream wind speed (CFD input). The different colors represent different maximum distances. The right column is the same as the left, but without error bars. Results correspond to the 5B-Demo, 1D induction model and all configurations.

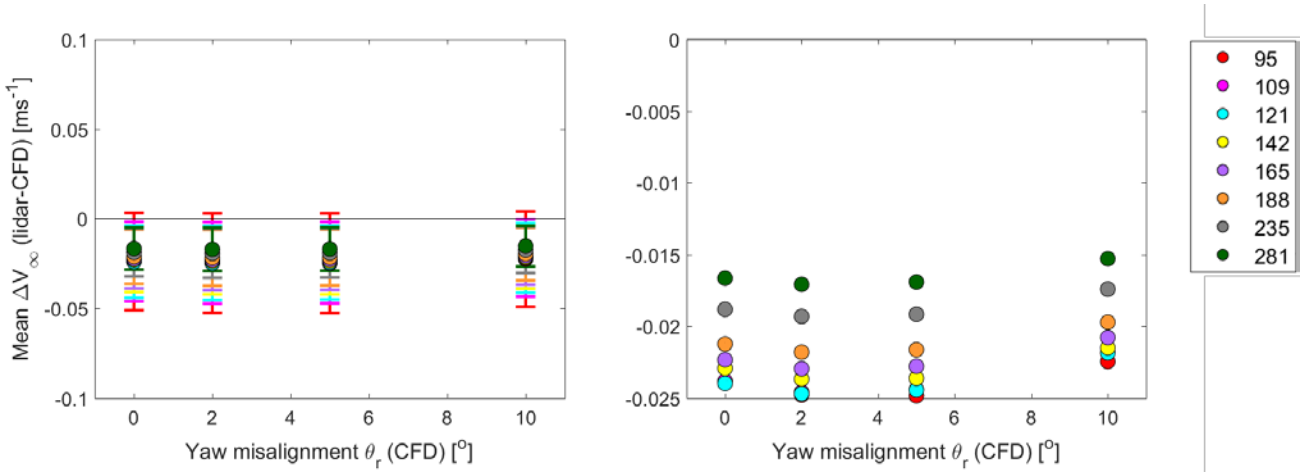

Figure A.35. Free stream wind speed error as a function of yaw misalignment (CFD input). The different colors represent different maximum distances. The right column is the same as the left, but without error bars. Results correspond to the 5B-Demo, 1D induction model and all configurations.

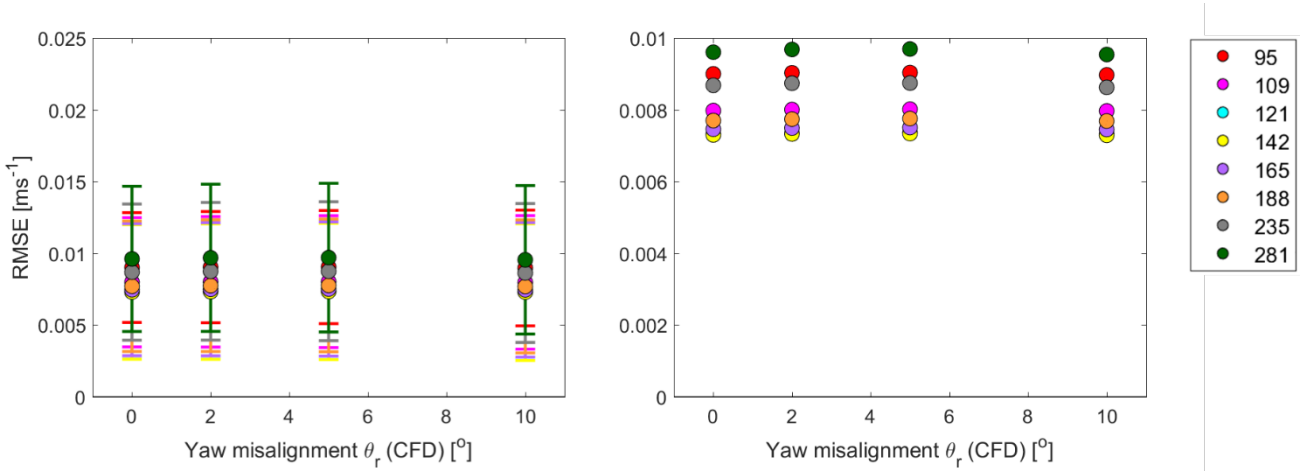

Figure A.36. RMSE as a function of yaw misalignment (CFD input). The different colors represent different maximum distances. The right column is the same as the left, but without error bars. Results correspond to the 5B-Demo, 1D induction model and all configurations.

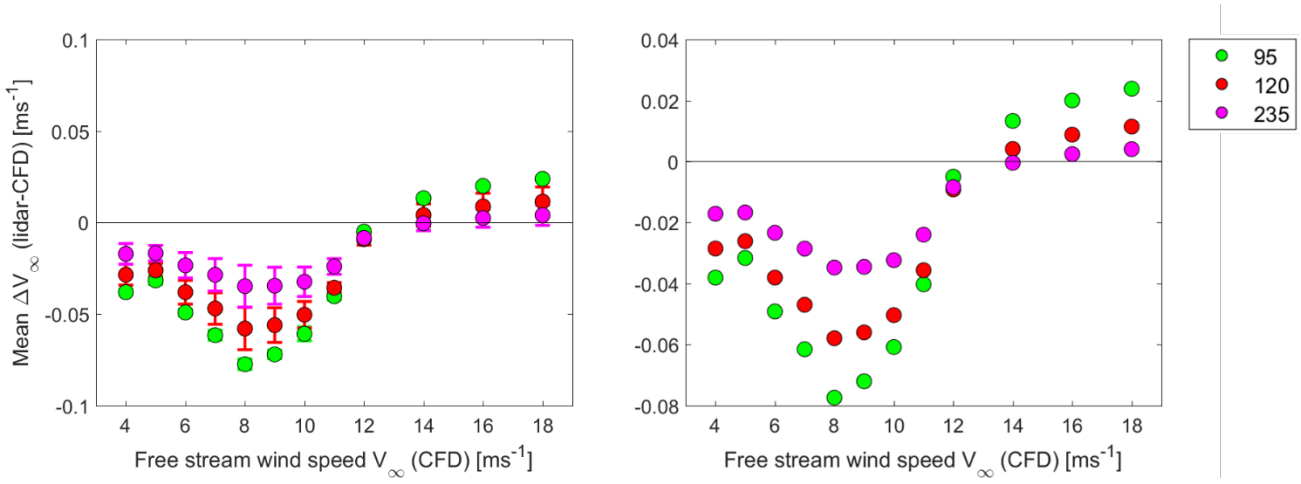

Figure A.37. Free stream wind speed error as a function of free stream wind speed (CFD input). The different colors represent different maximum distances. The right column is the same as the left, but without error bars. Results correspond to the ZDM, 1D induction model and all configurations.

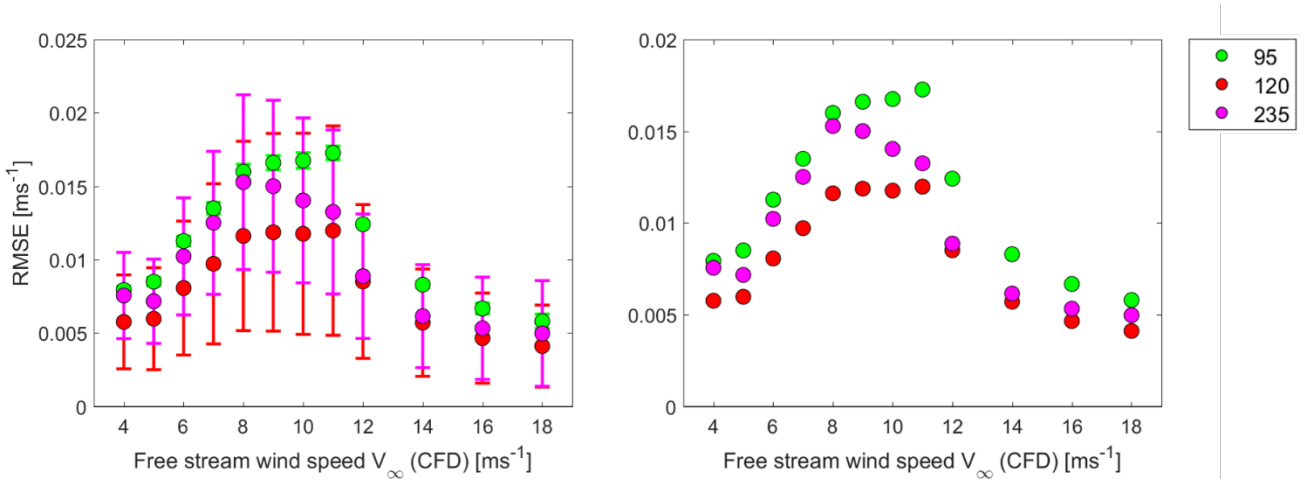

Figure A.38. RMSE as a function of free stream wind speed (CFD input). The different colors represent different maximum distances. The right column is the same as the left, but without error bars. Results correspond to the ZDM, 1D induction model and all configurations.

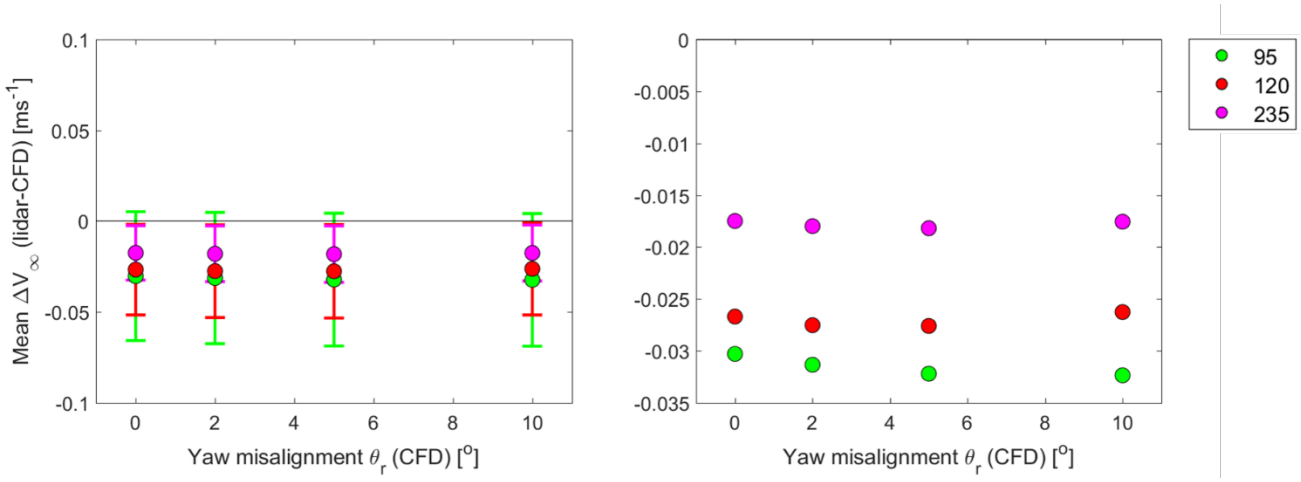

Figure A.39. Free stream wind speed error as a function of yaw misalignment (CFD input). The different colors represent different maximum distances. The right column is the same as the left, but without error bars. Results correspond to the ZDM, 1D induction model and all configurations.

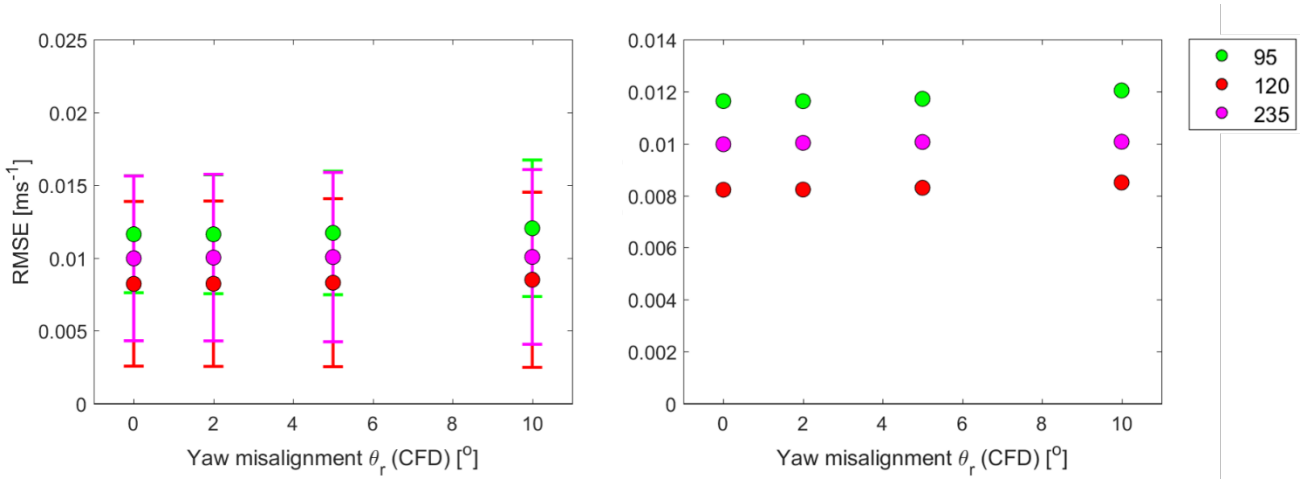

Figure A.40. RMSE as a function of yaw misalignment (CFD input). The different colors represent different maximum distances. The right column is the same as the left, but without error bars. Results correspond to the ZDM, 1D induction model and all configurations.

Annex I. Sensitivity to number of ranges (CFD)

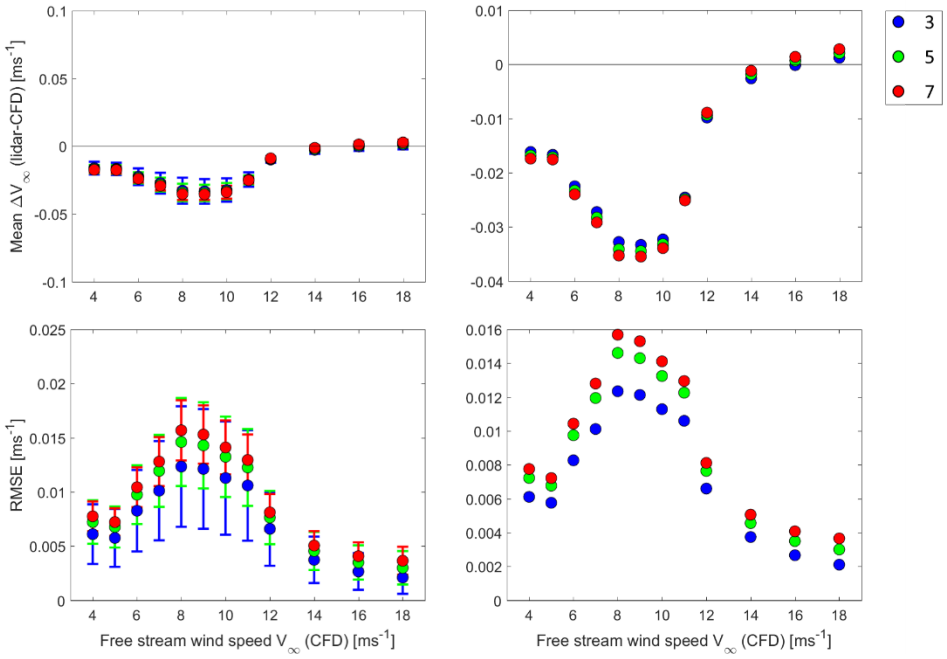

Figure A.41. Free stream wind speed error (top row) and RMSE (bottom row) as a function of free stream wind speed (CFD input). The different colors represent different number of ranges. The right column is the same as the left, but without error bars. Results correspond to the 5B-Demo and 1D induction model.

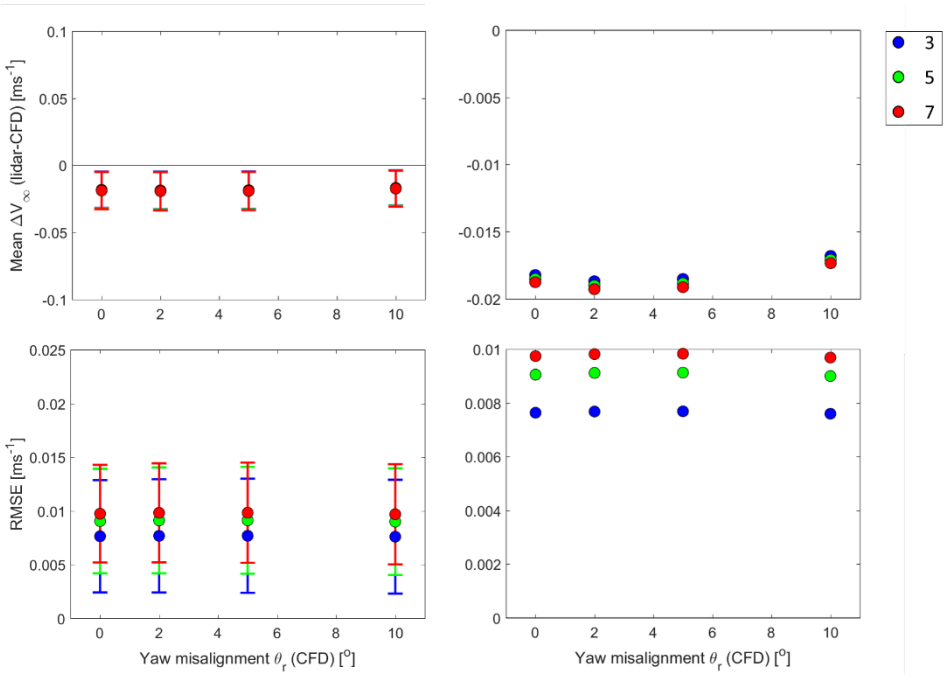

Figure A.42. Free stream wind speed error (top row) and RMSE (bottom row) as a function of yaw misalignment (CFD input). The different colors represent different number of ranges. The right column is the same as the left, but without error bars. Results correspond to the 5B-Demo and 1D induction model.

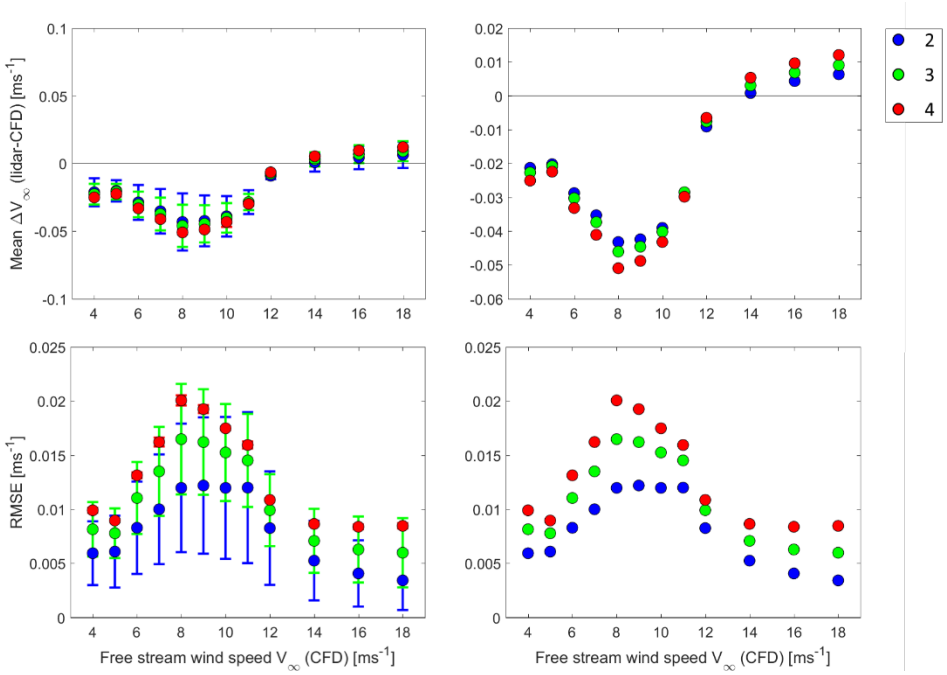

Figure A.43. Free stream wind speed error (top row) and RMSE (bottom row) as a function of free stream wind speed (CFD input). The different colors represent different number of ranges. The right column is the same as the left, but without error bars. Results correspond to the ZDM and 1D induction model.

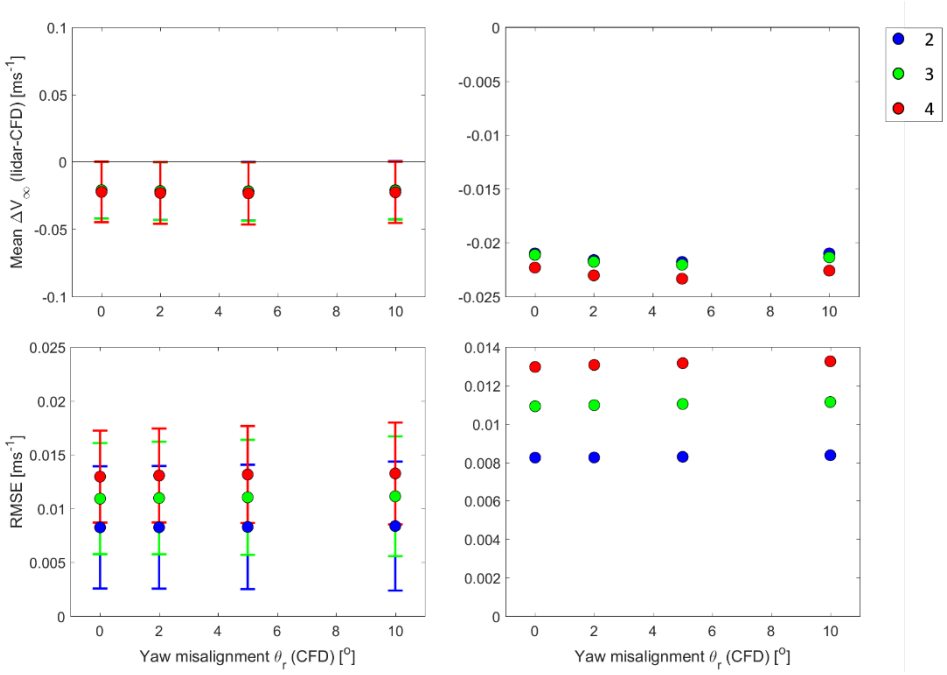

Figure A.44. Free stream wind speed error (top row) and RMSE (bottom row) as a function of yaw misalignment (CFD input). The different colors represent different number of ranges. The right column is the same as the left, but without error bars. Results correspond to the ZDM and 1D induction model.